



THE HONG KONG
POLYTECHNIC UNIVERSITY

香港理工大學

Pao Yue-kong Library

包玉剛圖書館

Copyright Undertaking

This thesis is protected by copyright, with all rights reserved.

By reading and using the thesis, the reader understands and agrees to the following terms:

1. The reader will abide by the rules and legal ordinances governing copyright regarding the use of the thesis.
2. The reader will use the thesis for the purpose of research or private study only and not for distribution or further reproduction or any other purpose.
3. The reader agrees to indemnify and hold the University harmless from and against any loss, damage, cost, liability or expenses arising from copyright infringement or unauthorized usage.

IMPORTANT

If you have reasons to believe that any materials in this thesis are deemed not suitable to be distributed in this form, or a copyright owner having difficulty with the material being included in our database, please contact lbsys@polyu.edu.hk providing details. The Library will look into your claim and consider taking remedial action upon receipt of the written requests.

The Hong Kong Polytechnic University

Department of Civil and Structural Engineering

**LINURON DEGRADATION BY PHOTO-AIDED
OXIDATION PROCESSES IN AQUEOUS PHASE -
- KINETIC STUDY AND REACTION
MECHANISMS**



RAO Yong Fang

A Thesis Submitted in Partial Fulfilment of the Requirements for the
Degree of Doctor of Philosophy

October 2009

CERTIFICATE OF ORIGINALITY

I hereby declare that this thesis is my own work and that, to the best of my knowledge and belief, it reproduces no material previously published or written, nor material that has been accepted for the award of any other degree or diploma, except where due acknowledgement has been made in the text.

Yong Fang, Rao

ABSTRACT

The widespread application of herbicides as a routine practice to control weed growth has led to increasing environmental concerns in the past decades because of their low biodegradability and long-term persistence in soil, which makes them ubiquitous. Most herbicides are diffused into aquatic environment via agricultural runoff or leaching. Linuron (N-(3, 4-dichlorophenyl)-N'-methoxy-N'-methylurea) (LNR), one of the most commercialized phenylurea herbicides, has received particular attention in recent years due to the toxicity, being frequently detected in the surface and underground waters, and possible endocrine disrupting properties of LNR and/or its metabolites. Till now, little is known about the degradability and reaction products of LNR by Vis (visible light)-induced photocatalysis. The knowledge regarding the LNR decomposition by UV, ozonation, and UV/ozone processes is far from complete although UV and ozonation has shown good performance in terms of LNR decay in some studies. In particular, the information about the intermediates and end products remains limited. Therefore, the aqueous degradation of LNR has been investigated by UV, ozonation, UV/ozone and $\text{TiO}_2/\text{H}_2\text{O}_2/\text{Vis}$ processes.

The investigation was conducted under idealized conditions and has taken into account both degradation kinetics and reaction mechanisms. It has been found that ozonation and UV/ O_3 are pH-dependent while UV is pH-independent in terms of LNR decomposition. Experimental results also indicated overall rate constants increased exponentially with pH above 9.0 while the increase of rate constants with pH below 9 is insignificant in sole- O_3 system. In UV photolysis study, the LNR

decay rate constant is linearly increased with the intensity of light. Linear models were proposed on the basis of reaction kinetics of LNR decay by these three processes. All dominant parameters such as quantum yield (Φ_{LNR}), k_{OOH} (rate constant for the formation of free radical HOO^{\bullet} from ozone decomposition at high pH), rate constant of linuron with ozone ($k_{o_3, LNR}$), rate constant of linuron with hydroxyl radical ($k_{OH, LNR}$), and α (the ratio of the production rate of HO^{\bullet} and the decay rate of ozone in UV/O₃ system), involved in the three processes were determined with the aid of proposed linear models. The effect of various anions on the performance of ozonation has also been examined.

Eight intermediates escaped from previous studies were detected in the sole-UV system in this study. *N*-terminus demethoxylation, photohydrolysis with dechlorination, hydroxylation on the benzene ring and *N*-terminus demethylation were found to be the major mechanisms in the linuron decay under the irradiation of UV at 254 nm while *N*-terminus demethoxylation, dechlorination and hydroxylation on the benzene ring were observed to be involved in the ozonation process. Different decay pathways were proposed based on the identified intermediates in the studied three processes. The release of chlorine and nitrogen as well as mineralization has also been quantified. UV/O₃ has demonstrated the best performance among these three processes in terms of LNR decay, mineralization, dechlorination and denitrogenation.

Furthermore, the degradation of LNR in TiO₂ suspension has been studied, with and without the aid of H₂O₂ under the irradiation of visible light. The removal of LNR in TiO₂-P25 suspension can be increased from 10% to nearly 100% after 3 hr of

reaction by simply adding H_2O_2 to the process. Various types of TiO_2 including anatase, rutile and TiO_2 -P25 exhibited different photocatalytic activities on LNR decay, while their performances were strongly dependent on the presence and/or absence of H_2O_2 . The H_2O_2 -assisted TiO_2 photocatalysis using visible light could be optimized by adjusting TiO_2 dosage, initial concentration of H_2O_2 and the initial pH of the system. The LNR decay rate, generally, increased with the increase of TiO_2 dosage, but too high the TiO_2 dosage was not cost-effective due to the light attenuation. The initial H_2O_2 concentration in the tested range did not show a significant influence on the reaction rate. A neutral initial pH level was found to be favorable for the H_2O_2 -assisted photocatalysis under visible light, which made the proposed process more attractive for real application.

The reaction mechanism of LNR degradation by the $\text{TiO}_2/\text{H}_2\text{O}_2/\text{Vis}$ process has been also examined through the investigation on the effects of various radical scavengers, monitoring the generation of photocurrent, examining the performance of other metal oxides in place of TiO_2 in this system, and comparing the intermediates and decay pathways of LNR by UV- TiO_2 and $\text{TiO}_2/\text{H}_2\text{O}_2/\text{Vis}$ processes with 16 and 17 intermediates identified, respectively. The generation of electrons was first confirmed by monitoring photocurrent with a TiO_2 -coated ITO electrode immersed in H_2O_2 solution under the irradiation of visible light. It has been revealed that demethoxylation and demethylation through alkylic-oxidation is the major mechanism of LNR degradation while dechlorination (hydroxylation at the chlorine site) and direct hydroxylation on the benzene ring is minor in both processes. The mineralization and the release of chlorine and nitrogen have been also studied.

Publications arising from the thesis

Journal Papers

- 1. Rao Y. F.,** Chu W., A New Approach to Quantify the Degradation Kinetics of Linuron with UV, Ozonation and UV/O₃ processes, *Chemosphere* 2009, 74(11), 1444-1449.
- 2. Rao Y. F.,** Chu W., Reaction Mechanism of linuron degradation in TiO₂ suspension under visible light irradiation with the assistance of H₂O₂, *Environmental Science & Technology* 2009, 43, 6183-6189.
- 3. Rao Y. F.,** Chu W. Linuron degradation in aqueous semiconductor suspension under visible light irradiation-with and without H₂O₂, *Chemical Engineering Journal*, 2010, 158 (2), 181-187.
- 4. Rao Y. F.,** Chu W. Degradation of linuron by UV, Ozonation, and UV/O₃ processes---Effect of Anions and Reaction Mechanism *Journal of Hazardous Materials*, 2010, 180 (1-3), 514-523.

Conference Presentation

- 1. Rao Y. F.,** Chu W., Modeling the Reaction Kinetics and Product Identification of Linuron Decay by UV/O₃ Process, *The 5th IWA Specialist Conference/ 10th IOA-EA₃G Berlin Conference on Oxidation Technologies for Water and Wastewater Treatment*, 30 March-02 April, Berlin, Germany, 2009.

ACKNOWLEDGEMENTS

I would like to express my deepest gratitude to my supervisor, Prof. Wei Chu, for his unwavering support throughout the project. Without his guidance and advice, the completion of this thesis is unattainable. I also wish to extend my thanks to the technicians in the Water and Wastewater Laboratory, especially Mr. Wai Shung Lam for his invaluable assistance and also Mr. Chi Wai Lau for his technical support.

The support from my former colleagues Dr. Ada K.H. Chan, Dr. Esther W.K. Choy and Dr. Catherine T.K. Lau is gratefully acknowledged for their precious advices. Thanks also go to my family for their constant encouragement and moral support throughout the period.

Last but not least, the financial support from the Hong Kong Polytechnic University (RGTN) is highly appreciated.

TABLE OF CONTENTS

Declaration	i
Abstract	ii
Publications	v
Acknowledgements	vi
Table of Contents	vii
List of Figures	xi
List of Tables	xvii
Chapter 1 Introduction	1
1.1 Background	1
1.2 Objectives of Study	3
1.3 Scope of Study	4
Chapter 2 Literature Review	7
2.1 Wastewater Treatment Processes	7
2.1.1 UV photolysis.....	7
2.1.2 Ozone-based Advanced Oxidation Processes	15
2.1.3 Photocatalysis.....	25
2.2 Description of Linuron	32
2.2.1 Background	32
2.2.2 Toxicological Effects	32
2.2.3 Environmental Fate	33
2.2.4 Previous degradation studies of LNR.....	34
Chapter 3 Materials and Methodology.....	35
3.1 Introduction	35
3.2 Materials	35
3.3 Experimental Setup	38

3.3.1 UV/O ₃ process.....	38
3.3.2 Photocatalysis process.....	40
3.4 Instrumental Analysis.....	42
3.4.1 Analysis by high performance liquid chromatography (HPLC).....	43
3.4.2 Analysis by LC/MS.....	43
3.4.3 Analysis by ion chromatography (IC).....	44
3.4.4 TOC measurement.....	44
3.4.5 pH measurement.....	45
3.4.6 X-ray diffraction analysis.....	45
3.4.7 Diffuse reflectance absorption analysis.....	46
3.4.8 Measurement of the emission spectra of lamps.....	46
3.4.9 Measurement of the photocurrent	46
 Chapter 4 Degradation Kinetics of LNR with UV, Ozonation and UV/O ₃ Processes	 48
4.1 Introduction.....	48
4.2 Results and Discussion.....	50
4.2.1 Decomposition and mineralization of LNR in UV/Ozone system	50
4.2.2 Effect of pH level on decay rate of the LNR ozonation	51
4.2.3 Quantum Yield determination in UV system.....	52
4.2.4 Rate Constant Determination in Ozone system.....	53
4.2.5 Derivation of Rate Models and rate constant determination in UV/O ₃ system	58

4.3 Summary	65
Chapter 5 Reaction Mechanism of LNR Degradation by UV Photolysis, Ozonation and UV/O ₃ Process.....	66
5.1 Introduction	66
5.2 Results and Discussion	67
5.2.1 The effect of initial pH level on the decay of LNR by UV, O ₃ and UV/O ₃ processes.....	67
5.2.2 The effect of varied anions on the LNR decay in sole- ozone system	70
5.2.3 Reaction mechanism of LNR degradation	72
5.3 Summary	88
Chapter 6 LNR Decomposition in Aqueous Semiconductor Suspension under Visible Light Irradiation-with and without H ₂ O ₂	89
6.1 Introduction	89
6.2 Results and Discussion	91
6.2.1 LNR degradation under visible light irradiation in TiO ₂ - H ₂ O ₂ system.....	91
6.2.2 Effect of TiO ₂ phase composition	95
6.2.3 The performance of different semiconductors under various conditions	97
6.2.4 Effect of TiO ₂ -P25 dosage	98
6.2.5 Effect of H ₂ O ₂ concentration.....	100
6.2.6 Effect of pH level	102
6.2.7 Effect of initial concentration of LNR	104
6.3 Summary	107

Chapter 7 Reaction Mechanism of LNR Degradation in TiO ₂ Suspension under Visible Light Irradiation with the Assistance of H ₂ O ₂	109
7.1 Introduction	109
7.2 Results and Discussion	111
7.2.1 LNR Degradation in Various Systems	111
7.2.2 Photocatalytic Degradation Mechanism of LNR under Visible Light.....	113
7.2.3 Effect of Wavelength	117
7.2.4 Photocatalytic Degradation Pathway of LNR under Visible Light or UV Irradiation.....	119
7.3 Summary	129
Chapter 8 Conclusion and Recommendation.....	130
8.1 Conclusion	130
8.1.1 The Degradation of LNR by using UV, Ozonation, and UV/Ozone.....	130
8.1.2 The Degradation of LNR by TiO ₂ /H ₂ O ₂ /vis (visible light) process	132
8.2 Limitation and Recommendation	134
References.....	136
APPENDIX I: Experimental runs	I-1
APPENDIX II: Mass spectrum of LNR and major intermediates	II-1
APPENDIX III: Absorption spectrum of LNR	III-1
APPENDIX IV: Experimental results	IV-1

LIST OF FIGURES

Figure 2-1:	The possible routes to loss of photochemically excited molecule.	9
Figure 2-2:	Schematic photoexcitation in a solid semiconductor followed by de-excitation events	26
Figure 2-3:	Chemical Structure of LNR.	32
Figure 3-1:	The top view and sectional view of the photoreactor Rayonet TM .	39
Figure 3-2:	Schematic diagrams of the photoreactor Luzchem CCP-4V.	41
Figure 3-3:	Schematic diagrams of the photoreactor with Xe lamp installed.	41
Figure 3-4:	Emission spectra of 420 nm lamps.	42
Figure 3-5:	Emission spectra of Xe lamp.	42
Figure 3-6:	XRD patterns of different TiO ₂ powders used in this study: (a) P25; (b) Rutile; (c) Anatase.	46
Figure 4-1:	Comparison of LNR decay (C/C_0) and TOC removal by the different treatment processes at pH 6 ($C_0 = 0.1$ mM)	50
Figure 4-2:	Pseudo first-order degradation of 0.1 mM LNR in ozone-alone system at various pH levels ($[O_3] = 1.71 \times 10^{-5}$ M).	52
Figure 4-3:	Pseudo first-order degradation of 0.1 mM LNR in sole-UV system under various light intensity irradiation.	53
Figure 4-4:	(a) Variation of decay rate constant of 0.1 mM LNR with various hydroxide ion concentrations at different ozone concentration levels in ozone-alone system; (b)	56

Correlations between $\text{int}_{\text{koverall}}$ and $[\text{O}_3]$ or Correlations between $\text{slope}_{\text{koverall}}$ and $3[\text{O}_3] / [\text{LNR}]$.

- Figure 4-5: Relationship between the degradation of atrazine and LNR (Notes: $[\text{LNR}]_0 = [\text{ATZ}]_0 = 10 \mu\text{M}$, $[\text{H}_2\text{O}_2]_0 = 20 \text{ mM}$, Initial light intensity = $3.0 \times 10^{-6} \text{ Einstein L}^{-1} \text{ s}^{-1}$). 57
- Figure 4-6: Variation of decay rate constant of 0.1 mM LNR under different light. 62
- Figure 5-1: (a). Pseudo first-order rate constants at different initial pH level by different degradation process; (b). The ratio of k_{UV/O_3} and $k_{\text{UV}} + k_{\text{O}_3}$. 68
- Figure 5-2: (a) The effect of varied anions on the performance of ozonation at pH 3; (b) The effect of varied anions on the performance of ozonation at pH 7; (c) The variation of pH during the ozonation of LNR with the presence of various anions. (Notes: $[\text{LNR}]_0 = 0.1 \text{ mM}$, $[\text{O}_3] = 0.0245 \text{ mM}$, $[\text{anions}] = 0.01 \text{ M}$). 71
- Figure 5-3: (a) The evolution profiles of LNR and intermediates in the photolysis of LNR at 254 nm; (b) UV absorption spectrum of the solution at different time intervals; (c) The evolution profiles of TOC, pH, Cl^{-1} , NO_3^{-1} , and NH_4^+ . (Notes: $[\text{LNR}]_0 = 0.285 \text{ mM}$, $\text{pH}_0 = 6.0$, $[\text{I}_0] = 9.0 \times 10^{-6} \text{ Einstein L}^{-1} \text{ s}^{-1}$). 78
- Figure 5-4: The evolution profiles of DCPMU and intermediates in the photolysis of DCPMU at 254 nm. 79
- Figure 5-5: The decay pathways of LNR under the irradiation by UV 80

at 254 nm.

- Figure 5-6: (a) The evolution profiles of LNR and intermediates for the degradation of LNR by ozonation; (b) The evolution profiles of TOC, pH, Cl^- , NO_3^- , and NH_4^+ for the degradation of LNR by ozonation. (Notes: $[\text{LNR}]_0 = 0.285 \text{ mM}$, $[\text{O}_3] = 0.0245 \text{ mM}$, $\text{pH}_0 = 6.0$). 83
- Figure 5-7: (a) The evolution profiles of LNR and intermediates for the degradation of LNR by UV/ O_3 ; (b) The evolution profiles of TOC, pH, Cl^- , NO_3^- , and NH_4^+ for the degradation of LNR by UV/ O_3 . (Notes: $[\text{LNR}]_0 = 0.285 \text{ mM}$, $[\text{O}_3] = 0.0245 \text{ mM}$, $[\text{I}_0] = 9.0 \times 10^{-6} \text{ Einstein L}^{-1} \text{ s}^{-1}$, $\text{pH}_0 = 6.0$). 85
- Figure 5-8: The degradation pathways of LNR by ozonation and UV/ O_3 processes. 86
- Figure 6-1: Diffuse reflection spectra of various TiO_2 powder. 92
- Figure 6-2: (a) LNR degradation under different reaction conditions; (b) H_2O_2 decomposition under different reaction conditions; (c) Effect of radical scavenger on visible-light photocatalysis of LNR with and without H_2O_2 . (Notes: initial LNR concentration is 0.1 mM, TiO_2 loading is 0.6 g/L, the initial concentration of H_2O_2 is 10 mM, initial pH value is 6.0). 94
- Figure 6-3: LNR degradation using different TiO_2 as photocatalysts with and without H_2O_2 (Notes: initial LNR concentration is 0.1 mM, TiO_2 loading is 0.6 g/L, the initial 96

concentration of H_2O_2 is 10 mM, initial pH value is 6.0, R denotes rutile, A represents anatase.).

- Figure 6-4: The performance of various semiconductors under different reaction conditions. (Notes: initial LNR concentration is 0.1 mM, semiconductor loading is 0.6 g/L, the initial concentration of H_2O_2 is 10 mM, initial pH value is 6.0). 98
- Figure 6-5: The effect of TiO_2 -P25 dosage on the LNR decay rate (Notes: initial LNR concentration is 0.1 mM, the initial concentration of H_2O_2 is 10 mM, initial pH value is 6.0). 99
- Figure 6-6: (a) The effect of H_2O_2 concentration on the LNR degradation; (b) The variation of H_2O_2 concentration during the reaction (Notes: initial LNR concentration is 0.1 mM, TiO_2 -P25 dosage is 0.4 g/L, initial pH value is 6.0). 101
- Figure 6-7: (a) LNR decomposition at different pH levels; (b) H_2O_2 decomposition at different pH levels. (Notes: initial LNR concentration is 0.1 mM, TiO_2 -P25 dosage is 0.4 g/L, the initial concentration of H_2O_2 is 5 mM.). 103
- Figure 6-8: (a) Degradation of LNR at different initial concentrations; (b) L-H plot of LNR decay (Notes: TiO_2 -P25 dosage is 0.4 g/L, the initial concentration of H_2O_2 is 5 mM, initial pH is 6.0). 106
- Figure 7-1: LNR degradation under different reaction conditions. (Notes: initial LNR concentration is 0.1 mM, TiO_2 112

loading is 0.6 g/L, the initial concentration of H₂O₂ is 10 mM, initial pH value is 6.0).

- Figure 7-2: Effect of radical scavengers on visible-light photocatalysis of LNR with the assistance of H₂O₂. (Notes: initial LNR concentration is 0.1 mM, TiO₂ loading is 0.6 g/L, the initial concentration of H₂O₂ is 10 mM, initial pH value is 6.0). 115
- Figure 7-3: LNR and H₂O₂ decomposition in various oxides suspension under visible light irradiation (Notes: initial LNR concentration is 0.1 mM, all oxides loading is 0.6 g/L, the initial concentration of H₂O₂ is 1 mM, initial pH value is 6.0). 116
- Figure 7-4: Visible-light-induced current (*I*_{ph}) generation on a TiO₂/ITO electrode in water with or without H₂O₂ (Notes: the concentration of H₂O₂ solution is 0.03 M). 117
- Figure 7-5: (a) The effect of wavelength of visible light on the LNR decay rate; (b) *I*_{ph} and the H₂O₂ consumption are compared as a function of the wavelength (Notes: initial LNR concentration is 0.1 mM, TiO₂ loading is 0.6 g/L, the initial concentration of H₂O₂ is 10 mM, initial pH value is 6.0). 119
- Figure 7-6: Comparison of the evolution profiles of intermediates between Vis/TiO₂/H₂O₂ and UV/TiO₂ system. (Notes: The initial concentration of LNR is 0.25 mM, the initial concentration of H₂O₂ is 10 mM, initial pH value is 6.0; 123

for UV/TiO₂ system, six 350 nm UV lamps were used).

- Figure 7-7: Degradation pathways of LNR for both Vis/TiO₂/H₂O₂ and UV/TiO₂ processes. 12
- Figure 7-8: (a) Process summary of Vis/TiO₂/H₂O₂ (where [Int] stands for the concentration of intermediates); (b) Process summary of UV/TiO₂ (where [Int] stands for the concentration of intermediates). 127
- Figure 7-9: The evolution of TOC, chloride, ammonium and nitrate ions during the Vis-induced photocatalytic reaction (The initial concentration of LNR is 0.25 mM, the initial concentration of H₂O₂ is 10 mM, initial pH value is 6.0). 128

LIST OF TABLES

Table 3-1:	List of chemicals used in this study.	35
Table 3-2:	Physical properties of LNR.	38
Table 4-1:	Summary of the principal reactions expected in UV/O ₃ aqueous system.	59
Table 4-2:	Summary of Rate Constant determination.	63
Table 4-3:	Comparison between the predicted k_{overall} from the proposed model and the observed k_{overall} .	64
Table 5-1:	Identified degradation products and their main fragments determined by LC/ESI-MS during LNR degradation by UV, Ozone and UV/O ₃ processes.	73
Table 7-1:	Identified degradation products and their main fragments determined by LC/ESI-MS during LNR degradation by UV/TiO ₂ and TiO ₂ /H ₂ O ₂ /Vis processes.	121

Chapter 1 Introduction

1.1 Background

Around one-fifth of the world's population has no access to safe water while two-fifths suffer the consequences of unacceptable sanitary conditions (United Nations Educational, 2003). More than one-third of the Earth's accessible renewable freshwater is used for agricultural, industrial, and domestic purposes, and the majority of these activities result in this precious water supply being polluted with numerous synthetic and geogenic compounds (Schwarzenbach et al., 2006). Therefore, it is not surprising that water-environment problems arising from chemical contamination have received increasing worldwide concerns in the past decade. Undoubtedly, micropollutants such as herbicides and pesticides coming from agricultural practice play an important role in water pollution. It has been reported that 140 million tons of fertilizers and several million tons of pesticides are applied every year (FAO, 2006). Unfortunately, less than 1% of total applied herbicides can reach their intended targets with the dominant majority being diffused into the aquatic environment via agricultural runoff or leaching (Pimentel, 1995). Herbicides have thus become some of the most frequently detected organic pollutants in natural waters.

Linuron (N-(3, 4-dichlorophenyl)-N'-methoxy-N'-methylurea) (LNR), one of the most commercialized phenylurea herbicides, has been widely used to control annual and perennial broadleaf and grassy weeds by inhibiting photosynthesis upon absorption in the roots of a wide range of crops such as soybean, cotton, potato, corn,

winter wheat, asparagus, carrot and various fruit. LNR is moderately persistent in soil with a half-life ranging from 38 to 67 days (Katsumata et al., 2005). LNR is frequently detected in surface and ground waters near or below the areas with intensive use. In one particularly extreme case, LNR was detected in a drinking-water well in concentration of up to 2.8 mg L⁻¹ (Caux et al., 1998). LNR and some of its naturally decayed intermediates (such as chloroaniline) have been suspected as a possible human carcinogen and endocrine disruptor (Lintelmann et al., 2003, Orton et al., 2009). LNR is also highly toxic to non-target aquatic organisms such as fish and shellfish. The LC50 for linuron in trout and bluegill is 16 mg/l, and 40 mg/l in crawfish (Wagner, 1983), which entails the design of effective, cost-efficient, environmentally friendly treatment techniques to eliminate LNR and its intermediates in aqueous phase.

As a result, LNR has succumbed to the increasing investigation of its treatability by various processes. It has been reported that physical treatments such as adsorption (Rodriguez-Cruz et al., 2008) and membrane filtration (Benitez et al., 2009) can successfully remove LNR from wastewater and water. However, the adsorption capacity of sorbent and retention capacity of membrane both decline due to interference with natural organic matter. In addition, membranes may also suffer fouling problem. For their successful application, both the adsorption and filtration processes thus entail regeneration strategy, which results in high operation cost of these two processes. Biological methods (Dejonghe et al., 2003; Sorensen et al., 2005) have also demonstrated fair performance in terms of decomposing LNR. The bacteria harboring the potential to mineralize LNR have been successfully isolated. However, biological degradation of LNR generally requires a long time and the operation of

biological process is quite delicate and involves intricate techniques since it is well-known that the activity of bacteria is extremely condition-dependent. These may rationalize the growing attention that AOPs have received in the past decade. AOPs are based on the *in situ* production of the highly-reactive hydroxyl radicals that can efficiently oxidize organic compounds to CO₂ and H₂O under mild experimental conditions. Due to the high reactivity of hydroxyl radicals (redox standard potential 2.8 eV *versus* NHE), their attack is non-selective, which is especially useful for the treatment of wastewater containing recalcitrant organic pollutants. It therefore comes as no surprise that LNR has also experienced varied AOPs such as photo-Fenton procedure (Benitez et al., 2007b; Farre et al., 2007), O₃/H₂O₂ (Benitez et al., 2007a; Chen et al., 2008), and photocatalysis (Lopez et al., 2005) under a wide range of experimental conditions. A major part of these studies, however, focuses on degradation kinetics of LNR. If the fate of the resulting products remains unanswered, the treatment process cannot be proposed as a trouble-free method since the decay of the parent compounds may result in the generation of more toxic organics than their parent compounds. Hence, the major objective of this study is to design new environmentally friendly treatment process for the degradation and mineralization of LNR.

1.2 Objectives of Study

In this study, the use of well-established treatment processes such as UV photolysis, ozonation and UV/O₃, as well as a newly-developed treatment technology---TiO₂/H₂O₂/vis (visible light) is studied to evaluate their potential to degrade and mineralize LNR, since detailed information is limited concerning the treatability of LNR by these methods, and the respective process design.

The primary aim of this study is to investigate the use of different treatment processes for removal of the herbicide before discharging to the public. The specific objectives of this study are as following:

- i) To examine the degradation kinetics of LNR by UV photolysis, ozonation, and UV/O₃;
- ii) To establish a treatment model for each process by the application of a quantum yield model for the UV process, a direct and indirect-radical oxidation model for the ozonation or UV/O₃ process;
- iii) To study the decay pathways of LNR by UV photolysis, ozonation, and UV combined with ozone;
- iv) To investigate the feasibility of degrading and mineralizing LNR by TiO₂/H₂O₂/Vis process;
- v) To explore the degradation mechanism of LNR in TiO₂ suspension under the irradiation of visible light with the assistance of H₂O₂ via monitoring the generation of photocurrent and comparing the products and decay pathways of LNR by UV/TiO₂ and TiO₂/H₂O₂/Vis processes;
- vi) To identify the parameters that affect the performance of these processes such as initial pH level, ozone dosage, light intensities, TiO₂ dosage, H₂O₂ dosage, and initial LNR concentration; and
- vii) To evaluate the efficiency of mineralization and dechlorination of each process.

1.3 Scope of Study

This thesis consists of eight chapters. The present chapter covers the background, objectives and organization of this thesis.

Literature review is presented in Chapter 2 where background information concerning LNR is described in detail and ozone-based treatment processes are given in-depth discussion. In particular, the theory of heterogeneous photocatalysis using TiO_2 as photocatalyst is discussed. Furthermore, a brief review of the efforts involved with shifting the optical response of TiO_2 from UV to visible spectral range is also presented in this chapter. Finally, the studies on the system of $\text{TiO}_2/\text{H}_2\text{O}_2/\text{Vis}$ are summarized.

Chapter 3 involves the detailed description of methodology.

A new approach to quantify the degradation kinetics of LNR by UV photolysis, ozonation, and UV/ O_3 processes will be presented in chapter 4 based on the investigation on the effect of varied parameters on the LNR decomposition.

In Chapter 5, the effects of pH values on the performance of UV photolysis, ozonation, and UV/ O_3 processes and varied anions on the performance of ozonation are investigated in terms of LNR decay rate. Furthermore, main intermediates of LNR decay by these three processes are identified by LC/MS, and decay pathways are proposed accordingly in this chapter.

Chapter 6 discusses the feasibility of LNR decomposition in semiconductor suspension under the irradiation of visible light with and without H_2O_2 . The

influences of varied parameters such as the type of TiO₂, initial pH level, H₂O₂ concentration, TiO₂ dosage, initial concentration of LNR on the performance of this process are given detailed description.

Chapter 7 presents in-depth investigation on the degradation mechanism of LNR by TiO₂/H₂O₂/Vis process through examining the effects of various radical scavengers and the performance of other metal oxides in place of TiO₂ in this system, monitoring the generation of photocurrent, and comparing the intermediates and decay pathways of LNR by UV-TiO₂ and TiO₂/H₂O₂/Vis processes.

In Chapter 8, conclusions are presented in company with the limitation of this work and the recommendations for future work.

Chapter 2 Literature Review

2.1 Wastewater Treatment Processes

2.1.1 UV photolysis

There is a long-standing interest in the use of photochemical reactions as a tool in the degradation of organic compounds such as herbicides (Crosby and Tang, 1969; Hayase and Takahashi, 1983; Funakoshi et al., 1988; Jirkovsky et al., 1997; Chan and Chu, 2005), dye or dye derivatives (Chu and Tsui, 2002; Rezaee et al., 2008; Ma et al., 2009), antibiotics (Edhlund et al., 2006), aromatic amino acid (Jin et al., 1995) and other organic pollutants (Lau et al., 2005; Chu and Jia, 2009). In order to obtain a deep insight into the photolysis mechanism of organic compounds, this review sets out with the basic principles of photochemical reaction. It was reported that Alexander the Great was one of the first exploiters of a photochemical process when he equipped his troops with a treated cloth ‘wristwatch’ which changed color under the influence of the sun. However, it is during the 20th century that a systematic understanding of photochemical processes has developed (Wayne, 1970).

(1) The Laws of photochemistry

All photochemical processes obey four photochemical laws which can be applied generally in photochemistry (Calvert and Pitts, 1966; Rabek, 1982):

- a. Only the light which is absorbed by a molecule can be effective in producing photochemical change in the molecule;

- b. The absorption of light by a molecule is a one-quantum process, so that the sum of the primary process quantum yields Φ must be unity;
- c. Each photon or quantum absorbed by a molecule has a certain probability of populating either the lowest excited singlet state (S_1) or the lowest triplet state (T_1); and
- d. The lowest excited singlet (S_1) and triplet (T_1) states are the starting levels (in solution) of most organic photochemical processes.

(2) The fates of electronic excitation

Photochemical processes involving the absorption of light can be divided into the act of absorption, which falls within the domain of spectroscopy, and the subsequent fate of the electronically excited species formed. In this study, the latter is the major concern.

Figure 2-1 illustrates, in simplified form, the various paths by which an electronically excited species may lose its energy (Wayne, 1988).

Energy transfer, corresponding to paths (iv) and (v) in the Figure 2-1, leads to excited species, which can then join any of the general processes.

Photochemical change can come about either as a result of dissociation of the absorbing molecule into reactive fragments (process i), or as a result of direct reaction of the electronically excited species (process ii); electronically excited species may also undergo spontaneous isomerization or rearrangement, as indicated by path (iii). A special case of dissociation is that of ionization, shown as path (viii).

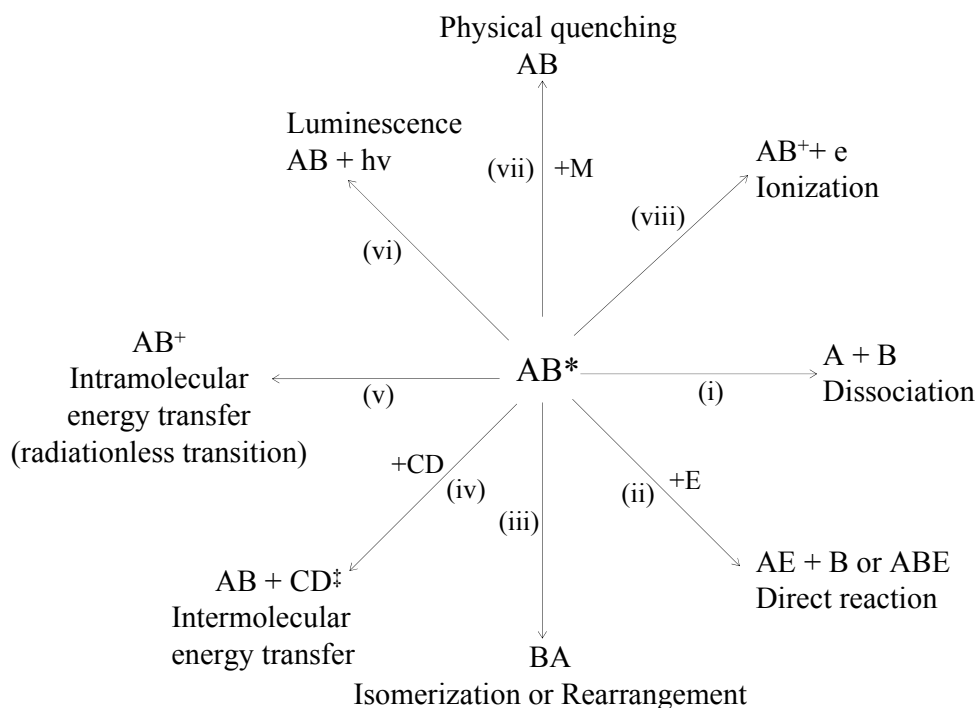


Figure 2-1: The possible routes to loss of photochemically excited molecule. The use of the symbols *, +, and ‡ is only intended to illustrate the presence of electronic excitation and not necessarily differences in states

Radiative loss of excitation energy (path vi) generates the phenomenon of luminescence: the terms *fluorescence* or *phosphorescence* are used to describe particular aspects of the general phenomenon.

Path (vii) demonstrated in Figure 2-1 is physical quenching. In this process an atom or molecule M can relieve AB^* of its excess energy. Physical quenching differs only formally from intermolecular energy transfer in that M, which must initially take up some excitation energy, does not make its increased energy felt in terms of its chemical behavior. The electronic excitation of AB^* is, in fact, frequently converted to translational or vibrational excitation of M.

(3) Photochemical reactions

Electronically excited molecules are highly energetic and have the potential for internal isomerization or rearrangement or reaction with other molecular species in the system. The general types of photochemical reaction are summarized as following (Wells, 1972):

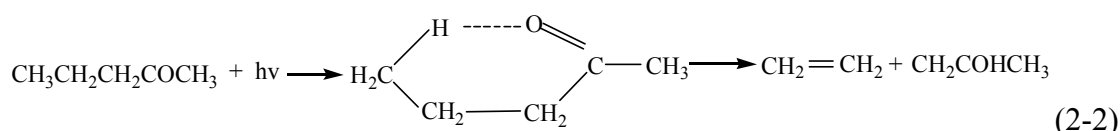
a. Photoreduction

The photoreduction occurs via the T_1 state of the photo-excited carbonyl compound in the great majority of cases. Molecules in this state react by abstracting hydrogen from a substrate species RH to give a hydroxymethyl radical and a radical R^\bullet :



The final reaction products are formed by self-combination and cross-combination reactions of the radicals produced in the hydrogen abstraction step. The efficiency of the hydrogen abstraction step is dependent upon factors such as the nature of the T_1 state of the carbonyl compound, the structure of the carbonyl compound, the dissociation energy of the R–H bond and the type of solvent used.

The hydrogen abstraction described above is an intermolecular process. Hydrogen abstraction is also one of the most important intramolecular reactions of excited species. The intramolecular abstraction of H is of particular importance in the photochemistry of most carbonyl compounds, since it is part of the sequence of events leading to the ‘Norrish Type II’ fragmentation. Equation 2-2 shows a six-membered transition state in the Type II fission of a ketone: this cyclic intermediate favors intramolecular H-abstraction over intermolecular abstraction from the solvent.



b. Photodimerization

Photodimerization involves the combination of an electronically excited molecule with a same ground state molecule to give a 1:1 photo-adduct. It has been reported that the dimerization pathway is the principal reaction during the photolysis process of butylated hydroxyanisole (BHA) at 254 nm, leading to the high yield of intermediate di-BHA (Lau et al., 2007).

c. Photo-addition

Photo-addition may be defined as the combination of an electronically excited molecule with a different ground state molecule to give a 1:1 photo-adduct.

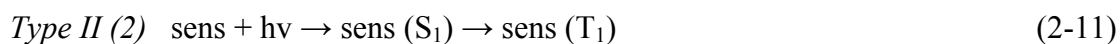
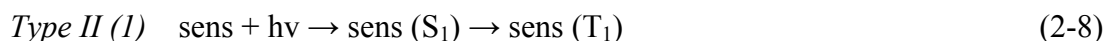
d. Photo-oxidation

Irradiation of organic compounds in the presence of a sensitizer and oxygen can lead to the involvement of oxygen in the photoreaction and the formation of oxygenated products. The presence of a sensitizer is believed to be necessary to the reaction and normally the photosensitized oxidations proceed via the T_1 state of the sensitizer. The sensitizer acts in one of the two ways --- either by abstracting hydrogen from the substrate to form radicals which subsequently react with the oxygen (Type I process) or by activating the oxygen so that a direct reaction can happen between oxygen and the substrate (Type II process).

The generalized mechanism for the Type I process is as follows:



In Type II photo-oxidations the reaction between oxygen and the organic substrate may occur either when (1) the oxygen is complexed with the sensitizer or when (2) the oxygen is in the S_1 state formed by energy transfer from the sensitizer. The two possible mechanisms for the Type II photo-oxidation are given below:



However, it has been reported photo-oxidation of organic compounds can also proceed in the absence of any sensitizer under the UV irradiation of 254 nm (Jin et al., 1995). In their study, the tyrosine triplet state ($^3\text{TYROH}$) is quenched by O_2 , leading to the generation of $^1\text{O}_2$ which reacts with TYROH by H abstraction. The

resulting intermediates TYRO^{\bullet} and HO_2^{\bullet} are believed to be the precursors of photo-oxidation products. In addition, another mechanism involving the generation of intermediate ‘endoperoxide’ has also been proposed in their study.

e. Photoisomerization and photorearrangement

Electronically excited molecules have considerable excess energy over ground state molecules and so it comes as no surprise that changes in the bonding system and of the positions of atoms in the molecular framework can happen in these energy rich species. Such rearrangement can give rise to ground state products which are isomeric with the original reactant. The reactant and products can be either *structural* isomers where groups or atoms in the isomers are located entirely differently or *valence-bond* isomers where the bonding system in the isomers differs.

(4) Quantum yields

To quantify the photodegradation of organic compounds, the decay rate and the quantum yield of their photodecomposition should be acquired. A pseudo first-order decay is expected at constant temperature, light intensity, and illumination wavelength (Chu and Tsui, 1999). The quantum yield for pollutant decay using a monochromatic light source, therefore, can be calculated from experimental first order decay rate as described by Choudhry and Webster (Choudhry and Webster, 1987):

$$\phi = \frac{k}{2.303 I_{\lambda,0} \epsilon_{p,\lambda} l} \quad (2-14)$$

where ϕ = quantum yield for the disappearance of LNR

$I_{\lambda,0}$ = intensity of the incident light at wavelength λ , Einstein $\text{L}^{-1}\text{s}^{-1}$

$\varepsilon_{p,\lambda}$ = molar absorptivity of LNR at wavelength λ , $\text{M}^{-1}\text{cm}^{-1}$

l = cell path length within the reactor, cm

k = the first order decay rate constant, s^{-1}

2.1.2 Ozone-based Advanced Oxidation Processes

Ozone has been widely applied in the treatment of municipal and industrial wastewaters and the disinfection of drinking water due to its high oxidation potential (2.08eV) (Chu and Ma, 2000; Graham et al., 2003; Hoigne and Bader, 1983). However, ozonation process is highly selective since high electrophilicity and selectivity of the reaction between O₃ and organic compound lead to organics with electron-donating substituent group (e.g. OH and CH₃) showing higher reactivity toward ozone and organics with electron-withdrawing substituents (e.g. Cl and NO₂) having lower ozone reactivity (Adewuyi, 2005). The coupling of ozonation with other processes such as ultrasound, UV, electrocoagulation and photocatalysis or chemical oxidation utilizing H₂O₂ or ferrous ion presents interesting and attractive approaches which can produce nonselective strong oxidants---hydroxyl radicals. Therefore, many recent efforts have been devoted to improving the efficiency of ozonation by exploiting the advantages of combinative or hybrid processes involving the simultaneous or sequential use of ozonation and other AOPs.

(1) US/O₃

Chemical effects of ultrasound are believed to be due to the phenomenon of acoustic cavitation, which involves the formation and subsequent collapse of microbubbles from acoustical wave-induced compression/rarefaction (Weavers and Hoffmann, 1998). In a collapsing cavitation bubble, the thermolytic decomposition of ozone and subsequent hydroxyl radicals formation occurs as follows:





These decomposition reactions occur in the gas phase. The reaction products migrate to the interfacial sheath of the bubble where they subsequently react in the aqueous phase. As we can see from eq. 2-15. and eq. 2-16., the combination of O₃ and ultrasound may be more effective since two HO[•] are formed per O₃ molecule consumed.

Weavers and Hoffmann (Weavers and Hoffmann, 1998) conducted cyclohexene degradation experiments using sonication (in the presence of O₂), ozonation, and sonolytic ozonation to determine the effect that ultrasound had on an O₃ gas bubble diffusing into a solution. The degradation experiments indicated that rates were the fastest when sonication was combined with ozonation, followed by sonication with O₂, and then ozonation alone in that order. Lall et al. investigated the decolorization of the dye Reactive Blue 19 by ozonation, ultrasound, and ultrasound-enhanced ozonation using a semibatch reactor. At dye concentration of 0.1 g/L and O₃ concentration of 9.4 mg/L with the presence of ultrasonic irradiations (20 kHz) at powers of 40, 80, and 120 W/L, rate constant increases 35.7, 75, and 139.9% for the respective ultrasonic powers as compared with ozone alone. They also studied the effect of ultrasonic power input on the overall mass transfer coefficient of ozone in solution. Using 5.4 mg/L O₃ and 0.03 g/L dye concentration at the maximum ultrasonic power input of 120 W/L, the ratio of mass transfer coefficient with ultrasound ($k_{L,a}^*$) to that without ultrasound ($k_{L,a}$) increased by 90%. The increase in overall rate was attributed to the combined effects of an increase in mass transfer and intrinsic kinetics resulting from cavitation (Lall et al., 2003). He et al. found the pseudo-first-order degradation rate constants of TOC reduction were 9.0×10^{-4} ,

7.3×10^{-3} and $1.8 \times 10^{-2} \text{ min}^{-1}$ for US, O₃ and a combination of US and O₃, respectively (He et al., 2007b).

(2) UV/O₃

The combined UV/O₃ system has been widely studied (Winarno and Getoff, 2002; Lau et al., 2007; Gong et al., 2008; Kim et al., 2008), and its overall oxidation reaction has been shown to be due to a synergistic effect of several individual reactions, such as direct (molecular) ozonation, direct photolysis, and indirect radical oxidation. Peyton and Glaze confirmed the formation of hydrogen peroxide as the first reaction intermediate of ozone photolysis. It was also proposed that the secondary reactions lead to the production of hydroxyl radical (HO•), the major oxidant in the UV/O₃ process (Peyton and Glaze, 1988). Hydroxyl radical (HO•) may then react with ozone to produce other radicals such as singlet oxygen and peroxy radicals, which is also believed to be involved in the overall oxidation reaction (Winarno and Getoff, 2002).

Lau et al. investigated the degradation of butylated hydroxyanisole (BHA) in UV, ozonation, and UV/O₃ processes. Their experimental results indicated that the degradation of BHA increases in order: UV photolysis, ozone, and UV/O₃. The TOC removal was insignificant in both the UV photolysis and ozonation processes, while 90% mineralization was achieved by using the UV/O₃ process after 180 min (Lau et al., 2007). Song et al. observed the total mineralization of CI Reactive Yellow 145 after 150 min in the UV, O₃, and UV/O₃ schemes was 4%, 63%, and 80%, respectively (Song et al., 2008).

(3) Catalytic Ozonation

Catalytic ozonation can be considered firstly as homogeneous catalytic ozonation, which is based on ozone activation by metal ions present in aqueous solution, and secondly as heterogeneous catalytic ozonation in the presence of metal oxides, metals/metal oxides on supports or other solid particles. Catalytic ozonation has been found to be effective for the removal of several organic compounds from drinking water and wastewater (Canton et al., 2003; Giraldez et al., 2007; Kastner et al., 2008; Zhang and Ma, 2008).

Homogeneous catalytic ozonation

Generally, two main processes can be considered when attempting to hypothesize the mechanism of homogeneous catalytic ozonation: ozone decomposition by means of active metal species, followed by the generation of free radicals, and complexes formation between the catalyst and organics followed by a final oxidation reaction.

The catalysts proposed for the process of homogeneous catalytic ozonation are transition metals such as Fe(II), Mn(II), Ni(II), Co(II), Cd(II), Cu(II), Ag(I), Cr(III), Zn(II). The nature of transition metal applied determines not only the reaction rate but also selectivity and ozone consumption (Kasprzyk-Hordern et al., 2003).

Legube and Leitner observed that, during the ozonation of wastewaters, Fe (II), Mn (II), Ni (II) and Co (II) sulphate induce an increase of total organic carbon (TOC) removal when compared with ozonation alone (Legube and Leitner, 1999). Trace amounts of cobalt (II) (2×10^{-6} M) were also found to be capable of accelerating the decay rate of organic compounds such as oxalic acid, which does not readily react with molecular ozone ($k_{O_3} = 0.04 \text{ M}^{-1} \text{ s}^{-1}$) (Pines and Reckhow, 2002). In their study, the degradation mechanism of oxalic acid was proposed in Co (II)/ozone

system: the first step in the catalytic ozonation reaction pathway is the formation of a cobalt (II) oxalate complex. Cobalt (II) oxalate is then oxidized by ozone to form cobalt (III) oxalate. The catalytic cycle is completed with decomposition of the cobalt (III) complex to form cobalt (II) and an oxalate radical. Xiao et al. have examined the effect of Mn^{2+} on the mineralization of 2, 4- dichlorophenol (DCP) by ozone. The results of their study show that trace amount of Mn^{2+} accelerates the mineralization of DCP. It was also observed that Mn^{2+} could induce the generation of more hydroxyl radicals via initiating the decomposition of ozone in catalytic ozonation system than those in sole-ozone system (Xiao et al., 2008).

Heterogeneous catalytic ozonation

The degradation mechanism of organic compounds by heterogeneous catalytic ozonation has not been well-understood till now. In the work of Beltrán et al., the decay mechanism of oxalic acid in TiO_2/O_3 system was proposed as following (Beltran et al., 2002):



Where S represents the free active centers on the surface of catalyst and B denotes oxalic acid. Based on this mechanism, it is believed that the adsorption of both ozone and oxalic acid on the surface of catalyst is critical to guarantee the catalytic effect.

Some authors, however, believe that an interaction between ozone and hydroxyl groups on the surface of catalysts leads to the generation of hydroxyl radicals (Ernst et al., 2004; Zhao et al., 2009). Zhao et al. examined the enhancement mechanism of heterogeneous catalytic ozonation by cordierite-supported copper for the degradation of nitrobenzene in aqueous solution. In their work, the production of hydroxyl radicals was confirmed by means of the spin trapping/EPR technique and a good correlation between density of surface hydroxyl groups and relative intensity of DMPO-OH adduct signal at the different loading percentage of Cu was found, indicating the formation of hydroxyl radicals is subjective to the density of the surface hydroxyl groups. In addition, Ernst et al. reported that the adsorption of organics on the catalyst's surface would not be necessary to provide the catalytic effect, and DOC (dissolved organic compounds) adsorption would probably inhibit the effect due to an overlaying of hydroxyl groups.

In some papers, the involvement of hydroxyl radicals into the heterogeneous catalytic ozonation is disagreed because the performance of ozonation is not influenced by the presence of radical scavengers like bicarbonates (Kaptijn, 1997; Logemann and Annee, 1997).

Other authors consider it possible that the improvement of direct ozonation results in the enhancement of heterogeneous catalytic ozonation. The pre-coating of γ -alumina by perfluorooctanoic acid stabilizes ozone, thus boosting its oxidation efficiency towards organic compounds in aqueous solution (Kasprzyk and Nawrocki, 2002).

In summary, there are generally three possible mechanisms of catalytic ozonation in heterogeneous systems (Kasprzyk-Hordern et al., 2003):

- chemisorption of ozone on the catalyst surface leading to the formation of active species which react with non-chemisorbed organic molecule;
- chemisorption of organic molecule (associative or dissociative) on the catalytic surface and its further reaction with gaseous or aqueous ozone; and
- chemisorption of both ozone and organic molecules and the subsequent interaction between chemisorbed species.

The main catalysts proposed for the process of heterogeneous catalytic ozonation are metal oxides (MnO_2 , TiO_2 , Al_2O_3), metals or metal oxides on metal oxide supports (e.g. $\text{Cu-Al}_2\text{O}_3$, Cu-TiO_2 , Ru-CeO_2 , V-O/TiO_2 , V-O/silica gel and $\text{TiO}_2/\text{Al}_2\text{O}_3$, $\text{Fe}_2\text{O}_3/\text{Al}_2\text{O}_3$) and activated carbon (Faria et al., 2008; Faria et al., 2009; Li et al., 2009) as well as some other material such as wood fly ash (Kastner et al., 2008), ceramic honeycomb (Zhao et al., 2008) and cordierite-supported copper (Zhao et al., 2009).

The efficiency of the catalytic ozonation process depends to a great extent on the catalyst and its surface properties as well as the pH of the solution that influences the properties of the surface active sites and ozone decomposition reactions in aqueous solutions.

The O_3/TiO_2 system was found to be efficient for oxalic acid degradation in water at acidic pH (Beltran et al., 2002). In the absence of catalyst, oxidation of oxalic acid was negligible at 20°C while around 70% removal of oxalic acid was achieved after 3 hr of reaction in the presence of TiO_2 . Alumina was also shown to be an effective catalyst for the ozonation of 2-chlorophenol. The highest efficiency (more than twice

as high) of catalytic ozonation when compared to ozonation alone was observed at neutral pH. At an acidic pH value, the usage of the $\text{Al}_2\text{O}_3/\text{O}_3$ system resulted in an increase of 83.7% of TOC degradation when compared to ozonation alone. Only a 17% increase of the efficiency of catalytic ozonation was obtained at a basic pH value, mainly because, under an alkaline environment, oxidation with hydroxyl radical from ozone decomposition initiated by OH^- is already strong (Ni and Chen, 2001). It was also reported that the catalytic ozonation with goethite (FeOOH) can substantially enhance nitrobenzene degradation compared with ozonation alone (Zhang and Ma, 2008).

Activated carbon is believed to act not only as the absorbent but also as a catalyst in promoting ozone oxidation. It was evidenced that the presence of activated carbon during ozonation increased the degradation rate of both oxamic and oxalic acid leading to mineralization (Faria et al., 2008). Giráldez et al. reported that AC (activated carbon) ozonation process significantly improved both polyphenol conversion and mineralization (Giraldez et al., 2007).

Photocatalytic ozonation

The photocatalytic oxidation, one of AOPs methods, has been widely investigated (Sanchez et al., 1998; Wang et al., 2002; Farre et al., 2005; Gimeno et al., 2007; Beltran et al., 2009). The process is based on the production of electron-hole pairs by semiconductor illuminated by light of suitable energy in an aqueous medium, which subsequently react with adsorbed species of suitable redox potential. In the presence of air, adsorbed molecular oxygen accepts photogenerated electrons, while water molecules can react with photogenerated holes to produce hydroxyl radicals (Sanchez et al., 1998; de Moraes et al., 2000):



Oxygen is usually introduced into the system as an oxidizing agent. The disadvantage of oxygen is the slow electron transfer from TiO_2 to oxygen. Ozone with its unique properties is a potential oxidant for the photocatalytic oxidation process (Gilbert, 2002).

In photocatalytic ozonation process, both direct and indirect reactions of ozone occur. With the presence of TiO_2 under illumination, ozone can generate HO^\bullet radicals through the formation of an ozonide radical ($\text{O}_3^{\bullet-}$) in the adsorption layer (Tanaka et al., 1996; Sanchez et al., 1998; Klare et al., 1999):



The generated $\text{O}_3^{\bullet-}$ species rapidly reacts with H^+ in the solution to give HO_3^\bullet and subsequently HO^\bullet (Sanchez et al., 1998; Klare et al., 1999):



The photocatalytic process in the presence of oxygen requires a total of three electrons for the generation of a single HO^\bullet species, which is a less favorable situation if compared with the one electron needed through the $\text{O}_3^{\bullet-}$ reaction pathway.

That is the reason why the presence of ozone is more effective in terms of the production of HO•.

Generally, the presence of dissolved ozone in the irradiated TiO₂ suspension significantly increases the OH radical production by means of two processes---inhibiting the recombination of electrons and holes and self-decomposition initiated by photogenerated electrons on the surface of TiO₂.

(4) Ozone-based other AOPs

Ozone combined with other oxidizing agents such as H₂O₂ has been proved effective treatment for the elimination of persistent and recalcitrant organic compounds (Chen et al., 2006; Al Momani et al., 2008). Al Momani et al. investigated the degradation of cyanobacteria toxin by ozone alone and O₃/H₂O₂ processes. It was found that at a fixed initial ozone concentration of 0.1 mg/L and different initial H₂O₂ concentrations, MC-LR degradation was enhanced from 65 to 95% as H₂O₂ initial concentrations increased from 0.001 to 0.005 mg/L. Complete MC-LR degradation was achieved in 80s with an initial H₂O₂ concentration of 0.01 mg/L (Al Momani et al., 2008). Kim et al. examined the degradability of 30 pharmaceuticals in water with O₃/H₂O₂ process. They observed k_{O_3/H_2O_2} values were 1.64 to 2.18 times higher than k_{O_3} values, and 1.37 to 1.77 times higher than $k_{O_3/UV}$ values for acetaminophen, ifenprodil and theophylline (Kim et al., 2008).

Furthermore, coupling ozonation and electrocoagulation (He et al., 2007a) or electrolysis (Kishimoto et al., 2005; Kishimoto et al., 2007; Kishimoto et al., 2008) has received growing attention recently. Ozonation combined with electrolysis

(ozone–electrolysis) is a new AOP. The advanced oxidation mechanism for ozone–electrolysis was estimated to be as follows (Kishimoto et al., 2008):



It was reported by Kishimoto et al. that the ozone consumption linearly increases with the electrolytic current in the hybrid system. They also observed that the rate constant k was directly proportional to the electrolytic current, which indicated hydroxyl radicals concentration is proportional to the electrolytic current (Kishimoto et al., 2008).

He et al. also observed synergistic effect achieved by coupling electrocoagulation with ozone for the decolorization of RY 84 and decolorization rate increased with the increase of current density (He et al., 2007a).

2.1.3 Photocatalysis

TiO₂ has received considerable attention as a photocatalyst since Fujishima and Honda discovered the photocatalytic splitting of water on TiO₂ electrode (Fujishima and Honda, 1972). In recent years, applications of TiO₂ to the cleanup of groundwater and wastewater have been one of the most active research areas in heterogeneous photocatalysis, which is inspired by the potential of TiO₂-based photocatalysis to destroy a wide range of organic compounds.

(1) Theory of TiO₂-based photocatalysis

TiO₂ can exist in one of three bulk crystalline forms: rutile, anatase, and brookite. Only rutile and anatase are stable enough and can be used as photocatalyst, with anatase showing a higher photocatalytic activity. The initial process for the photocatalytic degradation of organic and inorganic compounds in semiconductor heterogeneous system is the generation of electron-hole pairs. In general, a photon with energy equal to or higher than the bandgap energy of semiconductor can initiate the excitation of electron, e_{cb}^- from the valence band (VB) to the conduction band (CB), leaving a hole, h_{vb}^+ behind (Hoffmann et al., 1995b). Excited-state conduction-band electrons and the valence-band holes may suffer varied de-excitation pathways as shown in Figure 2-2.

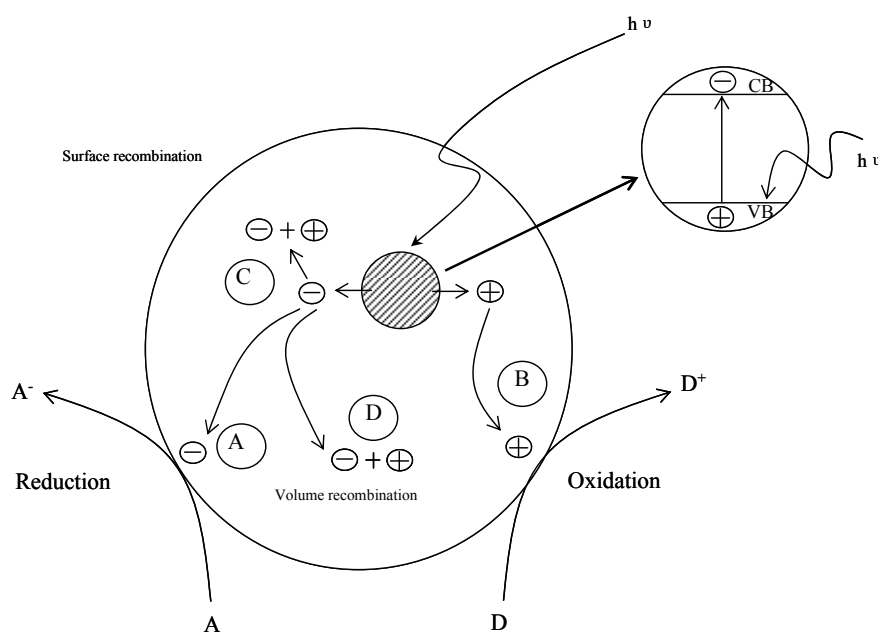


Figure 2-2: Schematic photoexcitation in a solid semiconductor followed by de-excitation events (Linsebigler et al., 1995)

The photoinduced electron transfer to adsorbed organic or inorganic species or the solvent stems from the migration of electrons and holes to the semiconductor surface. With the species adsorbed on the surface, the semiconductor can donate electrons to

reduce an electron acceptor (pathway C); in turn, a hole can migrate to the surface where an electron from a donor species can combine with the surface hole oxidizing the donor species (pathway D). The probability and rate of the charge transfer processes for electrons and holes depends on the respective positions of the band edges for the conduction and valence bands and the redox potential levels of the absorbate species (Linsebigler et al., 1995).

In competition with charge transfer to adsorbed species is electron and hole recombination. Recombination of the separated electron and hole can occur in the volume of the semiconductor particle (pathway B) or on the surface (pathway A) with the release of heat.

(2) Modification of TiO₂

Among all semiconductors, Titanium dioxide (TiO₂) is believed to be one of the most appropriate photocatalysts in terms of environmental application owing to its particularly optical properties, innocuity, low cost and enduring stability regarding photo- and chemical corrosion (Augugliaro et al., 1995; Hoffmann et al., 1995b). The widespread use of TiO₂ as an effective photocatalyst in practical application, however, has been curbed by its optical property that TiO₂ is only sensitive to UV light due to its large band gap ($E_g = 3.2$ eV and 3.0 eV for anatase and rutile phases, respectively). The sun can furnish an abundance of photons; however, UV light only accounts for a small portion (~ 5%) of the sun spectrum in comparison to the visible region (~ 45%). Driven by the need to utilize solar energy more efficiently, therefore, significant efforts have been dedicated to improve the utility of TiO₂ by shifting its optical response from the UV to the visible spectral range:

a. Combining TiO₂ with another semiconductor oxide

TiO₂ coupled with other semiconductor oxides such as CdS (Bessekhouad et al., 2006; Srinivasan et al., 2006), Cu₂O (Bessekhouad et al., 2005; Han et al., 2009), Fe₂O₃ (Pal et al., 1999; Liu and Gao, 2006), WO₃ (Chai et al., 2006; Lin et al., 2008) and Bi₂O₃ (Bian et al., 2008) has demonstrated photocatalytic activity under the irradiation of visible light. It is believed that the electrons on the valence band of a smaller band gap semiconductor such as CdS (2.4-2.6 eV), Cu₂O (2.0 eV), Fe₂O₃ (2.2 eV) and Bi₂O₃ (2.8 eV) excited by visible light to the conduction band can be transferred to the conduction band of a larger band gap semiconductor (TiO₂). This not only helps for charge separation by isolating electrons and holes in two distinct particles but at the same time, allows the extension of photoresponse of the composite photocatalyst to visible light range. The interparticle electron transfer theory was proposed by Serpone et al. for the first time (Serpone et al., 1995). Their work provides chemical evidence for electron and hole transfer between CdS and TiO₂.

b. Transition Metal Doping

The influence of transition metal dopants on the photocatalytic properties of TiO₂ has become another interesting area of semiconductor modification. Doping with transition metal ions such as Fe (Piera et al., 2003), Cr (Fan et al., 2008), V (Klosek and Raftery, 2001), Zr (Huang et al., 2006) and Co (Dvoranov et al., 2002), however, has shown both positive and negative effects on the photocatalytic activity of TiO₂; a number of authors claim that although metal ion doping could narrow the band gap of TiO₂, the metal ion may also serve as a

recombination center for electrons and holes, thus diminishing the overall activity of the photocatalyst (Thompson and Yates, 2006) .

c. Non-metal Doping

Asahi et al. (2001) reported doping TiO₂ with nitrogen allowed it being sensitive to the irradiation of visible light (less than 500 nm) (Asahi et al., 2001), which initiates extensive research interest in doping TiO₂ with anionic species (Yu et al., 2003; Tachikawa et al., 2004; Zaleska et al., 2008). It has been proposed that band gap narrowing may result from the mixing of the p states of the dopants with O 2p states forming the valence band of TiO₂ in the work of Asahi et al. A similar conclusion has also been reached by Lin et al. for the spectral changes observed for P-doped TiO₂ (Lin et al., 2005).

d. Surface Sensitization

Surface sensitization of TiO₂ via chemisorbed or physisorbed dyes also offers a way to extend the optical response of TiO₂ to the visible light range. The operating mechanism is the electrons from photoexcited dye molecules being injected into the conduction band of the semiconductor substrates, where the electrons can react with the electron acceptor such as oxygen or hydrogen peroxide to generate varied radicals or radical anions. Some common dyes used as sensitizers include phthalocyanine (Cao et al., 2003), thionine (Patrick and Kamat, 1992), and Ru(bpy)₃²⁺ (Khan et al., 1987; Zang and Rodgers, 2000). Such dye sensitizers, however, are not sufficiently stable in the aquatic environment and need to be prepared only in the acidic pH range. Therefore,

challenges still confront the researchers to find a way to apply dye-sensitized TiO₂ in environmental cleanup.

Whereas coupling, doping and photosensitization have demonstrated successful performance in either narrowing the band gap of TiO₂ or sensitizing photocatalytic properties of TiO₂ towards visible light irradiation, the preparation process of photocatalyst is time-consuming, technique-demanding and expensive and their photocatalytic activity under visible light irradiation is not high enough for the practical applications. Therefore, it still remains a big challenge to develop a cost-efficient and less technique-demanding TiO₂-based photocatalysis process which can work under the irradiation of visible light in the field of water treatment.

(3) H₂O₂-assisted Photocatalysis under Visible Light

It has also been reported that TiO₂ nanoparticles can work under the irradiation of visible light with the addition of H₂O₂ (Ohno et al., 2001; Li et al., 2001; Ogino et al., 2008). There are valence-unfilled Ti (IV) ion centers and O (II) centers which form basic $\equiv \text{TiOH}$ and acidic $\equiv \text{OH}$ on the surface of TiO₂ particle in aqueous solution, respectively (Regazzoni et al., 1998). In the presence of H₂O₂, the –OOH groups of H₂O₂ substitute the –OH groups of the basic $\equiv \text{TiOH}$ generating yellow surface complexes--Titanium peroxide. Fourier transform infrared spectroscopy and X-ray photoelectron spectroscopy of H₂O₂-treated TiO₂ suggested the formation of the surface complexes and the diffuse reflectance absorption spectra of H₂O₂-treated TiO₂ demonstrated marked red shift to the visible region (up to 550 nm) (Boonstra

and Mutsaers, 1975; Ohno et al., 2001). It was proposed that the epoxidation reaction of 1-decene could be initiated by a photochemical reaction of Ti- η^2 -peroxide with 1-decene (Ohno et al., 2001). On the other hand, the formation of active hydroxyl radicals was proven in TiO₂/H₂O₂ suspension under visible light irradiation in the work of Li et al (Li et al., 2001). A possible mechanism of the generation of hydroxyl radicals in this system was proposed. Titanium peroxide complex formed on the TiO₂ surface could extend the photoresponse to the visible region and can be excited by visible light. The excited surface complex injects an electron to the conduction band of TiO₂ where the electrons on the conduction band of TiO₂, then, initiate the decomposition of H₂O₂ to produce hydroxyl radicals. In addition, it was also reported that the water-oxide interface can lower the energy barrier for the H₂O₂ decomposition (the presence of oxides leads to the activation energy of the cleavage of the O – O bond in H₂O₂ being decreased from 210 kJ/mol to 40 kJ/mol) (Hiroki and LaVerne, 2005). As a result, hydroxyl radicals might be produced by the breakdown of H₂O₂ on the surface of TiO₂ under the irradiation of visible light (H₂O₂ + TiO₂ + vis → 2HO•) since the approximate energies of the visible radiation (from 400 nm to 700 nm) range from 293 kJ/mol to 167 kJ/mol (Wayne, 1970).

Although the interaction between H₂O₂ and TiO₂ is well-documented, the operating mechanism of TiO₂/H₂O₂ system under visible light irradiation is not well-understood.

2.2 Description of Linuron

2.2.1 Background

Linuron (LNR) is a substituted urea herbicide used to control annual and perennial broadleaf and grassy weeds on crop and non-crop sites. It is used as a pre and a postemergent herbicide. It works by inhibiting photosynthesis in target weed plants. It is labeled for use in soybean, cotton, potato, corn, bean, pea, winter wheat, asparagus, carrot, and fruit crops. It is also used on crops stored in warehouses and storerooms.

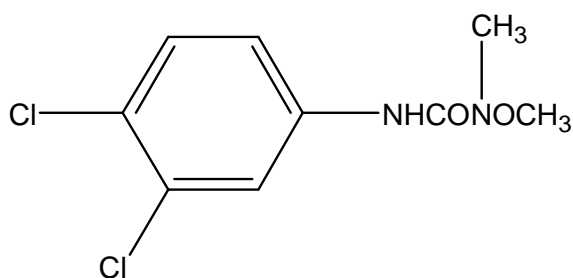


Figure 2-3: Chemical Structure of LNR

LNR is a Restricted Use Pesticide (RUP). Restricted Use Pesticides may be purchased and used only by certified applicators.

2.2.2 Toxicological Effects

LNR is classified by the EPA as a possible human carcinogen (EPA, 1984). LNR has been reported to be a weak competitive androgen receptor antagonist in vitro, inducing a positive response in the immature and adult rat Hershberger assay and suppresses androgen-dependent gene expression (Lambright et al., 2000; McIntyre et

al., 2000); it has been reported to inhibit the activity of 5 α -reductase which is one of the key enzymes of human androgen metabolism (Lo et al., 2007); Wilson et al. have observed that LNR reduces testosterone production from the fetal rat testis (Wilson et al., 2009); Orton et al. have found out the yeast exposed to LNR at a low concentration suffers a reduction of antiestrogenic and antiandrogenic activity, inhibition of ovulation in vitro and the decrease of testosterone production (Orton et al., 2009). Furthermore, some of its naturally decayed intermediates (such as chloroaniline) have also been suspected as endocrine disruptors (Lintelmann et al., 2003). LNR is highly toxic to non-target aquatic organisms such as fish and shellfish. The LC50 for LNR in trout and bluegill is 16 mg/l, and 40 mg/l in crawfish. It is moderately toxic to wild birds. Its LC50 in mallard ducks is 3,000 mg/kg, 3,500 mg/kg in pheasants, and 5,000 mg/kg in quail (EPA, 1984).

2.2.3 Environmental Fate

LNR is moderately persistent in soils. The rates of dissipation in agricultural soils determined by laboratory and field experiments are highly variable, with values ranging from days to several years (Fryer and Kirkland, 1970; Smith and Emmond, 1975; Kempsonjones and Hance, 1979; Caux et al., 1998). This compound is bound to soil (especially clay) and organic matter and does not move freely. The movement of the compound decreases as the organic content of the soil increases (Sorensen et al., 2005).

LNR is slightly to moderately soluble in water, and is not readily broken down in water. It is frequently detected in surface and ground waters near or below areas with

intensive use, and in one extreme case, LNR was detected in a drinking-water well in concentration up to 2,800 $\mu\text{g/L}$ (Caux et al., 1998).

2.2.4 Previous degradation studies of LNR

The toxicological effects and persistence of LNR in the environment promotes the need of developing effective treatment techniques to eliminate and mineralize this contaminant. There have been a few number of previous studies referred to the general degradation of LNR, such as biological methods (Dejonghe et al., 2003; Sorensen et al., 2005), $\text{O}_3/\text{H}_2\text{O}_2$ (Tahmassebi et al., 2002; Chen et al., 2008), direct photolysis (Faure and Boule, 1997), photo-Fenton procedure (Katsumata et al., 2005), ultrafiltration and nanofiltration process (Benitez et al., 2009) and UV/ TiO_2 (Lopez et al., 2005). However, there has been no information available concerning the degradation of LNR by using UV/ O_3 process and $\text{TiO}_2/\text{H}_2\text{O}_2/\text{Vis}$ (visible light) based on a review of the scientific literature. A detailed examination on the degradation of LNR by these two processes is, thus, important and of my major interest.

Chapter 3 Materials and Methodology

3.1 Introduction

This chapter describes the methodology of experimental setup for the water treatment processes (i.e. UV/O₃, UV/TiO₂ and TiO₂/H₂O₂/Vis) employed in this study. The sampling and analytic methods of target compounds can be found in this chapter, and also how the generated intermediates are determined qualitatively and quantitatively is explicated in detail. The characterization of photocatalysts by X-ray diffraction (XRD), UV–Visible spectrophotometer and the generation of photocurrent are also depicted in this chapter.

3.2 Materials

All the chemicals used in this study were tabulated in Table 3-1. All the chemicals were used without further purification. The water used in the preparation of all the solutions was 18 MΩ deionized distilled water obtained from a Barnstead NANO pure water purification system. Linuron (LNR) has been chosen as the target pollutant. Selected physical properties of LNR were listed in Table 3-2.

Table 3-1: List of chemicals used in this study

Chemicals	Molecular weight, g mol ⁻¹	Formula	Purchased from
<u>Target Compounds</u>			
Linuron (99.0%)	249	C ₉ H ₁₀ Cl ₂ N ₂ O ₂	SUPELCO

Cont'd

Semiconductors or Metaloxides

Titanium dioxide (P25)	79.87	TiO ₂	Degussa
Titanium dioxide (Anatase)	79.87	TiO ₂	Shanghai
Titanium dioxide (Rutile)	79.87	TiO ₂	Shanghai
Zinc oxide	81.38	ZnO	Aldrich
Tungsten (VI) oxide	231.85	WO ₃	Aldrich
Aluminium Oxide (99.9%)	101.96	Al ₂ O ₃	Alfa Aesar
Silicon Dioxide	60.08	SiO ₂	Alfa Aesar

Oxidants

Hydrogen Peroxide (35%)	34.00	H ₂ O ₂	Riedel-deHaën
-------------------------	-------	-------------------------------	---------------

Intermediates

1-(3,4-dichlorophenyl)-3- methylurea (98%)	218	C ₈ H ₈ Cl ₂ N ₂ O	Aldrich
1-(3,4- dichlorophenyl)urea	203	C ₇ H ₆ Cl ₂ N ₂ O	Aldrich

Solvents

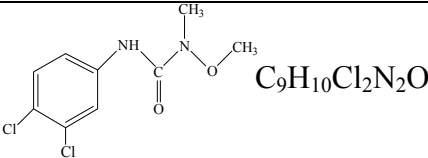
Acetonitrile (HPLC grade)	41.05	C ₂ H ₃ N	Tedia
Acetone (AR grade)	58.08	C ₃ H ₆ O	Tedia
Methanol (HPLC grade)	32.04	CH ₄ O	Tedia
tert-butanol (99%)	74.12	C ₄ H ₉ OH	Tedia

Cont'd

Acetic acid (99.8%)	88.11	CH ₃ COOH	Lab-scan
<hr/>			
<u>Others</u>			
Sodium Carbonate (99.7%)	105.99	NaCO ₃	AnalaR
Sodium Bicarbonate (99.9%)	84.01	NaHCO ₃	AnalaR
Sodium Chloride (99.99%)	58.44	NaCl	Riedel-dehaën
Sodium Sulfate (anhydrous)	142.04	Na ₂ SO ₄	BDH
	141.96	Na ₂ HPO ₄	BDH
titanium oxide sulfate hydrate (99.5%)	69.00	TiOSO ₄ •xH ₂ O	International Laboratory
Sulfuric Acid	98.08	H ₂ SO ₄	Tedia
Sodium Hydroxide (96%)	40.00	NaOH	Uni-Chem
Sodium Azide	65.00	NaN ₃	Aldrich
Ammonia Acetate	77.08	CH ₃ COONH ₄	Aldrich
Sodium Thiosulfate	158.11	Na ₂ S ₂ O ₃	BDH

Table 3-2: Physical properties of LNR

(<http://pmep.cce.cornell.edu/profiles/extoxnet/haloxyp-methylparathion/linuron-ext.html>)

Formula	 <chem>CN(C)OC(=O)Nc1ccc(Cl)c(Cl)c1</chem> $C_9H_{10}Cl_2N_2O$
Molecular mass	249.11
Physical state	White crystalline solid
Melting point (°C)	93~94
Boiling point (°C)	180~190
Vapor pressure	1.5×10^{-6} mm Hg at 24 °C
Water solubility	75 mg/l at 25 °C
Solvent solubility	slightly soluble in aliphatic hydrocarbons, moderately soluble in ethanol, soluble in acetone
Maxima of absorption spectrum	210 and 246 nm

3.3 Experimental Setup

3.3.1 UV/O₃ process

For the tests involving UV photolysis, 600 mL sample was irradiated in a 800 mL (97.8 mm ID×125 mm H) quartz beaker with magnetic stirring. The beaker was

placed in the center of a Rayonet™ RPR-200 photoreactor manufactured by the Southern New England Ultraviolet Co., which was equipped with phosphor-coated low-pressure mercury lamps, emitting 253.7 nm monochromatic UV at a light intensity of 1.5×10^{-6} Einstein $L^{-1}s^{-1}$ (See Figure 3-1).

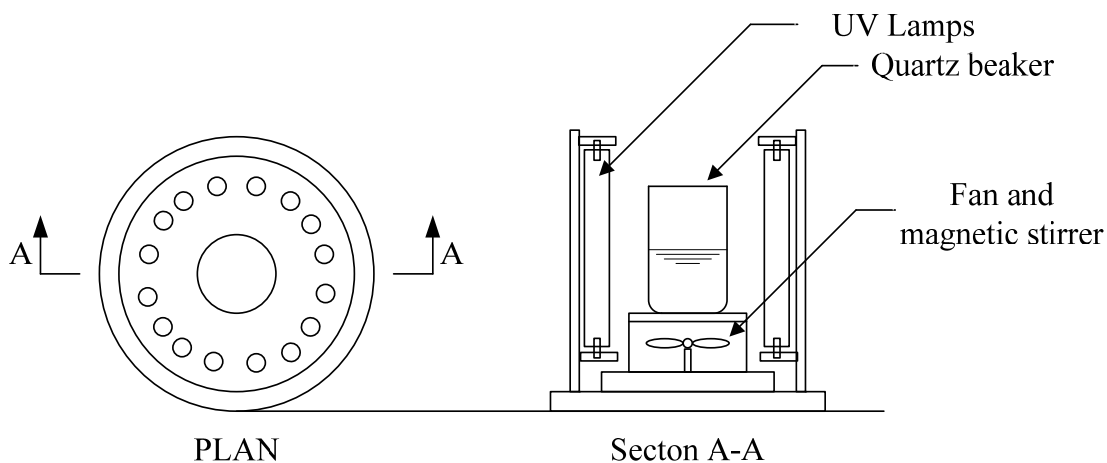


Figure 3-1: The top view and sectional view of the photoreactor Rayonet™.

For the tests involving ozonation, 400 mL of deionized water was pre-ozonated for 15 min (to produce a saturated ozone solution), after adding 200 mL of linuron stock solution into the pre-ozonated solution, a small reduction of dissolved ozone was observed at the beginning of the reaction, which was considered insignificant and could be replenished easily and quickly by continuous feeding of ozone gas into the reactor through a glass sparger (pore size ranges from 16-40 μm) located just above the bottom of the reactor. Ozone gas was produced by the OZAT ozone generator (CFS-1A from Ozonia, Ltd.). The flow rate of ozone/oxygen mixture into the reactor varied from 1.3-2.0 $L \text{ min}^{-1}$, which resulted in a 9.96×10^{-6} to 3.09×10^{-5} M ozone concentration in the solution. The concentration of ozone was determined by the Indigo spectrometric method. For the UV/O₃ experiments, simultaneous UV irradiation was provided during the ozonation period. The remaining ozone in the

collected sample was quenched by sodium thiosulfate before quantification of linuron.

3.3.2 Photocatalysis process

For UV-induced photocatalytic reactions, they were also conducted in a RayonetTM RPR-200 photochemical reactor. Six phosphor-coated low-pressure mercury lamps at 350 nm were installed on the photoreactor. To ensure a thorough mixing, 150 mL of solution was dispensed into a 300 mL quartz cylinder with mechanical stirring before and during the illumination.

For the investigation on the degradation kinetics of LNR by $\text{TiO}_2/\text{H}_2\text{O}_2/\text{Vis}$ system, the photodegradation of LNR was conducted in a Luzchem CCP-4V photochemical reactor controlled by a computer. To ensure a thorough mixing, 150 mL of solution was dispensed into a 300 mL quartz cylinder with mechanical stirring before and during the illumination. Twelve low-pressure mercury lamps centered at 420 nm were installed in the photoreactor as shown in Figure 3-2. The emission spectra of 420 nm lamp are shown in Figure 3-4.

For the examination on the degradation mechanism of LNR by $\text{TiO}_2/\text{H}_2\text{O}_2/\text{Vis}$ system, Vis (visible light)-induced photocatalytic reactions were conducted in a cylindrical glass vessel with a recycling water jacket to avoid overheating. To ensure a thorough mixing, 200 mL of solution was dispensed into the reactor with mechanical stirring before and during the illumination. The suspension was irradiated

by a 300 W Xe lamp (Beijing Perfectlight Co Ltd), which emits both UV and visible light over a wide wavelength as indicated in Figure 3-5. The experimental setup is shown in Figure 3-3. To limit the irradiation wavelength, the light beam was passed through both UV cutoff and other filters of varied wavelength (420, 435, 450, 500 nm).

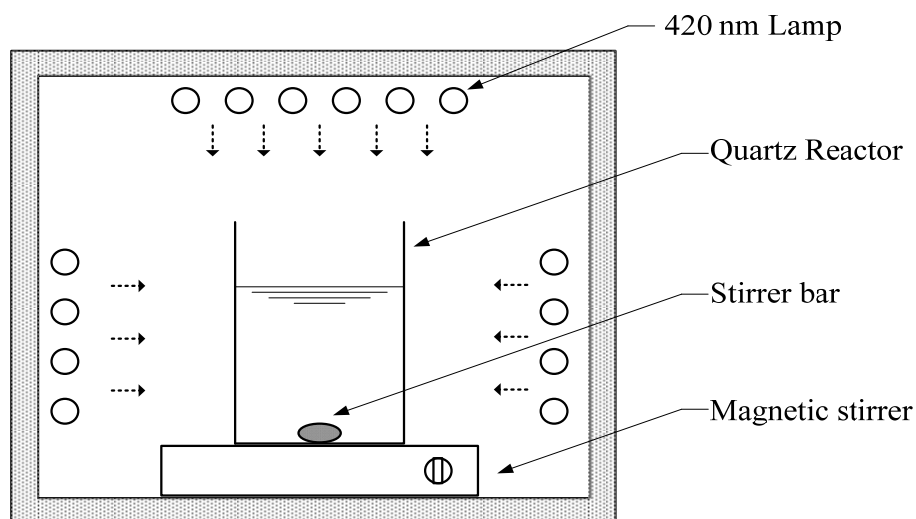


Figure 3-2: Schematic diagrams of the photoreactor Luzchem CCP-4V.

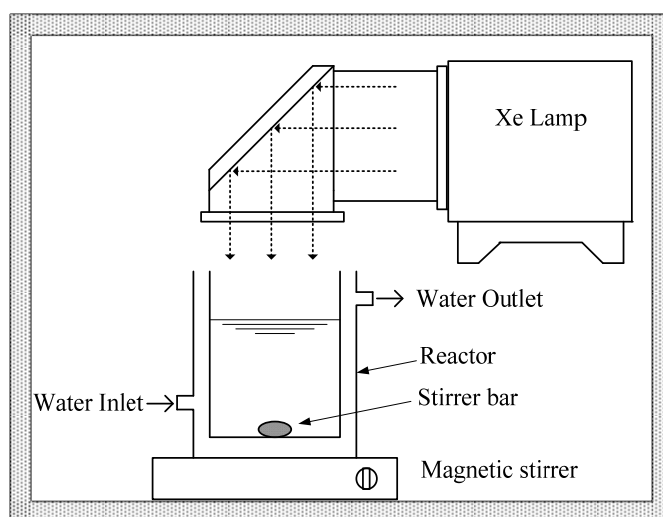


Figure 3-3: Schematic diagrams of the photoreactor with Xe lamp installed.

Samples were withdrawn at a predetermined interval and were filtered through a 0.2 μm PTFE membrane to keep the particles free from the solution prior to

quantification. All experiments were carried out at room temperature (air-conditioned) at $23 \pm 2^\circ\text{C}$ in duplicate.

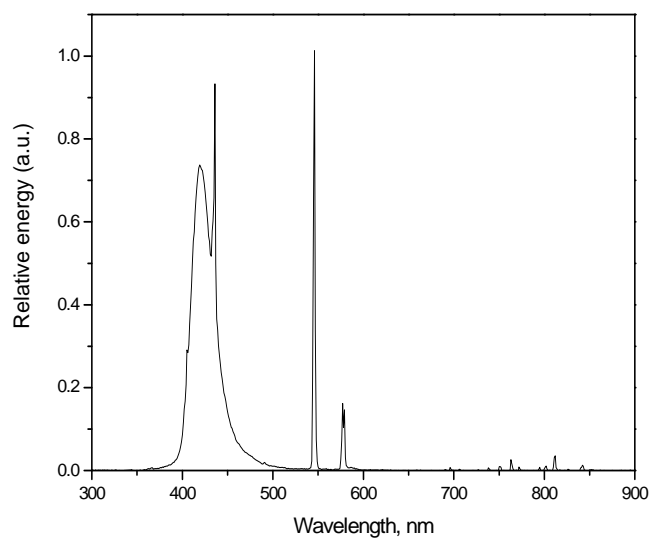


Figure 3-4: Emission spectra of 420 nm lamps

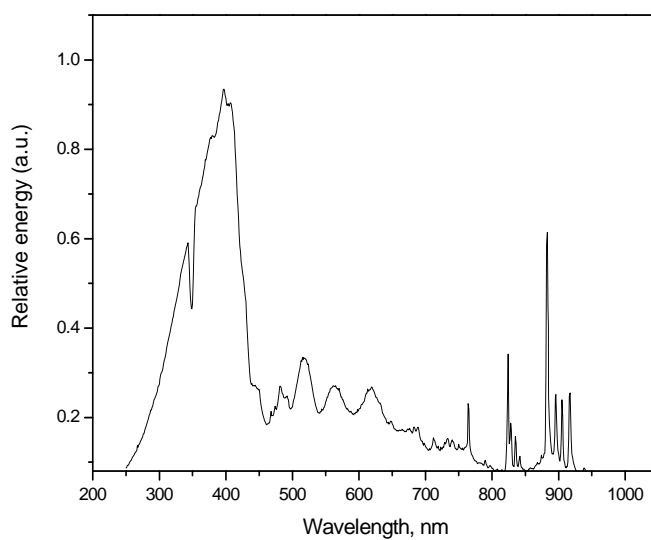


Figure 3-5: Emission spectra of Xe lamp

3.4 Instrumental Analysis

3.4.1 Analysis by high performance liquid chromatography (HPLC)

Remaining LNR after reaction was determined by HPLC (Waters). The system was comprised of a Waters 515 HPLC pump, Waters 2489 Dual λ Absorbance Detector, an Agilent Hypersil ODS column (5 μ m, 0.46 \times 25 cm), and Waters 717plus Autosampler. The maximum adsorption wavelength (λ_{max}) was selected as 246 nm for LNR (spectrum was shown in Appendix III). A mixture of 60% acetonitrile and 40% water was used as the mobile phase running at a flow rate of 1 mL/min. Four-point calibration was conducted for every batch of analysis.

3.4.2 Analysis by LC/MS

The identification of intermediates was carried out at an initial [LNR] of 0.29 mM. A Thermo Quest Finnigan LCQ Duo Mass Spectrometer system was used to identify the reaction intermediates, which consisted of a PDA-UV detector, and an electrospray ionization with a quadrupole ion-trap mass spectrometer operating at a negative mode at a capillary temperature of 225 °C. The mobile phase was a mixture of (A) 5mM ammonia acetate (pH 4.6) and (B) acetonitrile (100%). The composition of the mobile phase was changed according to the following gradient: 95% of A was kept during the first 2 minutes. From 2 to 26 min, B was steadily increased from 5% to 95%. From 26 to 27 min, B was kept at 95%. Finally, the mobile phase turned to the initial composition until the end of the run. Ionization of the HPLC elute was performed with the following settings: vaporizer temperature 270 °C, spray voltage 4.0 kV, current 5 μ A, sheath gas and auxiliary gas (N₂) flow rates (arbitrary units) 80 and 20, capillary temperature and voltage 150 °C and 3 V, respectively, and data collected from m/z 50–400.

Those intermediate compounds whose standards are not available commercially were quantified in terms of ion intensity relative to the initial LNR concentration for comparison. This approximation is acceptable on the basis of the fact that the UV absorbance may be ascribed to the resonance structure of the ring, which is basically identical (Adams and Randtke, 1992).

3.4.3 Analysis by ion chromatography (IC)

The generation of chloride, nitrite and nitrate ions were quantified by the ion chromatography (Dionex Series 4500i) composed of an anion column (Dionex IonPac® AS14 (4 mm × 250mm), Dionex CD25 Conductivity Detector and Dionex AS 40 Automated sampler. A mixture of 1 mM of NaHCO₃ and 3.5 mM of Na₂CO₃ was used as the mobile phase eluting at 1 mL min⁻¹. For the quantification of the ammonium ion produced during the reaction, Dionex IonPac® CS12 (4 mm × 250mm) was used as a cation column and 0.022 M MSA (methane sulphonic acid) was used as the mobile phase eluting at 1 mL min⁻¹.

3.4.4 TOC measurement

The total organic carbon (TOC) concentration was analyzed by a Shimadzu TOC-5000A analyzer equipped with an ASI-5000A autosampler to determine the total mineralization degree of the organic pollutants during the advanced oxidation process. The principle of it is to break down the single carbon units and convert them to single carbon molecular form (i.e. carbon dioxide) that can be measured quantitatively. The inorganic carbon is first removed by acidification and sparging. Each sample is acidified to pH 3 prior to TOC analysis. The analyzer is calibrated bi-

monthly. The sample is loaded into the analyzer by automatic sampler and the carrier gas, O₂, will carry the sample right into the reactor. A high temperature catalytic combustion is used to convert organic carbons to carbon dioxide (CO₂). The resulting CO₂ is then measured directly by an infrared analyzer. The TOC content is calculated and displayed in mg/L by the computer.

3.4.5 pH measurement

Solution pH was adjusted by the addition of diluted H₂SO₄ or NaOH. Measurement was carried out by the pH meter (Cole Parmer) and thorough mixing was ensured by magnetic stirrer.

3.4.6 X-ray diffraction analysis

X-ray diffraction (XRD) was employed to investigate the phase homogeneity of the titanium dioxide. Powder XRD patterns of the samples were recorded on a Bruker D8 Advance X-ray diffractometer with Cu K α radiation ($\lambda = 1.54178 \text{ \AA}$) at a scan rate of $0.05^\circ 2\theta/s$. The accelerating voltage and applied current were 40kV and 40mA, respectively. The XRD patterns of the three TiO₂ tested in this study are shown in Figure 3-6.

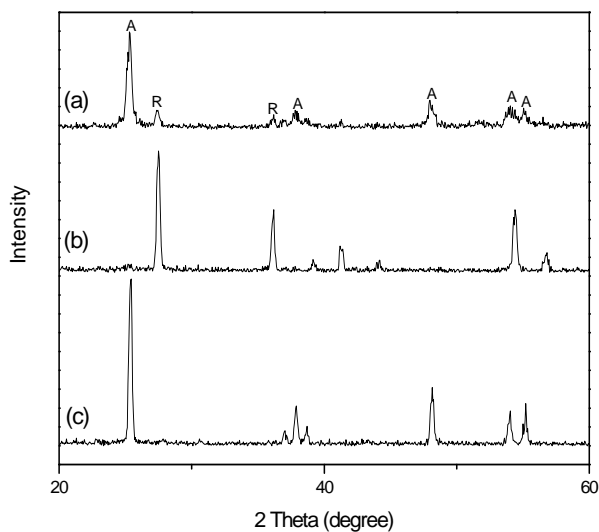


Figure 3-6: XRD patterns of different TiO_2 powders used in this study: (a) P25; (b) Rutile; (c) Anatase.

3.4.7 Diffuse reflectance absorption analysis

A Varian CARY 300 UV-Visible Spectrophotometer were used to obtain the ultraviolet-visible diffuse reflection spectra (UV-vis DRS) of the samples over a range of 200-800nm. Baseline correction was conducted using a calibrated sample of barium sulphate (BaSO_4).

3.4.8 Measurement of the emission spectra of lamps

The emission spectra of 420 nm lamp and Xe lamp were recorded by ILT900 Wideband Rapid Portable Spectroradiometer (InternationalLight TECHNOLOGIES).

3.4.9 Measurement of the photocurrent

Photocurrent generation was measured with TiO_2/ITO electrode immersed in aqueous solution of H_2O_2 . For preparing the TiO_2/ITO electrode, the ITO plates were

first cleaned by sonication in acetone, ethanol and DDW for 30 min, respectively. Then ITO plates were spin-coated with TiO₂ film from 25 g/L P25 ethanol suspension with the addition of 25 g/L glycerol. The TiO₂-coated ITO plates were calcined at 450°C for 30 min to burn off organics and bind the TiO₂ film to the ITO plate. The TiO₂/ITO electrode, a saturated calomel electrode (SCE), and Pt plate were immersed in the reactor as working, reference, and counter electrodes, respectively. Photocurrents were recorded in aqueous solution with or without H₂O₂ as a function of elapsed time with application of a potential (+0.5 V vs SCE) using a potentiostat (VersaSTAT 3) connected to a computer.

Chapter 4 Degradation Kinetics of LNR with UV, Ozonation and UV/O₃ Processes

4.1 Introduction

The phenylurea herbicides have been widely applied as effective weed killers by inhibiting photosynthesis upon absorption in the roots in the conventional production of corn, cereals, vegetables and fruits since their discovery in 1950 (Sorensen et al., 2005). Generally, these chemicals are characterized as persistent in the environment (half-life in soil was reported to be 38-67 days) (Caux et al., 1998) and thus have been found frequently in surface and ground waters (Garmouma et al., 1997). Linuron (N-(3, 4-dichlorophenyl)-N'-methoxy-N'-methylurea) (LNR), one of the most commercialized phenylurea herbicides, was selected as probe compound. The toxicity and possible endocrine disrupting effects of LNR and its metabolites lead to pressing demand for effective treatment techniques to eliminate and mineralize this contaminant.

Ozone process has widely been applied in the treatment of particular organic substances of concern, such as 2, 4- dichlorophoxyacetic acid (Chu and Ching, 2003), trichlorophenol (Graham et al., 2003) and atrazine (Acero et al., 2000). However, the reactions between organic substances and ozone are highly electrophilic and selective (Yao and Haag, 1991), which limit the application of the ozonation as a sole treatment process in meeting drinking water requirements. Therefore, intensive efforts have been put into the research about ozone associated with other oxidation

processes, such as O_3/H_2O_2 (Chen et al., 2006), Ultrasound/ O_3 (He et al., 2007b), UV/ O_3 (Lau et al., 2007), ozonation coupled with photocatalysis (Sanchez et al., 1998), and ozonation combined with electrolysis (Kishimoto et al., 2008), in which hydroxyl radical oxidation is believed to play a key role in the mineralization of organic substances due to its non-selective property.

LNR is subjected to growing attentions for investigating its treatability by various techniques, such as biological methods (Sorensen et al., 2005; Dejonghe et al., 2003), O_3/H_2O_2 (Tahmassebi et al., 2002), direct photolysis (Faure and Boule, 1997), photo-Fenton procedure (Katsumata et al., 2005), and photocatalysis (Lopez et al., 2005). However, the study of LNR under UV/ O_3 process in aqueous phase is still superficial and the inside study of the individual reaction pathway is very limited. The combined UV/ O_3 process has been widely studied (Lau et al., 2007), and its overall oxidation reaction is believed to result from a synergistic effect of several individual reactions, such as direct ozonation, direct photolysis, and indirect radical oxidation. UV irradiation can lead to ozone being transformed into hydrogen peroxide which can be further photolyzed into HO^\bullet and then initiate a chain of radical reactions (Gurol and Akata, 1996). It is believed that the UV/ O_3 process could provide an effective treatment of LNR and its toxic intermediates present in contaminated waters.

In this chapter, the degradation and mineralization of LNR was examined under direct photolysis, O_3 , and UV/ O_3 processes in aqueous phase. In addition, the effects of initial pH levels, ozone dose and light intensity on the decay rate of LNR were also investigated. The information was used in subsequent model derivations and rate constants determination for the involved sole-UV, O_3 and UV/ O_3 systems.

4.2 Results and Discussion

4.2.1 Decomposition and mineralization of LNR in UV/Ozone system

The degradation and mineralization of 0.1 mM LNR in sole UV, sole Ozone and combined UV/ozone system was investigated with pH level set at 6.0, ozone concentration and light intensity were fixed at 0.0171 mM and at 6.0×10^{-6} Einstein $L^{-1} s^{-1}$, respectively. As indicated in Figure 4-1, the decay rate of LNR increases in the order of UV photolysis, ozone and UV/ozone. In addition, LNR (0.1 mM) can be completely removed by the three proposed processes. It takes 35 minutes to fully decompose 0.1 mM LNR for UV illumination, while 22.5 and 10 minutes were required for ozonation and UV/ozone, respectively. The photolysis and oxidation of LNR were found to follow pseudo first-order kinetics. As also demonstrated in Figure 4-1, no TOC removal was observed in sole UV process, and TOC removal was insignificant in ozonation process (about 15% mineralization after 100 minutes). However, nearly 80% mineralization was achieved by using UV/ozone process after 100 minutes, suggesting the use of UV/ozone is a promising and clean process for the final disposal of LNR.

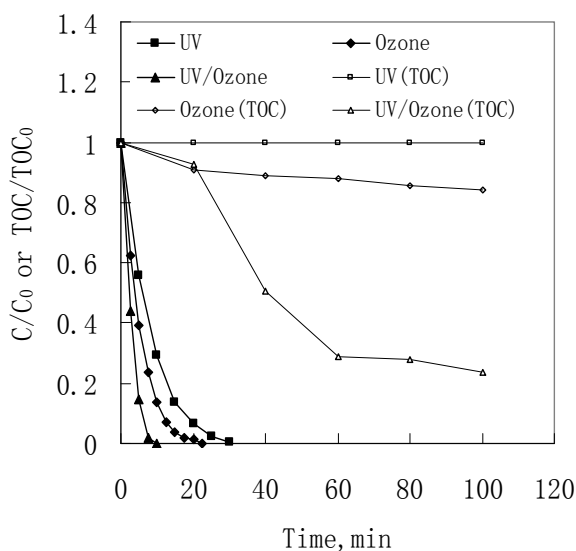


Figure 4-1: Comparison of LNR decay (C/C_0) and TOC removal by the different treatment processes at pH 6 ($C_0 = 0.1$ mM)

4.2.2 Effect of pH level on decay rate of the LNR ozonation

The decay rate of LNR was tested at various pH levels (from 3 to 11) by ozonation process with ozone concentration fixed at 0.0171 mM. As indicated in Figure 4-2, an increased degradation rate was observed at elevated pH levels. Furthermore, it is interesting to note that the overall rate constants increased linearly at lower pH level (< 9), but exponentially at higher pH level (> 9) as indicated in the inset of Figure 4-2. This can be rationalized by the different oxidation pathways. At lower pH level, the oxidation by ozone molecules is the dominant reaction, while a much faster oxidation by hydroxyl radicals plays a key role under basic conditions (Chu and Ma, 2000).

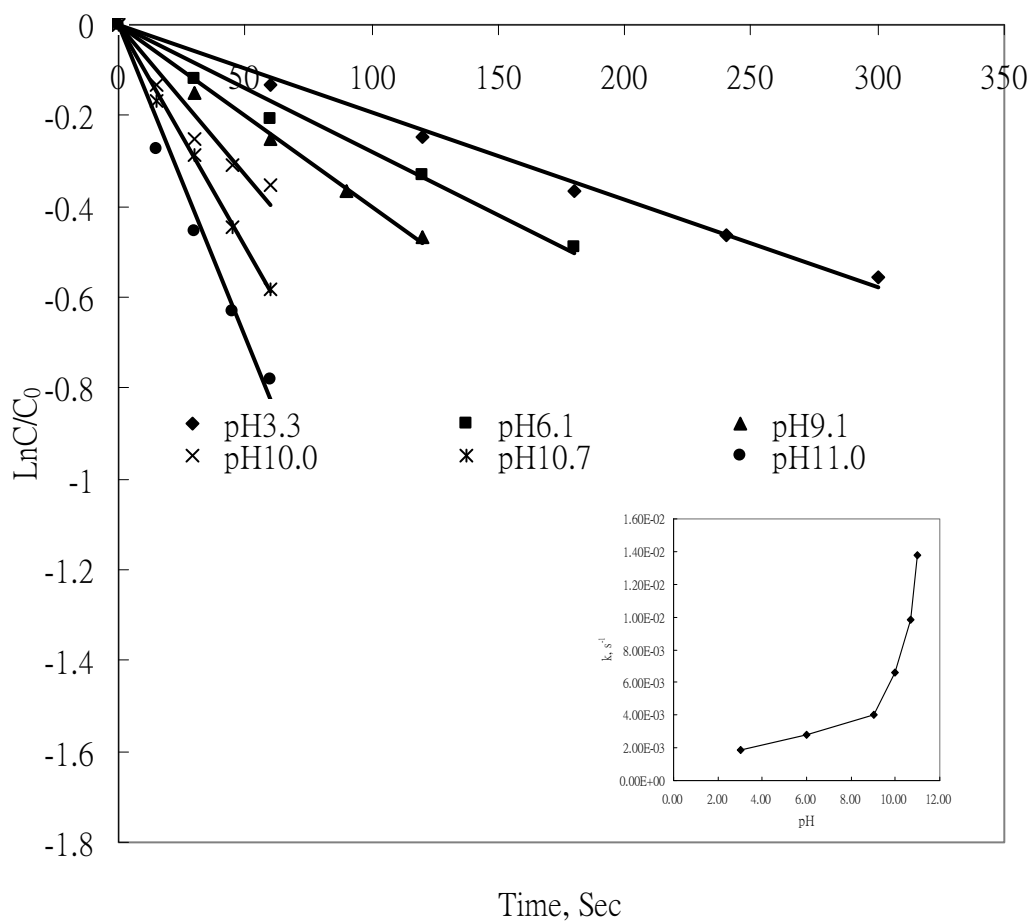


Figure 4-2: Pseudo first-order degradation of 0.1 mM LNR in ozone-alone system at various pH levels ($[O_3] = 1.71 \times 10^{-5} \text{ M}$)

4.2.3 Quantum Yield determination in UV system

The photodecay of LNR by sole-UV (at 253.7 nm) was investigated by using four different levels of light intensity at 3.0, 6.0, 9.0 and $12.0 \times 10^{-6} \text{ Einstein L}^{-1} \text{ s}^{-1}$ with other parameters unchanged. The results shown in Figure 4-3 suggested that the LNR decay rate constant is linearly increased with the intensity of light. Theoretically, it is possible to determine the quantum yield of LNR decay by simple pseudo first-order kinetics under an optical dilute condition. The decay rate of LNR by sole-UV therefore can be formulated as:

$$-\frac{d[LNR]}{dt} = k_{obs}[LNR] = 2.303\phi_{LNR}\varepsilon_{LNR}I_0[LNR] \quad (4-1)$$

$$k_{obs} = 2.303\phi_{LNR}\varepsilon_{LNR}I_0 \quad (4-2)$$

where ϕ_{LNR} is the quantum yield of LNR decay, k_{obs} is the observed pseudo first-order rate constant (s^{-1}), I_0 is intensity of the incident light at 253.7 nm (Einstein $L^{-1}s^{-1}$), ε_{LNR} is the molar absorptivity of LNR at 253.7 nm ($13,254 M^{-1}cm^{-1}$), and l is the optical path length of the quartz beaker (9.78 cm). The observed rate constant k_{obs} was found to be linearly correlated to initial light intensity as shown in Figure 4-3. Therefore, ϕ_{LNR} is calculated to be 0.00122 by the slope of the curve divided by $2.303 \varepsilon_{LNR} l$.

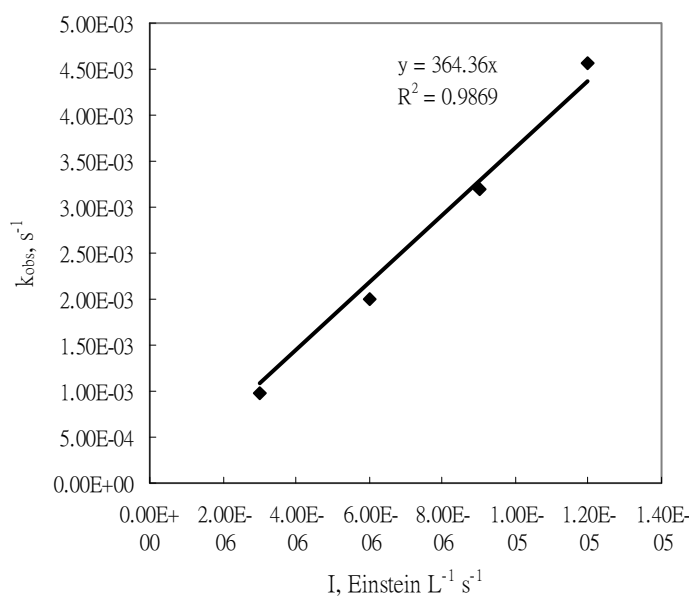


Figure 4-3: Pseudo first-order degradation of 0.1 mM LNR in sole-UV system under various light intensity irradiation

4.2.4 Rate Constant Determination in Ozone system

The degradation of LNR was found to follow a pseudo first-order reaction (See Figure 4-2) at different pH levels during ozonation. It is well known that the oxidization reaction in ozone system comes from either ozone molecule or hydroxyl

free radical with substrates. The decay rate of LNR therefore can be theoretically interpreted by Eqn. (4-3)

$$-\frac{d[LNR]}{dt} = k_{overall}[LNR] = k_{o_3, LNR}[LNR][O_3] + k_{OH, LNR}[LNR][HO^\bullet] \quad (4-3)$$

The formation of hydroxyl radicals depends on the pH level of the solution; under a pseudo steady state condition, the concentration of hydroxyl radicals can be estimated by the following equation (Benitez et al., 1994):

$$[HO^\bullet] = \frac{3k_{OOH}[O_3][OH^-]}{k_{OH, LNR}[LNR]} \quad (4-4)$$

where k_{OOH} is the rate constant for the formation of free radical HOO^\bullet from ozone decomposition at high pH (Staehelin and Hoigne, 1982). By combining Eqns. (4-3) and (4-4), the oxidation rate of LNR in ozone system can be derived as following:

$$k_{overall}[LNR] = k_{o_3, LNR}[LNR][O_3] + 3k_{OOH}[O_3][OH^-] \quad (4-5)$$

in terms of rate constant, Eqn. (4-5) would be:

$$k_{overall} = k_{o_3, LNR}[O_3] + 3k_{OOH}[O_3] \frac{[OH^-]}{[LNR]} \quad (4-6)$$

In order to determine the k_{O_3} and k_{OOH} , the variations of overall rate constant at different levels of $[O_3]$ and $[OH^-]$ were investigated and plotted in Figure 4-4a. Depending on $[O_3]$, $k_{overall}$ has a good linear correlation with $[OH^-]$ (r^2 ranging between 0.967 and 0.997). According to Eqn. (4-6), the intercepts of these lines would be the $k_{o_3, LNR}[O_3]$ for the corresponding $[O_3]$, while the slopes stand for the $3k_{OOH} \frac{[O_3]}{[LNR]}$. Therefore, k_{O_3} can be determined by plotting the intercepts (from

Figure 4-4a) at different $[O_3]$ as a function of the corresponding ozone concentration as shown in Figure 4-4b. Also, k_{OOH} can be calculated by plotting the slopes (from

Figure 4-4a) at different $[O_3]$ as a function of the term $\frac{3[O_3]}{[LNR]}$ (see Figure 4-4b). The correlation lines going through the origin in Figure 4-4b result in $k_{o_3, LNR}$ and k_{OOH} as $293 \text{ M}^{-1}\text{s}^{-1}$ and $14.2 \text{ M}^{-1}\text{s}^{-1}$, respectively. The different orders of these two rate constants suggest that the second term of Eqn. (4-5) (i.e. the oxidation due to hydroxyl radical) can be ignored when the hydroxide ion concentration level is much lower than the concentration of the compound. In order to verify the hypothesis that the ozone concentration was close to a constant during the reaction, Hatta number was calculated to compare diffusion time with reaction time based on the Eqn. (4-7) (Benitez et al., 1994).

$$Ha = \frac{\sqrt{k_{O_3, LNR} D_{O_3} C_{LNR} + 3k_{OOH} D_{O_3} [OH^-]}}{k_L} \quad (4-7)$$

where D_{O_3} is the ozone diffusion coefficient in the liquid and k_L is the ozone transfer coefficient to the liquid. D_{O_3} is reported to be $1.76 \times 10^{-9} \text{ m}^2 \text{ s}^{-1}$ in the water at $20 \text{ }^\circ\text{C}$ (Johnson and Davis, 1996). $k_L a$ was determined to vary from 0.013 to 0.025 s^{-1} according to Huang (Huang and Shu, 1995). The gas-liquid interfacial area per unit of liquid volume (a) was estimated by the Eqn. (4-8) (Lan et al., 2008) and Eqn. (4-9) (Bin et al., 2001).

$$a = \frac{6H_g}{d_{bs}} \quad (4-8)$$

$$H_g = 5.54U_g^{1.03} \quad (4-9)$$

where U_g is superficial velocity varied from 2.9×10^{-3} to $4.4 \times 10^{-3} \text{ m s}^{-1}$ in this study and d_{bs} is the Sauter bubble diameter calculated from the correlation of Bouaifi and Roustan (Bouaifi and Roustan, 1998). As a result, Hatta number was estimated

to be ranged from 0.0046 to 0.0217 which is below 0.03, indicating the kinetic regime is very slow.

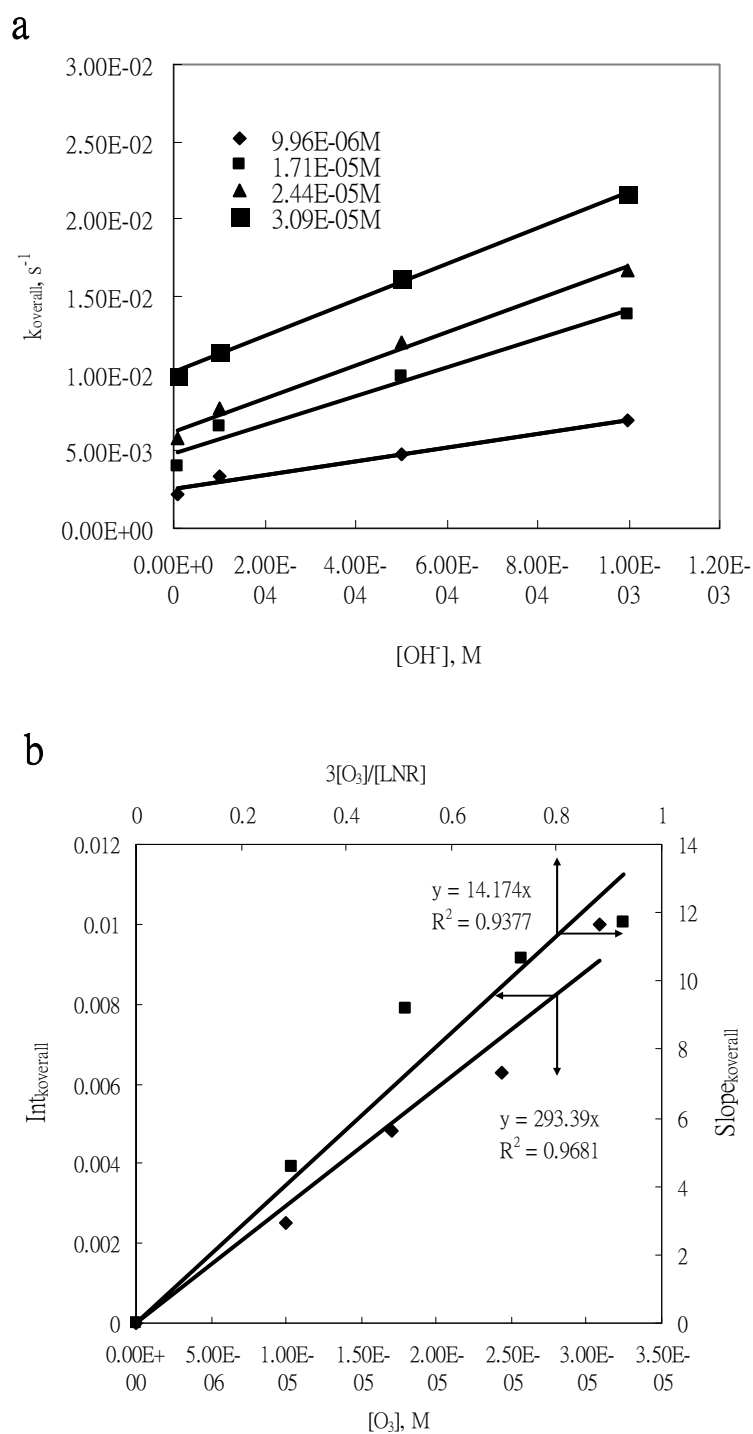


Figure 4-4: (a) Variation of decay rate constant of 0.1 mM LNR with various hydroxide ion concentrations at different ozone concentration levels in

ozone-alone system; (b) Correlations between $\text{int}_{\text{koverall}}$ and $[\text{O}_3]$ or
Correlations between $\text{slope}_{\text{koverall}}$ and $3[\text{O}_3] / [\text{LNR}]$

To determine the $k_{\text{OH},\text{LNR}}$, an independent UV/H₂O₂ experiment using ATZ as a reference compound was conducted, where the LNR decay due to sole-UV has been deducted from the reaction data. In theory, $k_{\text{OH},\text{LNR}}$ can be determined by using Eqn. 4-10 under the same reaction conditions in oxidizing the model compound ATZ:

$$\text{Ln} \frac{[\text{LNR}]_0}{[\text{LNR}]_t} = \frac{k_{\text{OH},\text{LNR}}}{k_{\text{OH},\text{ATZ}}} \text{Ln} \frac{[\text{ATZ}]_0}{[\text{ATZ}]_t} \quad (4-10)$$

By plotting $\text{Ln} \frac{[\text{LNR}]_0}{[\text{LNR}]_t}$ versus $\text{Ln} \frac{[\text{ATZ}]_0}{[\text{ATZ}]_t}$ as shown in Figure 4-5, a straight line

was observed, which gave a slope of 1.015 in terms of $\frac{k_{\text{OH},\text{LNR}}}{k_{\text{OH},\text{ATZ}}}$. Since $k_{\text{OH},\text{ATZ}}$ was

reported to be $2.7 \times 10^9 \text{ M}^{-1}\text{s}^{-1}$ (Acero et al., 2000), the value of $k_{\text{OH},\text{LNR}}$ was

determined to be $2.74 \times 10^9 \text{ M}^{-1}\text{s}^{-1}$.

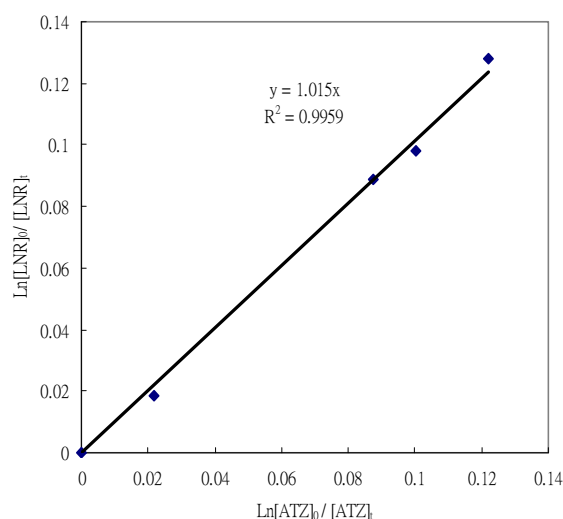


Figure 4-5: Relationship between the degradation of atrazine and LNR ($[\text{LNR}]_0 = [\text{ATZ}]_0 = 10 \text{ } \mu\text{M}$, $[\text{H}_2\text{O}_2]_0 = 20 \text{ mM}$, Initial light intensity = 3.0×10^{-6} Einstein $\text{L}^{-1} \text{ s}^{-1}$)

4.2.5 Derivation of Rate Models and rate constant determination in UV/O₃ system

The decomposition of LNR in UV/O₃ system is an extremely complicated process since many individual reactions, such as direct photolysis, direct (molecular) ozonation, and various free radical oxidation are believed to be involved in this system. According to Gurol and Akata, the principal reactions expected in UV/O₃ aqueous system are summarized in Table 4-1 (Gurol and Akata, 1996).

From the table, the inclusion of all sub-reactions to develop kinetic model in this system will be difficult and the result is likely impracticable due to the involvement of too many parameters. Therefore, a different approach using ozone molecule oxidation, hydroxyl radical oxidation, and UV-induced oxidation to describe the overall process were proposed. The decay of LNR in UV/O₃ system therefore can be described as below:

$$-\frac{d[LNR]}{dt} = k_{overall}[LNR] = k_{O_3,LNR}[LNR][O_3] + k_{OH,LNR}[LNR][HO^\bullet] + 2.303\phi_{LNR}\epsilon_{LNR}II[LNR] \quad (4-29)$$

The [HO[•]] of the second term in the Eqn. (4-29) theoretically may come from the hydroxide ion initiated decomposition of ozone and the photolysis of ozone by UV. Under acidic condition, however, the contribution of the hydroxide ion initiated decomposition of ozone to the production of HO[•] is insignificant at low pH levels as discussed previously. The photolysis of ozone can be assumed as the only source of HO[•] in UV/O₃ system.

Table 4-1: Summary of the principal reactions expected in UV/O₃ aqueous system

Reaction	Rate Constant (M ⁻¹ s ⁻¹) and Equilibrium Constant (pK _a)	eq
$O_3 + hv \rightarrow H_2O_2$		4-11
$H_2O_2 + hv \rightarrow 2HO^\bullet$		4-12
$H_2O_2 \leftrightarrow HO_2^- + H^+$	$pK_{a,10} = 11.8$	4-13
$HO_2^- + O_3 \rightarrow O_3^{\bullet-} + HO_2^\bullet$	$k_{11} = 2.8 \times 10^6$	4-14
$HO_2^\bullet \leftrightarrow H^+ + O_2^{\bullet-}$	$pK_{a,12} = 4.8$	4-15
$O_2^{\bullet-} + O_3 \rightarrow O_3^{\bullet-} + O_2$	$k_{13} = 1.6 \times 10^9$	4-16
$O_3^{\bullet-} + H^+ \rightarrow HO^\bullet + O_2$	$k_{14} = 5.2 \times 10^{10}$	4-17
$HO^\bullet + H_2O_2 \rightarrow HO_2^\bullet + H_2O$	$k_{15} = 2.7 \times 10^7$	4-18
$HO^\bullet + HO_2^- \rightarrow HO_2^\bullet + OH^-$	$k_{16} = 7.5 \times 10^9$	4-19
$HO^\bullet + O_3 \rightarrow HO_2^\bullet + O_2$	$k_{17} = 3.0 \times 10^9$	4-20
$2HO^\bullet \rightarrow H_2O_2$	$k_{18} = 5.5 \times 10^9$	4-21
$2HO_2^\bullet \rightarrow H_2O_2 + O_2$	$k_{19} = 7.6 \times 10^5$	4-22
$HO_2^\bullet + O_2^{\bullet-} + H_2O \rightarrow H_2O_2 + O_2 + OH^-$	$k_{20} = 8.9 \times 10^7$	4-23
$O_3 + OH^- \rightarrow HO_2^- + O_2$	$k_{21} = 14.2$	4-24
$O_3 + LNR \rightarrow \text{products}$	$k_{O_3,LNR} = 293$	4-25
$LNR + uv \rightarrow \text{products}$		4-26
$HO^\bullet + LNR \rightarrow \text{products}$	$k_{OH,LNR} = 2.74 \times 10^9$	4-27
Other radicals + LNR \rightarrow products		4-28

Since HO^\bullet is so reactive that it does not accumulate to an appreciable level in the solution, a steady-state approximation can be made (from the equations listed in Table 4-1):

$$\begin{aligned} \frac{d[HO^\bullet]}{dt} = & 2 \frac{d[H_2O_2]}{dt} + k_{14}[O_3^{\bullet-}][H^+] - k_{15}[HO^\bullet][H_2O_2] - k_{16}[HO^\bullet][HO_2^-] \\ & - k_{17}[HO^\bullet][O_3] - k_{18}[HO^\bullet]^2 - k_{OH,LNR}[HO^\bullet][LNR] = 0 \end{aligned} \quad (4-30)$$

$$\begin{aligned} \text{or } 2 \frac{d[H_2O_2]}{dt} + k_{14}[O_3^{\bullet-}][H^+] = & k_{15}[HO^\bullet][H_2O_2] + k_{16}[HO^\bullet][HO_2^-] + k_{17}[HO^\bullet][O_3] \\ & + k_{OH,LNR}[HO^\bullet][LNR] \end{aligned} \quad (4-31)$$

Under acidic conditions (the reaction condition of this test), HO_2^- concentration would be at extremely low level (judging from the pKa of 11.8 as shown in Eqn. (4-13)), which means $O_3^{\bullet-}$ as a source of HO^\bullet is negligible (from Eqns. (4-14) to (4-17)) comparing to H_2O_2 (Eqn. 4-12). In addition, the contribution of Eqn. 4-16 to HO^\bullet consumption can also be ignored. Furthermore, the termination of HO^\bullet through radical-radical termination reactions as presented by Eqns. (4-21) to (4-23) is insignificant and can be neglected due to very low HO^\bullet radical concentrations (Gurol and Akata, 1996). According to Table 1, k_{15} is much smaller than k_{17} and $k_{OH,LNR}$ (more than 100 times), while $[O_3]$ (a continuous input) is much higher than $[H_2O_2]$, the Eqn. (4-18) can therefore be ignored. Thus, Eqn. (4-31) can safely be simplified to:

$$2 \frac{d[H_2O_2]}{dt} = k_{17}[HO^\bullet][O_3] + k_{OH,LNR}[HO^\bullet][LNR] \quad (4-32)$$

In Eqn. (4-32), $[HO^\bullet]$ still cannot be calculated since the variation of $[H_2O_2]$ is difficult to be determined. However, if Eqns (4-11) and (4-12) are merged together, the left-hand side of Eqn. (4-32) can be redefined as $-\alpha \frac{d[O_3]}{dt}$ (α is defined as the

ratio of the production rate of HO^\bullet and/or the decay rate of ozone) since the rate of Eqn. (4-11) is likely much faster than that of Eqn. (4-12). Then Eqn. (4-32) becomes:

$$-\alpha \frac{d[O_3]}{dt} = 2.303\alpha\phi_{O_3}I\varepsilon_{O_3}l = k_{17}[HO^\bullet][O_3] + k_{OH,LNR}[HO^\bullet][LNR] \quad (4-33)$$

where ϕ_{O_3} is the quantum yield of ozone decay, l is the optical light path (i.e. the diameter) of the quartz beaker and ε_{O_3} is the molar absorptivity of ozone ($3600 \text{ L mol}^{-1} \text{ cm}^{-1}$) (Bahnmann and Hart, 1982) at 253.7nm.

or

$$[HO^\bullet] = 2.303 \frac{\alpha\phi_{O_3}I\varepsilon_{O_3}l}{k_{17}[O_3] + k_{OH,LNR}[LNR]} \quad (4-34)$$

The decay rate of LNR can therefore be defined in Eqn. (4-35) by incorporating Eqs. (4-29) and (4-34):

$$k_{overall} = k_{O_3,LNR}[O_3] + 2.303I \left\{ k_{OH,LNR} \frac{\alpha\phi_{O_3}\varepsilon_{O_3}l}{k_{17}[O_3] + k_{OH,LNR}[LNR]} + \phi_{LNR}\varepsilon_{LNR}l \right\} \quad (4-35)$$

It should be noted that many chemicals in the solution are capable of absorbing UV light at 253.7nm, which may result in an effect of light attenuation. This is specially noticeable when their concentration or the associated molar absorptivity is high. Since this study focused on the initial rate, the contribution to light attenuation from intermediates can be negligible, which makes LNR and ozone the major components contributing to the attenuation effect. The attenuated light intensity can be quantified by the following equation in a cylindrical reactor (Chu et al., 2005):

$$I = \frac{I_0}{-2.303A} [e^{-2.303A} - 1] \quad (4-36)$$

Where $A = \sum_{i=1}^n \varepsilon_i c_i l = \varepsilon_{O_3} C_{O_3} l + \varepsilon_{LNR} C_{LNR} l$. Due to high molar absorptivity of ozone and LNR (as indicated before), the term $e^{-2.303A}$ approaches zero, then the Eqn. (4-36) can be further simplified to:

$$I = \frac{I_0}{2.303A} \quad (4-37)$$

By substituting Eqn. (4-37) into Eqn. (4-35), the Eqn. (4-35) becomes:

$$k_{overall} = k_{O_3, LNR} [O_3] + \frac{I_0}{A} \left\{ k_{OH, LNR} \frac{\alpha \phi_{O_3} \varepsilon_{O_3} l}{k_{17} [O_3] + K_{OH, LNR} [LNR]} + \phi_{LNR} \varepsilon_{LNR} l \right\} \quad (4-38)$$

The tested results of $k_{overall}$ under different light intensity were correlated to $\frac{I_0}{A}$ as shown in Figure 4-6, where a linear curve was observed as predicted in Eqn. (4-38). The slope of the linear curve would be the complex term inside the bracket of Eqn. (4-38), and the intercept revealed the $k_{O_3, LNR} [O_3]$. Because ϕ_{O_3} was reported to be 0.48 and the other parameters are all known, the α is determined to be 6.92×10^{-5} . The calculated parameters and the corresponding equations and/or figures are summarized in Table 4-2.

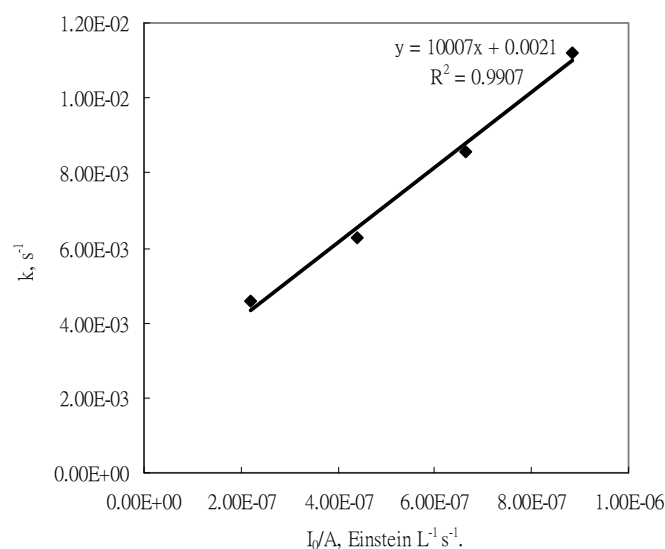


Figure 4-6: Variation of decay rate constant of 0.1 mM LNR under different light

intensity irradiation in UV/O₃ system (Notes: pH₀ = 4.03, [O₃] = 1.71 × 10⁻⁵ M)

Table 4-2: Summary of Rate Constant determination

parameter	value	unit	Involved equations and figures
Φ_{LNR}	0.00122	mol Einstein ⁻¹	Eq. 4-2(slope) and Fig. 4-3
$k_{o_3,LNR}$	293	M ⁻¹ s ⁻¹	Eq. 4-6 (int.) and Fig. 4-4b
k_{OOH}	14.2	M ⁻¹ s ⁻¹	Eq. 4-6 (slope) and Fig. 4-4b
$k_{OH,LNR}$	2.74 × 10 ⁹	M ⁻¹ s ⁻¹	Eq. 4-10 (slope) and Fig. 4-5
α	6.92 × 10 ⁻⁵	fraction	Eq. 38 (slope) and Fig. 4-6

A high $k_{o_3,LNR}$ value (293 M⁻¹s⁻¹) and low k_{OOH} (14.2 M⁻¹s⁻¹) justifies the observation that OH⁻ plays a much more important role at pH levels above 9 than pH levels below 9. It has been reported that $k_{o_3,LNR}$ is 1.9 M⁻¹s⁻¹ (Benitez et al., 2007a) or 3.1 M⁻¹s⁻¹ at pH 2.0 (DeLaat et al., 1996), which is lower than the value obtained in this study. This can be rationalized by the pKa value of LNR and the highly electrophilic property of ozone. The pKa of phenylurea was reported to vary in the range from 4.3 to 5.5 (Lopez et al., 2005), as a result, LNR would be charged positively at pH 2 while charged negatively at pH 9-11 in this study. The negatively-charged compounds show higher reactivity toward ozone than positively-charged one (Hoigne and Bader, 1983), leading to a higher $k_{o_3,LNR}$ value under basic conditions. The k_{OOH} is lower than the value (48 ± 12 M⁻¹s⁻¹) reported previously (Forni et al., 1982). It is probably because the value reported by Forni was determined at pH levels of 11.2-12.3 while pH level in this study varied from 9 to 11. The $k_{OH,LNR}$ was

determined to be $2.74 \times 10^9 \text{ M}^{-1}\text{s}^{-1}$ which is about the same order of the value $(4.2 \pm 0.4) \times 10^9 \text{ M}^{-1}\text{s}^{-1}$ with 248 nm UV irradiation reported by López et. al. (Lopez et al., 2005).

The observed LNR decay rate and predicted overall decay rate by the proposed model under various conditions were compared and shown in Table 4-3, where the error ranges from 2.2% to 11.5%, indicating the proposed models offer an accurate way to predict the LNR decay in the UV, O₃ and UV/O₃ under varied conditions.

Table 4-3: Comparison between the predicted k_{overall} from the proposed model and the observed k_{overall}

Reaction conditions	Predicted k_{overall} based on the proposed model (s^{-1})	Observed k_{overall} in this study (s^{-1})
Sole-UV system		
$I_0 = 9.0 \times 10^{-6} \text{ Einstein L}^{-1}\text{s}^{-1}$ [LNR] ₀ = 0.1 mM	3.27×10^{-3}	3.20×10^{-3}
Ozone system		
[O ₃] = $1.71 \times 10^{-5} \text{ M}$ pH = 11.0 [LNR] ₀ = 0.1 mM	1.23×10^{-2}	1.38×10^{-2}
Ozone system		
[O ₃] = $9.96 \times 10^{-6} \text{ M}$ pH = 11.0 [LNR] ₀ = 0.1 mM	7.16×10^{-3}	7.00×10^{-3}
UV/Ozone system		
[O ₃] = $3.09 \times 10^{-5} \text{ M}$ $I_0 = 6.0 \times 10^{-6} \text{ Einstein L}^{-1}\text{s}^{-1}$ pH = 6.0 [LNR] ₀ = 0.1 mM	1.304×10^{-2}	1.154×10^{-2}

4.3 Summary

In this chapter, the degradation for LNR by UV, O₃, and UV/O₃ processes has been investigated. The decay rate of linuron by UV/O₃ process was found to be around 3.5 times and 2.5 times faster than sole-UV and ozone-alone, respectively. No TOC removal was observed in sole UV process, and TOC removal was insignificant in ozonation process (about 15% mineralization after 100 minutes). However, nearly 80% mineralization was achieved by using UV/ozone process after 100 minutes. The overall rate constants increase exponentially with pH above 9.0 while the increase of rate constants with pH below 9 is insignificant in O₃ system. All predominating parameters involved in the three processes were determined in the assistant of proposed linear models. The proposed approach could furnish a useful method to explore the major kinetic constants, while minimizing the requirement in defining the minor rate constants. This is helpful in real applications for determining a quick but accurate prediction in system design.

Chapter 5 Reaction Mechanism of LNR Degradation by UV Photolysis, Ozonation and UV/O₃ Process

5.1 Introduction

Herbicides have been widely used as a regular and effective practice to increase the productivity of crop fields. The enormous majority of herbicides, however, are diffused into aquatic environment via agricultural runoff or leaching, only a tiny part of total applied herbicides reaching the target pests. (Pimentel, 1995). Herbicides, therefore, have been some of the most frequently detected organic contaminants in natural waters. On the other hand, increasing demand of high quality water results in intensive concern about the possible effect of such substances on human health and ecological environment (Colborn et al., 1993; Daam et al., 2009).

LNR was still chosen as target compound in this chapter. Various treatment techniques has been developed to destruct LNR in recent years (Faure and Boule, 1997; Dejonghe et al., 2003; Farre et al., 2007; Chen et al., 2008; ; Benitez et al., 2009). A major part of the investigation, however, focuses on the removal or decomposition of LNR. If the fate of the resulting products remains unanswered, the treatment process cannot be proposed as a trouble-free method since the decay of the parent compounds may result in the generation of more toxic organics than parent compounds. The intermediates from the transformation of LNR vary with treatment methods since different methods offer differed reaction mechanisms. Even LNR is treated by the same process, the identification and fate of intermediates could still

vary with researchers since the decay of LNR is condition-dependent. As a result, the investigation of the resulting products is necessary in each process.

Only four photoproducts have been identified during the phototransformation of LNR in aqueous phase under the irradiation of UV at 254nm in earlier study (Faure and Boule, 1997) and the evolution and destination of these products still remains unanswered. In addition, the information about the reaction mechanism of LNR by UV/O₃ process and the fate of intermediates generated during this process is scanty so far. Therefore, in this study, the degradation intermediates of LNR by UV, O₃, and UV/O₃ were investigated and the decay pathways were proposed accordingly for these three processes, respectively. The effect of initial pH level on the decay of LNR by these three processes and the influence of various anions on the decomposition of LNR by ozonation have also been examined. And some major products which escaped identification in the earlier studies are presented in this chapter.

5.2 Results and Discussion

5.2.1 The effect of initial pH level on the decay of LNR by UV, O₃ and UV/O₃ processes

The decomposition of LNR was tested at varied pH levels (from 3 to 11) by different treatment processes: (1) UV photolysis, (2) ozone, and (3) combined UV/ozone system. The photolysis and oxidation of LNR were found to follow pseudo-first-order kinetics at various initial pH levels and the observed rate constants are summarized in Figure 5-1a. As indicated in Figure 5-1a, an increased degradation rate was observed at elevated pH levels both in ozone and UV/ozone systems. It is

well-known that the hydroxide ion can initiate the decomposition of ozone to produce hydroxyl radicals which is a stronger oxidant than ozone in aqueous solution (Forni et al., 1982). The pH level, therefore, plays a major role in the reactions involved with ozone. It is also interesting to observe that photolysis of LNR is pH-independent. No decay of LNR after 50 min was observed at three different pH levels 3, 7, and 11 in a separate test, suggesting there is no acid-or-alkaline catalyzed hydrolysis.

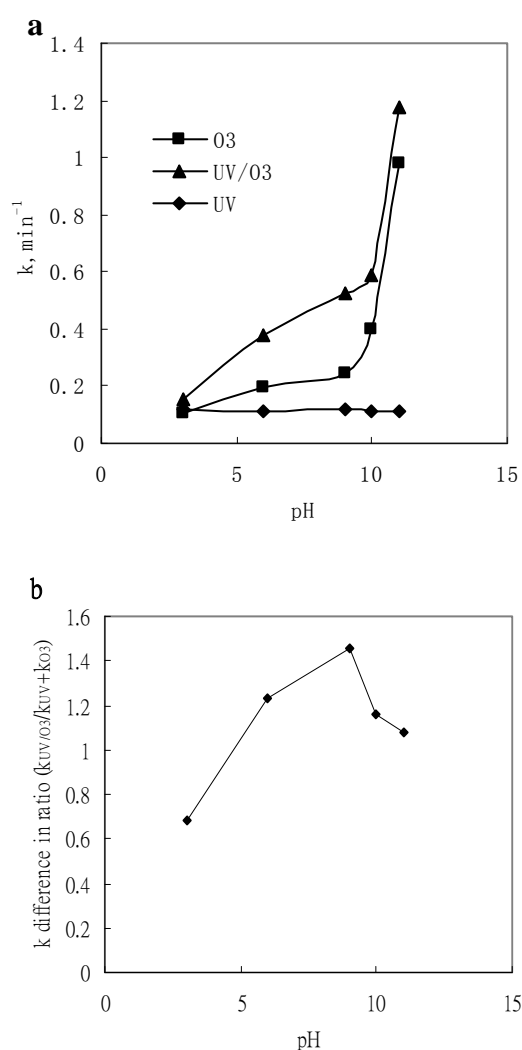


Figure 5-1: (a). Pseudo first-order rate constants at different initial pH level by different degradation process. (b). The ratio of $k_{\text{UV/O}_3}$ and $k_{\text{UV}} + k_{\text{O}_3}$ (Notes: $[\text{LNR}]_0 = 0.1 \text{ mM}$, $[\text{O}_3]_0 = 0.0171 \text{ mM}$, $[\text{I}_0] = 6.0 \times 10^{-6} \text{ Einstein L}^{-1} \text{ s}^{-1}$)

It is believed that the combined UV/O₃ system can offer a synergistic effect of individual reactions: direct ozonation, direct photolysis, and HO[•] oxidation. In this study, the UV/O₃ process has proved that it is an effective treatment of LNR from neutral to high pH levels (Figure 5-1a) and 80% TOC removal could be achieved within 100 min reaction as presented in chapter 4. In order to optimize the UV/O₃ process at different pH levels, the synergistic effect was examined by comparing the ratio of reaction rate constants of UV/O₃ versus the summation of direct ozonation and direct photolysis as illustrated in Figure 5-1b. At pH 3, the ratio is smaller than unity indicating no synergistic effect at all. It was reported that UV irradiation at 254 nm led to all the ozone being photolyzed into hydrogen peroxide which is much weaker oxidant when compared to ozone and hydroxyl radicals (Canton et al., 2003). In addition, hydrogen peroxide is very stable at acidic pH, the chance for forming hydroxyl radicals due to the interaction between UV and H₂O₂ is minimal. Therefore, no significant rate improvement was observed by combining UV and O₃ at pH 3 (Chu, 2001).

As pH level gradually increased, the synergistic effect becomes more perceptible, and reaches a maximum at around pH 9. This is resulting from the formation of hydroxyl radicals from both ozone molecules and UV/H₂O₂ process.

However, it is interesting to note that the synergistic effect drops as pH is further increased. This is because the intermediate H₂O₂ is very unstable at very high pH levels. The H₂O₂ can easily decay into water and oxygen and the total oxidation capability of the process reduced. This phenomenon may be rationalized by another possible reason that high concentration of hydroxide ion can also initiate the

decomposition of ozone into hydroxyl radicals in sole-ozone system. UV, thus, may not play a key role in terms of the generation of hydroxyl radicals in UV/O₃ system.

5.2.2 The effect of varied anions on the LNR decay in sole-ozone system

The effect of various cations such as Mn²⁺, Fe²⁺, Co²⁺, Zn²⁺, Cu²⁺ and Ti²⁺ on the performance of ozonation process has been well documented (Pines and Reckhow, 2002; Canton et al., 2003; Ni et al., 2003; Xiao et al., 2008). The information about whether or not the anions may influence the functioning of sole-ozone process still remains very limited.

In this section, the effect of various anions on the LNR decay was investigated at pH 3 and 7 in sole-ozone system. As indicated in Figure 5-2, the existence of 0.01 M chloride leads to the significant retardance in the decay rate of LNR at pH 3 while Chloride does not show considerable influence on the degradation of LNR at pH 7. It was reported chloride could react with ozone under acidic conditions as shown in Eqn. 5-1 and Eqn. 5-2 (Yeatts and Taube, 1949):



The first reaction is the rate-determining reaction while the second one is reversible. High concentration of hydrogen ion favors the second reaction proceeding towards the right side. Therefore, at pH 3, chloride ions can effectively compete for O₃ with LNR to produce Cl₂ which is much weaker oxidant than ozone. On the other hand, at pH 7, lower proton concentration deactivates the above reactions, restricts the reaction between ozone and chloride, and minimizes the competition between

chloride and LNR for O_3 . In addition, a little retardance in the LNR decay rate was observed after 4 min reaction at pH 7 with the existence of 10 mM chloride (See Figure 5-2b). This is possibly due to the decrease of pH during the reaction as shown in Figure 5-2c.

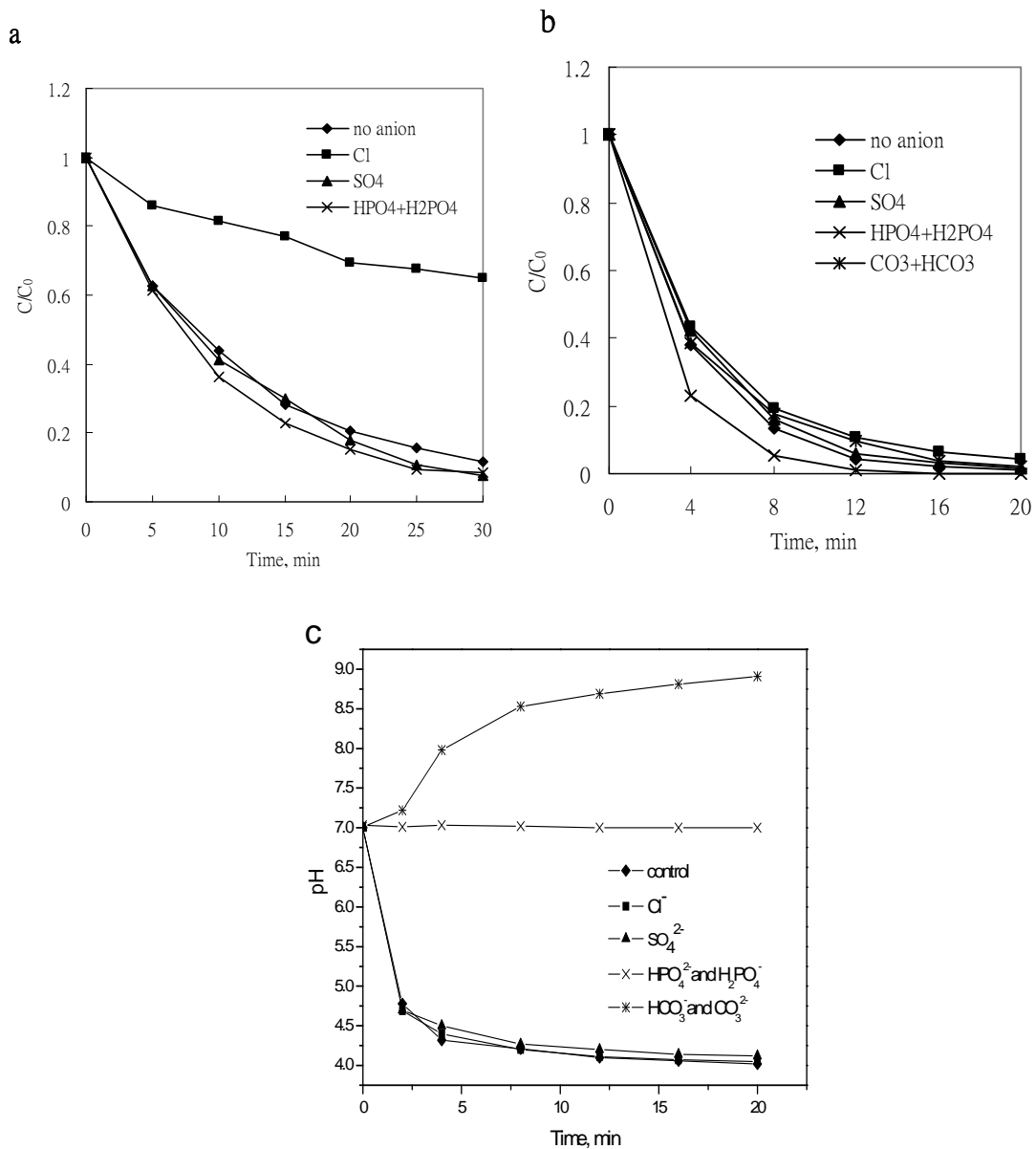


Figure 5-2: (a) The effect of varied anions on the performance of ozonation at pH 3; (b) The effect of varied anions on the performance of ozonation at pH 7; (c) The variation of pH during the ozonation of LNR with the presence

of various anions. (Notes: $[\text{LNR}]_0 = 0.1 \text{ mM}$, $[\text{O}_3]_0 = 0.0245 \text{ mM}$, $[\text{anions}] = 0.01 \text{ M}$)

It is also interesting to note the LNR decay rate accelerates with the existence of HPO_4^{2-} and H_2PO_4^- at pH 7 while such an effect is not significant at pH 3, in which the solution pH remains stable during the reaction for every scenario (data not shown). At pH 7, the buffer ability of HPO_4^{2-} and H_2PO_4^- made the pH of the solution very stable during the reaction while the pH value decreased from 7 to 4.78 during the first 2 min reaction in the case of no anion as indicated in Figure 5-2c. The higher pH level may result in the faster decay of LNR in the reaction with the existence of HPO_4^{2-} and H_2PO_4^- , as discussed previously.

When 0.01 M Na_2CO_3 was added into the solution at pH 7, another interesting point is the increase of pH level during the reaction did not guarantee an improvement of LNR decay rate even though the higher pH should theoretically favors the faster decay of LNR. This may be because carbonate ions can quench the hydroxyl radicals in the solution to generate hydroxide ions as described in Eqn. 5-3:



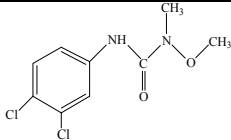
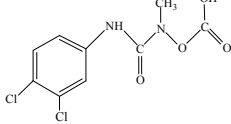
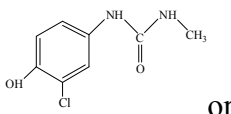
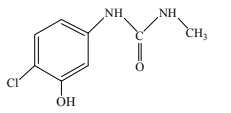
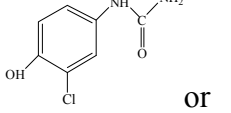
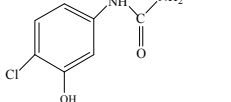
Since carbonate and bicarbonate can compete for hydroxyl radicals with LNR, which can hinder the beneficial effect resulting from the increment of pH level, these two effects counteract each other and this rationalizes no appreciable influence of bicarbonate and carbonate ions on the LNR degradation rate.

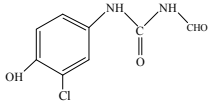
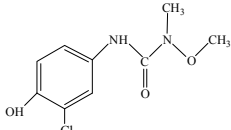
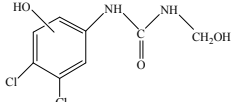
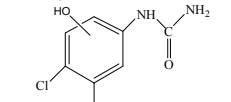
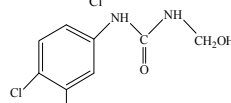
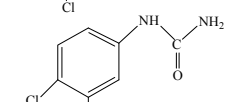
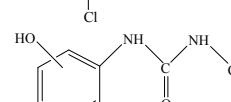
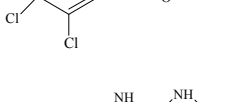
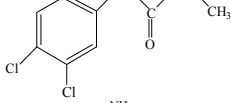
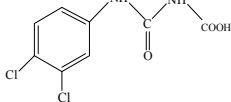
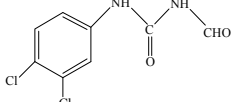
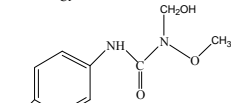
5.2.3 Reaction mechanism of LNR degradation

In order to gain a deep insight into the LNR degradation by UV, ozone and UV/ozone processes, the intermediates were identified and the evolution of major

intermediates was investigated in each process. Seventeen intermediates were identified during LNR degradation by these three processes. The information on the intermediates including the mass of deprotonated ion ($[M-H]^+$) of the daughter compounds, the proposed molecular structure, and the proposed fragments is summarized in Table 5-1. Actually, $[M + \text{acetate}]^-$ ions were obtained as a base peak of the mass spectra for most intermediates and LNR (See Appendix II) due to 5 mM ammonium acetate being used as mobile phase and negative-ion mode being employed in this study (Barcelo and Albaiges, 1989). Some of their mass spectra are shown in Appendix II.

Table 5-1: Identified degradation products and their main fragments determined by LC/ESI-MS

Compound	Retention time	Molecular weight	Molecular ion and main fragments	Structural formula	Detected in		
					UV	O ₃	UV/O ₃
LNR	20.93	248	247, 217, 188, 160, 109		√	√	√
1	10.25	278	277, 250, 233, 217, 119				√
2 and 3	10.61, 12.62	200	199, 142	 or 	√	√	√
4	11.61	186	185, 165, 141, 119	 or 	√		√

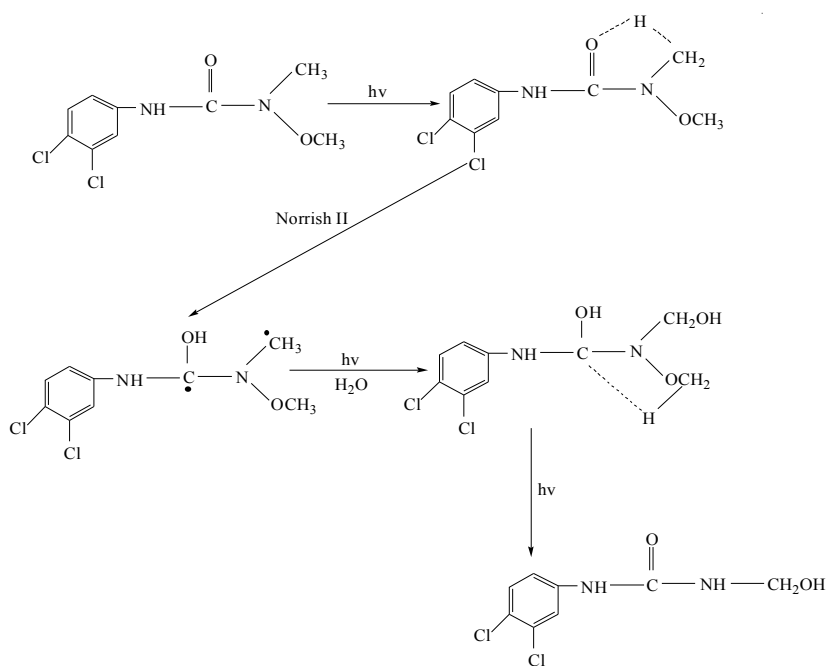
5	13.12	214	213		√	√
6 and 7	14.11 and 15.40	230	229, 37, 119, 109		√	√
8	14.90	250	249, 219, 202, 176, 137, 119, 109			√
9	15.44, 15.56	220	219, 203, 176, 137, 119, 109			√
10	15.68	234	233, 203, 160, 137, 119, 109		√	√
11	16.31	204	203, 160, 137, 119, 109		√	√
12	16.93	234	233, 202, 176, 137, 119, 109		√	√
13	17.46	218	217, 160, 137, 119, 109		√	√
14	18.74	248	247, 202, 204		√	√
15	18.93	232	231, 202, 188, 160, 137, 119, 109		√	√
16 and 17	19.30, 19.72	264	263, 233, 217, 202, 188, 156, 119, 109	 or 		√

(1) UV photolysis

The direct photolysis of LNR and evolution profiles of intermediates by UV at 254 nm is shown in Figure 5-3. The LC-MS analysis revealed that twelve intermediates were produced during the reaction. The “demethoxylation” pathway is believed to be one of major reaction pathways since compound 13 (DCPMU) is the dominating intermediate during photolysis of LNR as indicated in Figure 5-3a. Similar observation has been reported earlier (Faure and Boule, 1997). The formation of intermolecular hydrogen bond between one hydrogen atom of *N*-methoxyl and the oxygen of neighboring C=O bond and subsequent generation of formaldehyde was proposed to be the mechanism of this demethoxylation pathway. Faure and Boule reported four intermediates (compounds 6, 7, 11 (DCPU) and 13 (DCPUM)) in the photolysis of LNR by UV at 254 nm (Faure and Boule, 1997) while eight new intermediates (compounds 2, 3, 4, 5, 10, 12, 14 and 15) were detected in this study. Photohydrolysis-dechlorination is believed to be another major reaction mechanism during the photolysis of LNR by UV at 254 nm, judging from the yields of the products from photohydrolysis-dechlorination and chloride ions during the reaction (See Figure 5-3c). There are two pairs of isomers (6 and 7, 2 and 3) which are the products of Photohydrolysis-dechlorination among these intermediates. Compounds 6 and 7 are believed to come from the hydroxylation on the ring with simultaneous dechlorination of LNR. Compounds 2 and 3 originate from the photohydrolysis-dechlorination of compound 13 (DCPMU), and the photohydrolysis-dechlorination of compound 11 (DCPU) produces compound 4, which have been corroborated by two individual tests using compound 13 (DCPMU) and 11 (DCPU) as initial probe compounds by UV process at 254 nm. In addition, compound 12 was detected in the degradation of both LNR and compound 13 (DCPMU) by UV irradiation at 254 nm, indicating this product is from the hydroxylation of benzene ring of DCPMU. The

hydroxylation of benzene ring has been reported by other researchers (Jin et al., 1995; Lau et al., 2007). Jin et al. proposed two possible mechanisms (One is the presence of oxygen leading to the production of $O_2^{\bullet-}$ and HO_2^{\bullet} , and another one is that benzene ring of the parent compound is hydroxylated via endoperoxide not involving free radicals). Oxygen was believed to be involved in both mechanisms, and it was suggested that the presence of oxygen could significantly increase the decay rate of tyrosine (Jin et al., 1995). This, however, is not observed in this study. In a separate test that the LNR solution was deoxygenated by argon before and during the irradiation by UV at 254 nm, the same twelve intermediates were identified and no reduction in LNR decay rate was observed in the absence of oxygen.

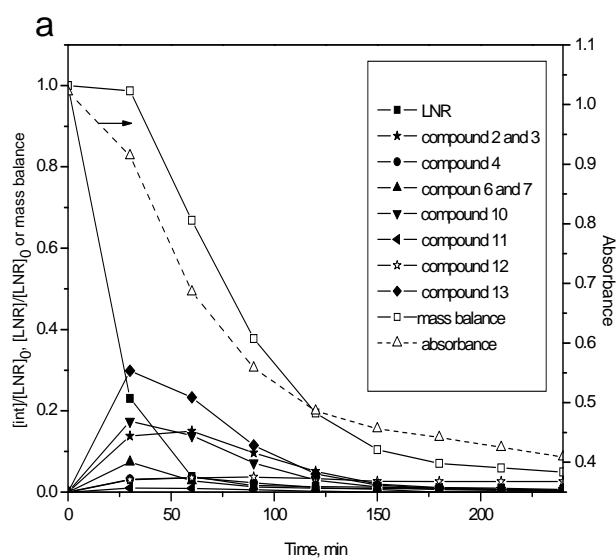
A different mechanism---direct hydrolysis of benzene ring of DCPMU, not involving oxygen, thus, is proposed and may rationalize the generation of compound 12. Compound 10 also escaped from the identification in earlier study. It is reasonable to assume that compounds 10 and 11 (DCPU) originate from *N*-oxidation and subsequent demethylation of DCPMU, respectively as observed in the work of Jirkovsky et al. (Jirkovsky et al., 1997). However, it is interesting to note that compounds 10 and DCPU were not detected in the photolysis of DCPMU, indicating DCPMU is not the source of compound 10. Compound 10 and 11 were detected in the photolytic degradation of LNR without the existence of oxygen, suggesting that oxygen was not involved in the production of these two compounds, either. The possible mechanism for the generation of compound 10, therefore, was proposed as below:



DCPU is believed to result from compound 10 since the photolysis of DCPMU does not generate DCPU. Therefore, the decay pathway of LNR by UV process was proposed (Figure 5-5) on the basis of the evolution profile analysis of intermediates during the photolysis of LNR and the information about the intermediates from the photolysis of DCPMU and DCPU. The percentages in Figure 5-5 stand for the fraction of LNR transformed to a particular product during the initial phase (30 minutes). Figure 5-5 also reveals that demethoxylation is predominant decay mechanism of LNR by UV process at 254 nm since 63.1% ($[\text{DCPMU}] + [\text{compound 2 and 3}] + [\text{compound 12}] / [\text{LNR}]_{\text{removed}}$) of LNR was eliminated via this pathway. Furthermore, the individual test using DCPMU as the initial compound reveals that photohydrolysis-dechlorination is the dominating mechanism in terms of the photolysis of DCPMU (96.9% of DCPMU was removed via this pathway) (See Figure 5-4).

Figure 5-3b shows UV spectrum of the reaction solution at different time intervals. It is well-known that a benzene ring has two absorption bands (One occurs near 205

nm, and another one appears near 250 nm). As indicated in Figure 5-3b, both absorption bands are dwindling during the photolysis reaction. Judging from the mass balance of benzene ring and the decreased absorbance of the solution at 254 nm (See Figure 5-3a and Figure 5-3b), it is believed that ring-opening occurs during the photolytic decomposition of LNR. Unfortunately, mineralization of LNR was not observed in this process due to the lack of oxidants as demonstrated in the TOC curve (Figure 5-3c). Figure 5-3c also demonstrates that photohydrolysis-dechlorination led to considerable decrease of pH level from 6.0 to 3.59. It was observed that around 98% of chlorine on the benzene ring was released and trace amount of NH_4^+ and NO_3^- was detected, indicating de-nitrogenation could be achieved in the photolytic degradation of LNR by UV at 254 nm.



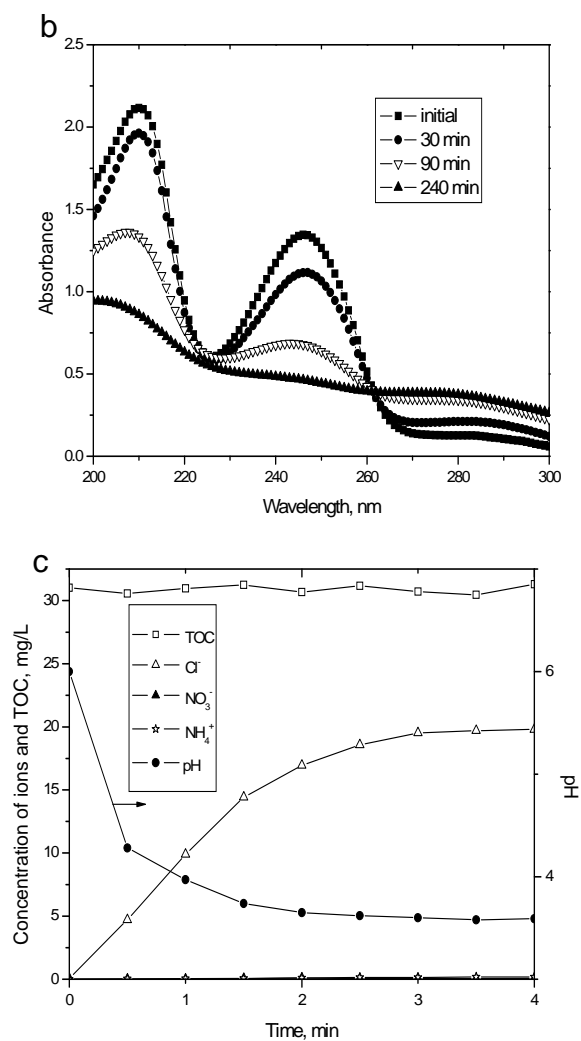


Figure 5-3: (a) The evolution profiles of LNR and intermediates in the photolysis of LNR at 254 nm; (b) UV absorption spectrum of the solution at different time intervals; (c) The evolution profiles of TOC, pH, Cl^- , NO_3^- , and NH_4^+ .

(Notes: $[\text{LNR}]_0 = 0.285 \text{ mM}$, $\text{pH}_0 = 6.0$, $[I_0] = 9.0 \times 10^{-6} \text{ Einstein L}^{-1} \text{ s}^{-1}$)

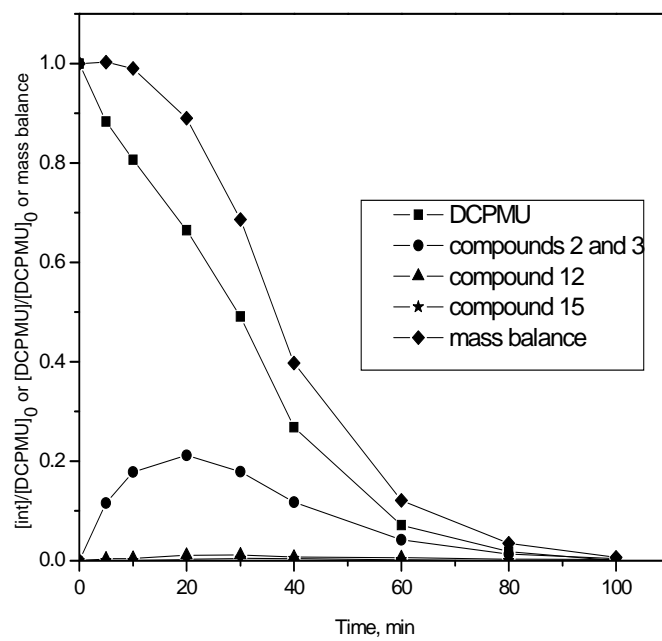


Figure 5-4: The evolution profiles of DCPMU and intermediates in the photolysis of DCPMU at 254 nm

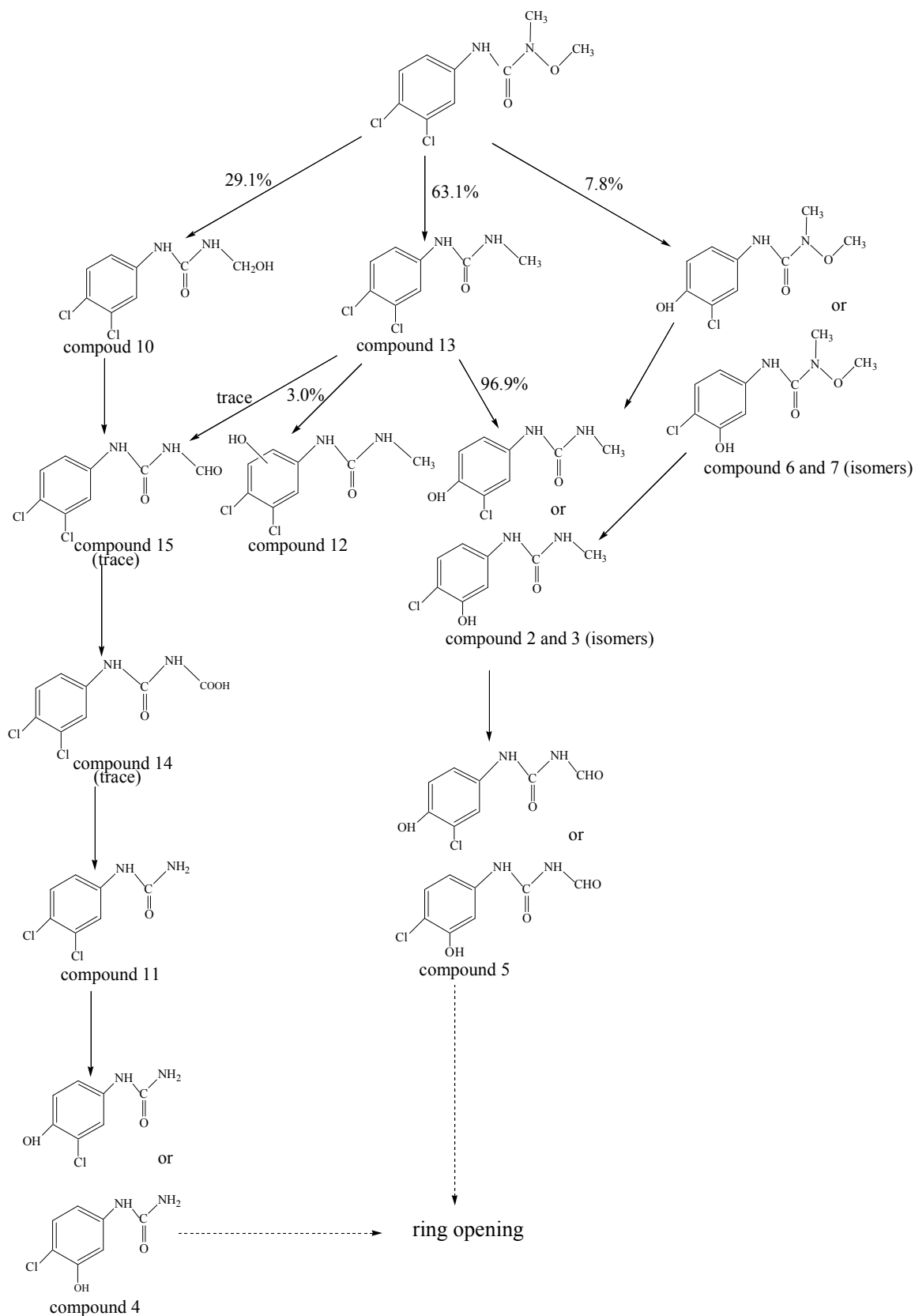


Figure 5-5: The decay pathways of LNR under the irradiation by UV at 254 nm.

(2). Ozonation

Benzene ring is susceptible to electrophilic attack (by electrophilic agents) due to its exposed π electrons. However, substituted groups on the benzene ring are believed to exert a significant influence on the reactivity of electrophilic reaction. LNR is tri-substituted by two chlorines and a side chain ($\text{NHCHON} \begin{matrix} \text{OCH}_3 \\ \text{CH}_3 \end{matrix}$). Bi-substitution by chlorine may result in decrease on the electron density of benzene ring due to electron-withdrawing ability of chlorine while the side chain can be a moderately activating substituent because the unshared electron pair on the nitrogen atom adjacent to the benzene ring may make a contribution to the electron density on the benzene ring through resonance (Solomons, 2006). Ozone is highly electrophilic agent. The degradation of LNR by ozonation, therefore, becomes very complicated. Ten intermediates were identified and summarized in Table 1 in this study. The evolution profiles of LNR and four major intermediates (compound 6 or 7, 10, 11, 13) were demonstrated in Figure 5-6a. It is interesting to note that the profile of mass balance is quite similar to that of LNR, indicating the intermediates only account for a small portion to the total mass. This may be because most intermediates are susceptible to ozonation process. In addition, trace amount of six intermediates (compound 2 and 3, 12, 15, 16 and 17) were detected in this system. Compound 6 or 7 is believed to come from the dechlorination-hydroxylation of LNR while compound 16 and 17 may originate from the *N*-terminus oxidation of LNR. Demethoxylation of LNR leads to the generation of compound 13 (DCPMU). All six other intermediates (compounds 2 and 3, 10, 11, 12 and 15) are believed to come from DCPMU, which was confirmed by an independent test using DCPMU as initial probe compound in this system. Compounds 2 and 3 are from dechlorination-

hydroxylation of DCPMU. *N*-terminus oxidation of DCPMU produces compound 10 and 15. Compound 11 (DCPU) is believed to result from the demethylation of DCPMU while hydroxylation of benzene ring of DCPMU gives rise to the production of compound 12. A decay pathway of LNR by ozonation, thus, was proposed accordingly (See Figure 5-8).

Judging from the low yield of compound 6 or 7, the dechlorination is likely to be minor mechanism of LNR decay by ozonation while *N*-terminus oxidation may be major mechanism. However, more than 50% of total chlorine was released after 20 min of reaction as shown in Figure 5-6b, which contradicts to the previous assumption. One possible explanation is that dechlorination-hydroxylation intermediates may not accumulate to appreciable level due to fast decay. When chlorine is substituted by hydroxyl, the electron-donating resonance effect of hydroxyl favors the enhancement of the electron density on the benzene ring and the susceptibility of these dechlorination-hydroxylation intermediates to ozonation.

Although mass balance of benzene ring nearly approaches zero, the TOC removal is only around 25% after 120 min (See Figure 5-6b). This may be due to the high selectivity of ozone leading to its incapability to degrade some small organic compounds resulting from the cleavage of benzene ring. As shown in Figure 5-6b, pH decreases significantly during the initial 20 minutes of the reaction due to the release of chloride and probably the generation of aliphatic acid. Figure 5-6b also reveals that 13% of nitrogen was released to the solution as nitrate and ammonia ions after 120 min.

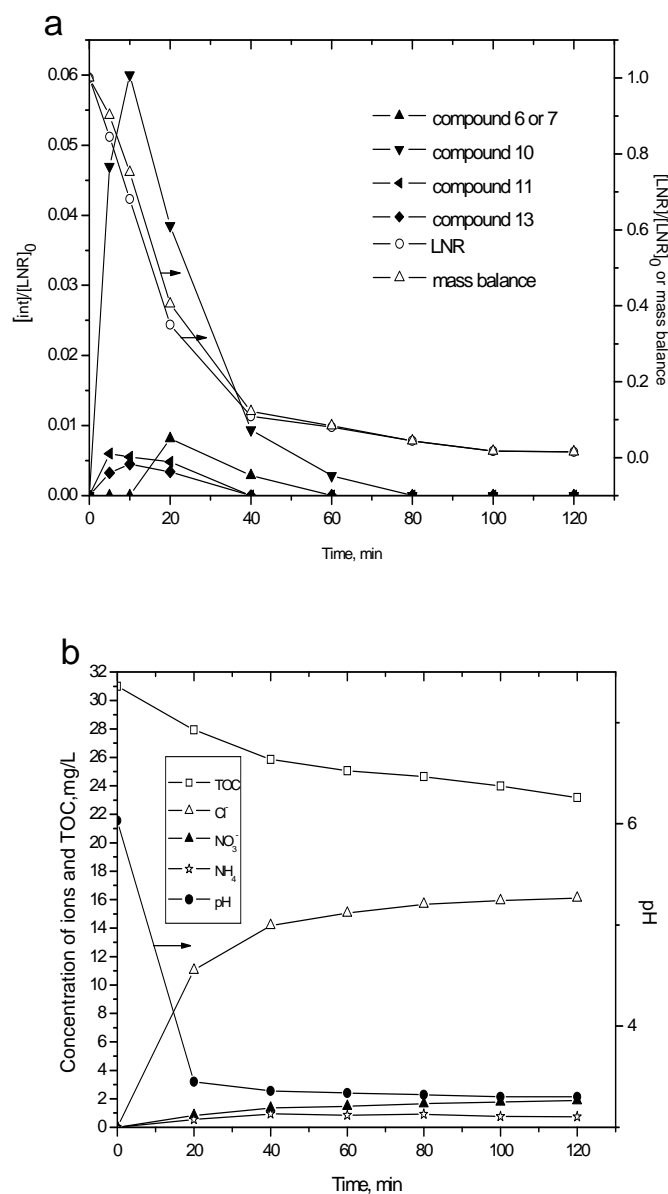


Figure 5-6: (a) The evolution profiles of LNR and intermediates for the degradation of LNR by ozonation; (b) The evolution profiles of TOC, pH, Cl^- , NO_3^- , and NH_4^+ for the degradation of LNR by ozonation.

(Notes: $[LNR]_0 = 0.285$ mM, $[O_3] = 0.0245$ mM, $pH_0 = 6.0$)

(3) UV/ O_3 process

It is generally agreed that several individual reactions such as direct (molecular) ozonation, direct photolysis, and radical oxidation (mainly hydroxyl radical) involve

the degradation of organic compounds by UV/O₃ process. Therefore, more intermediates (seventeen) were detected in this system than sole-ozone and sole-UV (See Table 5-1). The evolution profiles of LNR and major products were shown in Figure 5-7 a. The decay pathway of LNR by UV/O₃ was proposed as illustrated in Figure 5-8, where the degradation pathways by UV/O₃ are quite similar to that of ozonation. However, the yield of major intermediates is much higher in UV/O₃ system than that of major products in sole-ozone system as indicated in Figure 5-7a. This is likely because these intermediates originate from more decay mechanisms in parallel including photolysis, radical oxidation and oxidation offered by ozone molecule. At the initial stage of reaction, photolysis may play a major role in the degradation of LNR since both UV/O₃ and UV processes produce the same dominating intermediates (the yield of compound 13 is the highest and followed by compound 10) (See Figure 5-3a and Figure 5-7a). This phenomenon can be rationalized by the following:

- (a) Ozone can be rapidly photolyzed into hydrogen peroxide under UV irradiation at a wavelength of 254 nm due to its high molar absorptivity ($3600 \text{ M}^{-1} \text{ cm}^{-1}$) and quantum yields (0.48) (Gurol and Akata, 1996); and
- (b) The low absorption coefficient of H₂O₂ ($19.6 \text{ M}^{-1} \text{ cm}^{-1}$) (Gurol and Akata, 1996) may make H₂O₂ incapable of competing with LNR (the absorption coefficient of LNR is $13254 \text{ M}^{-1} \text{ cm}^{-1}$) for photons to produce hydroxyl radical.

The evolution of TOC, pH and varied ion products in this system was also investigated in this study (See Figure 5-7b). As demonstrated in Figure 5-7, the UV/O₃ process have shown several advantages over sole-UV and ozonation including: (1) more than 86% mineralization; (2) faster degradation of LNR (Complete decomposition of LNR was observed after 25 min); (4) greater and faster

removal in terms of mass balance; (3) greater and faster dechlorination and denitrogenation (Complete release of chlorine was achieved after 80 min and around 56% of nitrogen was released as ammonia and nitrate ions after 120 min).

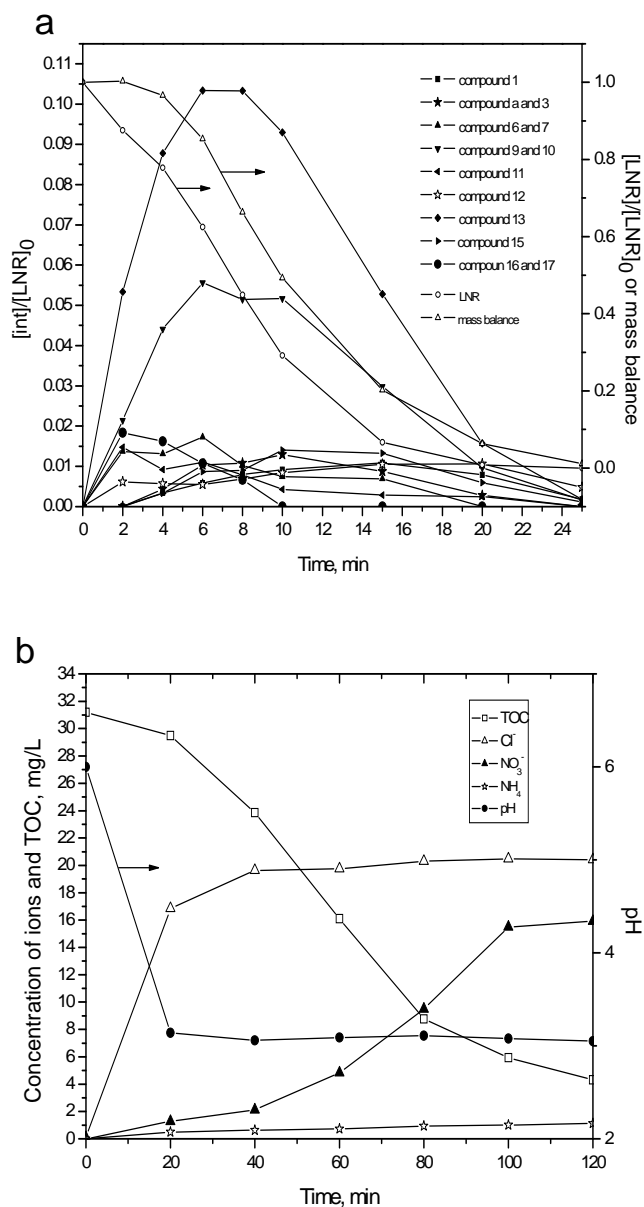


Figure 5-7: (a) The evolution profiles of LNR and intermediates for the degradation of LNR by UV/O₃; (b) The evolution profiles of TOC, pH, Cl⁻, NO₃⁻, and NH₄⁺ for the degradation of LNR by UV/O₃. (Notes: $[LNR]_0 = 0.285$ mM, $[O_3] = 0.0245$ mM, $[I_0] = 9.0 \times 10^{-6}$ Einstein L⁻¹ s⁻¹, $pH_0 = 6.0$)

5.3 Summary

The degradation of LNR by UV, O₃ and UV/O₃ processes was examined. It has been found the LNR decay is highly pH-dependent (especially in basic range) in both ozonation and UV/O₃ processes while UV process is pH-independent in terms of LNR decay. The effect of varied anions on the performance of ozonation was also investigated. Chloride ion was observed to significantly retard the degradation of LNR at pH 3 while it exerted no effect on the performance of ozonation at pH 7. The presence of phosphate ion led to the increase of LNR decay rate at pH 7 due to its buffer ability to keep pH stable and had no influence on the LNR degradation. In addition, the reaction mechanisms were proposed via identification of intermediates and evolution profile analysis of intermediates in UV, O₃ and UV/O₃ system. Among these three treatment processes, UV/O₃ process has exhibited the best overall performance. It demonstrated significant advantages not only in the decay rate of LNR but also achieving 86% mineralization at the end of the process (120 min).

Chapter 6 LNR Decomposition in Aqueous Semiconductor Suspension under Visible Light Irradiation-with and without H₂O₂

6.1 Introduction

Semiconductor-induced photocatalysis has received intensive attention as an environmental remediation technology over the past decades (van Schalkwyk et al., 2003; Spamer et al., 2003; Fu et al., 2006; Liu and Sun, 2007; Garcia-Lopez et al., 2007). Among all semiconductors, Titanium dioxide (TiO₂) is believed to be one of the most appropriate photocatalysts in terms of environmental application owing to its particularly optical properties, innocuity, low cost and enduring stability regarding photo- and chemical corrosion (Augugliaro et al., 1995; Hoffmann et al., 1995a). In general, a photon with energy higher than the bandgap energy ($E_g = 3.2$ eV and 3.0 eV for anatase and rutile phases, respectively) of TiO₂ can initiate the excitation of electron from the valence band (VB) to the conduction band (CB), leaving a hole, h_{vb}^+ behind (Hossain et al., 2008). These charged species are believed to induce the generation of free radicals such as HO• and O₂•⁻ which play a major part coupling with h_{vb}^+ in the oxidation of organic compounds (Hoffmann et al., 1995a). The widespread use of TiO₂ as an effective photocatalyst, however, has been curbed by its poor light absorption in the visible region due to its large band gap. Therefore, efforts have been devoted to improve the utility of TiO₂ by shifting its optical response from the UV to the visible spectral range. Using transition metal and nonmetal doping to lower the threshold energy for the excitation of electron in the valence band plays a

big part in these efforts (Asahi et al., 2001; Piera et al., 2003; Tachikawa et al., 2004; Huang et al., 2006; Niishiro et al., 2007; Zaleska et al., 2008). In addition, recently photosensitization via surface adsorbed organic dyes and coordination metal complexes also holds promise for extending TiO₂ absorption into the visible region (Cho et al., 2001; Fung et al., 2003; Wang et al., 2007). Whereas both doping and photosensitization have demonstrated successful performance in either narrowing the band gap of TiO₂ or sensitizing photocatalytic properties of TiO₂ towards visible light irradiation, the preparation process of photocatalyst is time-consuming and expensive, which may hinder the use of TiO₂ in practical applications. In this chapter, a novel and cost-efficient process was developed to allow the degradation of organic compounds in TiO₂ suspension under visible light irradiation with the assistant of H₂O₂.

The widespread application of herbicides as a regular and effective practice to control weed growth has led to increasing environmental concerns in the past decades because of their low biodegradability and long-term persistence in soil. Most herbicides are diffused into aquatic environment via agricultural runoff or leaching (Canle et al., 2001), which makes them ubiquitous. Linuron (LNR), selected as the probe contaminant in this chapter, has received particular attention in recent years due to the toxicity, being frequently detected in the surface and underground waters, and possible endocrine disrupting properties of LNR and/or its metabolites (Sorensen et al., 2005). Therefore, various treatment techniques have been developed to remove LNR in the aqueous phase, including biological methods (Dejonghe et al., 2003; Sorensen et al., 2005), direct photolysis (Faure and Boule, 1997), O₃/H₂O₂ (Tahmasseb et al., 2002), photo-Fenton procedure (Katsumata et al., 2005; Farre et

al., 2007), UV/H₂O₂ (Benitez et al., 2006) and photocatalysis under UV irradiation (Lopez et al., 2005). The information regarding the photocatalytic decay of LNR under visible light, however, is very limited.

In view of these, the major objectives of this chapter are to explore a new and effective approach to utilize visible light to degrade LNR with the aid of H₂O₂ in semiconductor suspension. The performance of the LNR degradation was investigated in this study under different conditions, such as selection of semiconductors, the effects of TiO₂ phase composition, TiO₂ dosage, the concentration of H₂O₂, and initial pH levels.

6.2 Results and Discussion

6.2.1 LNR degradation under visible light irradiation in TiO₂-H₂O₂ system

Many studies have shown that, under UV irradiation, H₂O₂ play a dual role in enhancing the semiconductor-sensitized photocatalytic degradation of organic compounds by acting either as an electron scavenger to prevent the recombination of e⁻ and h⁺ or as a direct source of hydroxyl radicals (Poulios et al., 2003; Wong and Chu, 2003; Kaniou et al., 2005; Nienow et al., 2008). However, under visible light, such information is limited.

In this section, the degradation of LNR was investigated under various conditions including the presence or absence of TiO₂ (P25), the processes with or without H₂O₂, and the use of visible light irradiation or in the dark. As shown in Figure 6-1a, it is interesting to observe that the elimination of LNR is insignificant in the systems of

P25/H₂O₂ (in the dark), Vis/P25 and Vis/H₂O₂ with LNR decay level of 8%, 10% and 8%, respectively, after a 3 hr of reaction. However, in the system of P25/H₂O₂/Vis, a pronounced enhancement of the reaction rate was observed resulting in a nearly complete decay of LNR.

Though the H₂O₂ itself could not degrade the LNR directly, by using P25/H₂O₂ in the dark about 8% of LNR removal was observed. This may result from the TiO₂ surface adsorption and the formation of an oxidizing agent, i.e., a titanium peroxide complex due to the interaction between H₂O₂ and valance-unfilled Ti (IV) on TiO₂ surface (Ohno et al., 2001; Li et al., 2001). It could be verified by both the color change on TiO₂ surface (turned into pale yellow) after the addition of H₂O₂ and the increase of H₂O₂ consumption to 9% comparing to that of 0% when no TiO₂ was involved (Figure 6-1b).

The use of visible light irradiation in the presence of P25, however, can slightly increase the LNR degradation to 10%. The upper threshold wavelength that P25 can absorb is 410 nm (Figure 6-2), which is within the emission spectra of the 420 nm lamps (Figure 3-4) and therefore likely leading to the production of trace amount of e⁻ and h⁺. However, another mechanism that might also contribute to the LNR decay was the surface complexation between organic compounds and TiO₂. It was reported that the formation of complex between the organic compounds harboring function groups such as -OH, -COOH, -NH₂ and ≡TiOH groups on the TiO₂ surface might initiate the degradation of organic compound upon absorbing visible light through ligand-to-metal charge transfer (Agrios et al., 2004; Paul et al., 2007). An additional test was conducted to verify the latter mechanism by adding 1 M MeOH, a well

known hydroxyl radical scavenger, into the reaction and no LNR decay was observed as demonstrated in Figure 6-1c. The result suggested that the hydroxyl radical, not the complex, was responsible for the LNR decay.

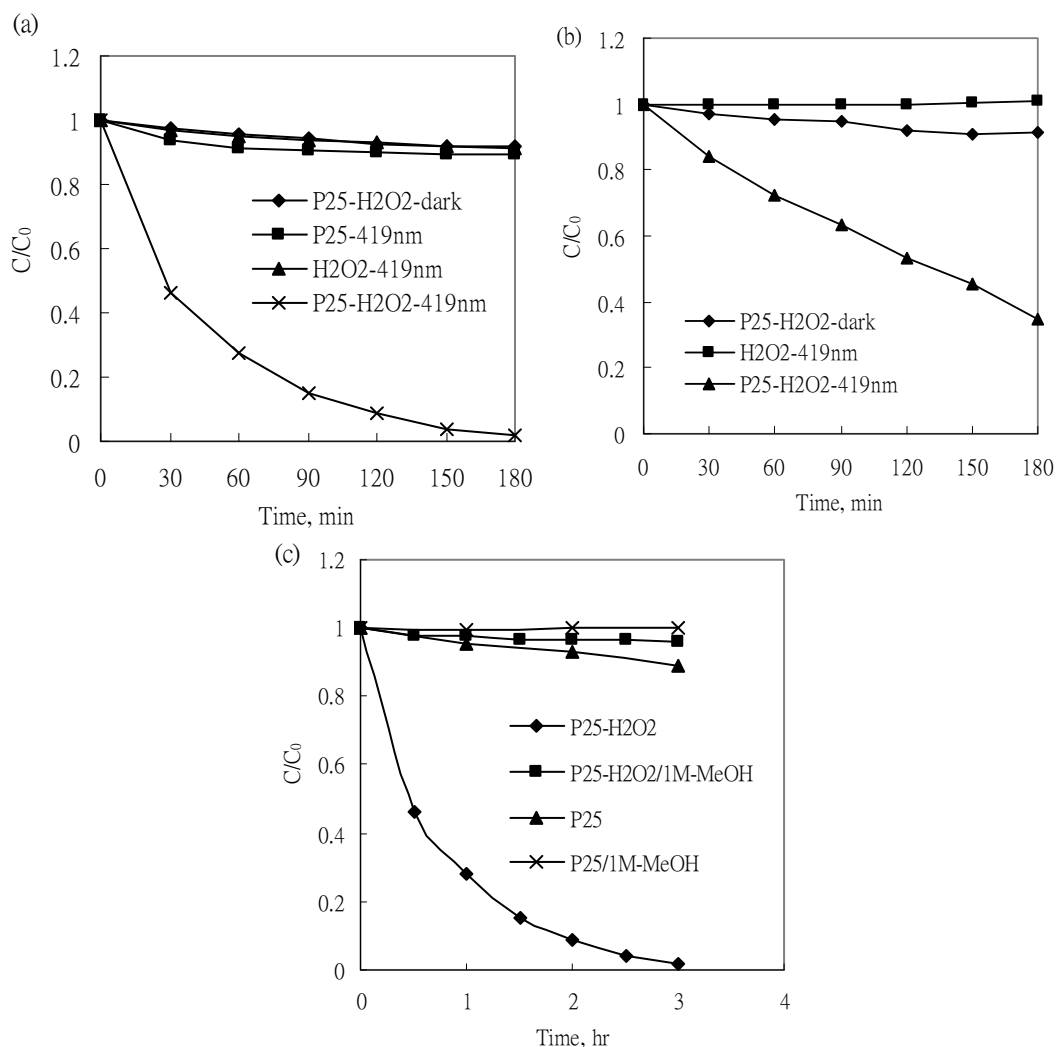


Figure 6-1: (a) LNR degradation under different reaction conditions; (b) H_2O_2 decomposition under different reaction conditions; (c) Effect of radical scavenger on visible-light photocatalysis of LNR with and without H_2O_2 . (Notes: initial LNR concentration is 0.1 mM, TiO_2 loading is 0.6 g/L, the initial concentration of H_2O_2 is 10 mM, initial pH value is 6.0)

It was interesting to reveal a synergistic effect in the process of P25/H₂O₂/Vis for a quick and complete removal of LNR. The possible explanations for this synergistic effect are: (1) H₂O₂ acts as an electron acceptor to prevent the recombination of e⁻ and h⁺ and/or offering additional hydroxyl radicals (Eqn. 6-1); (2) The interaction between H₂O₂ and TiO₂ leads to the formation of titanium peroxide complex on the TiO₂ surface which may act as oxidizing species under visible light (Ohno et al., 2001); (3) Titanium peroxide complex on the TiO₂ surface extend the photoresponse of TiO₂ to the visible region, leading to the visible-light-induced surface electron transfer from surface complexes to the conduction band of TiO₂. The electrons on the conduction band of TiO₂ initiate the decomposition of H₂O₂, which gives rise to the generation of hydroxyl radicals (Eqn. 6-2) (Li et al., 2001); and (4) It was reported that the water-oxide interface can lower the energy barrier for the H₂O₂ decomposition (Hiroki and LaVerne, 2005). As a result, additional hydroxyl radicals might be produced by the breakdown of H₂O₂ on the surface of TiO₂ under the irradiation of visible light (Eqn. 6-3).



where e_{direct}^- is the electron directly excited from the valence band to the conduction band of TiO₂ and e_{transfer}^- is the electron transferred from surface complexes to the conduction band of TiO₂. The addition of 1 M MeOH significantly inhibits the LNR degradation in this process as shown in Figure 6-1c, indicating that the LNR decay is dominated by various radicals that generated upon the irradiation of visible light while the direct oxidation of titanium peroxide complex may make a trivial contribution to the LNR decay.

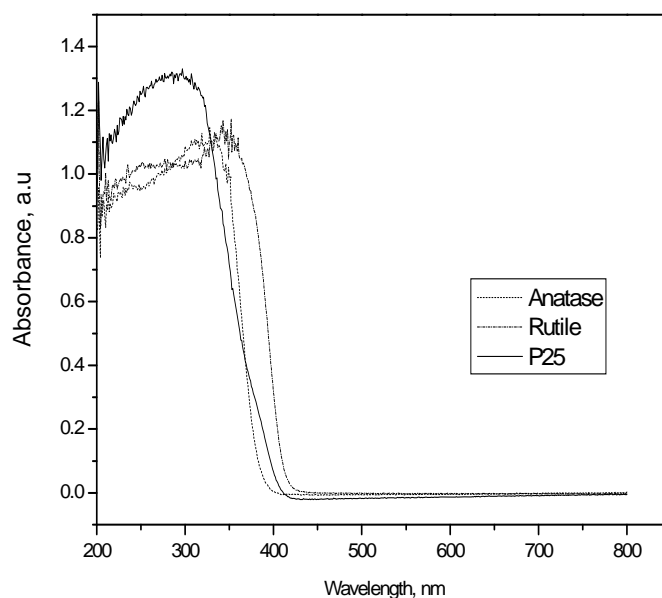


Figure 6-2: Diffuse reflection spectra of various TiO₂ powder

6.2.2 Effect of TiO₂ phase composition

The LNR degradation has been investigated in three different TiO₂ suspensions with or without H₂O₂ under visible light irradiation. Figure 6-3 shows that, in the absence of H₂O₂, anatase exhibited the highest reactivity (nearly 20% decomposition of LNR was achieved) and rutile was the worst. However, in the presence of H₂O₂, P25 demonstrated the best performance and followed by rutile and anatase. It is not unexpected that rutile displayed the lowest photocatalytic activity due to its narrow band gap unfavorable for the separation of photo-induced charges (Jing et al., 2008).

On the contrary, in the presence of H₂O₂, rutile showed a much better performance than anatase. The advantage of rutile in comparison with anatase is that the former can absorb a larger fraction of the emission spectrum of 419 lamps. Rutile powder can absorb photon up to 440nm while anatase shows absorption only up to 402nm

(data are not shown here). In addition, it was reported that Ti- η^2 -peroxide and Ti- μ -peroxide were the dominant bonds to be formed on the surface of rutile and anatase, respectively, in the presence of H₂O₂ (Ohno et al., 2001). By combining with our previous findings, it's very likely that the Ti- η^2 -peroxide has a better performance than the Ti- μ -peroxide in generating free radicals. The P25 demonstrated the best performance when using H₂O₂ as the additional hydroxyl radical source and this is because of its finest particle sizes (or largest surface area) as suggested by many researchers (Ohno et al., 2001; Hiroki and LaVerne, 2005).

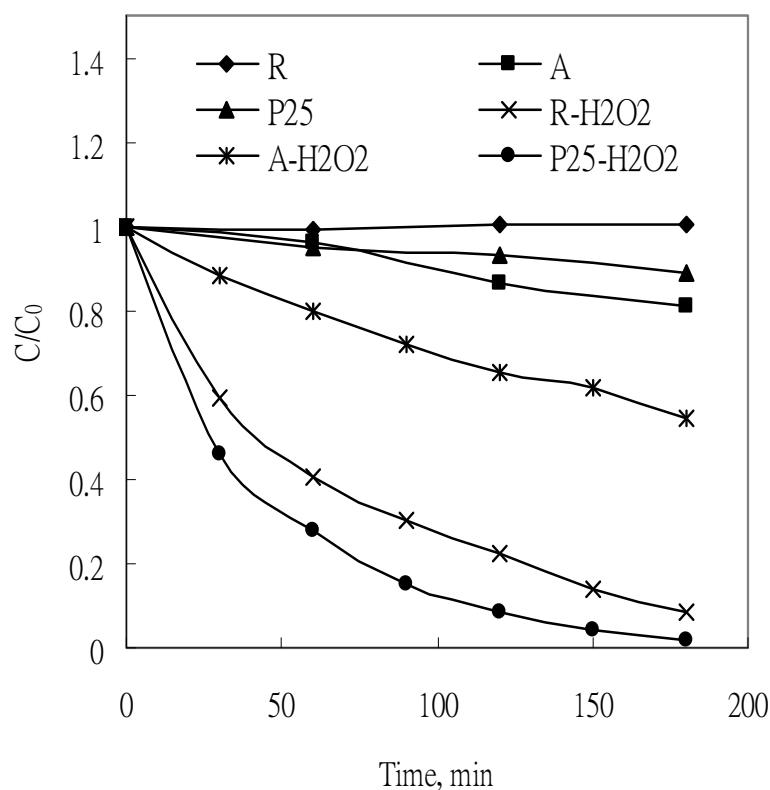


Figure 6-3: LNR degradation using different TiO₂ as photocatalysts with and without H₂O₂ (Notes: initial LNR concentration is 0.1 mM, TiO₂ loading is 0.6 g/L, the initial concentration of H₂O₂ is 10 mM, initial pH value is 6.0, R denotes rutile, A represents anatase.)

6.2.3 The performance of different semiconductors under various conditions

Several semiconductors were also examined as alternatives in this study. ZnO has been considered as a suitable replacement to TiO₂ since both are relatively inexpensive and have almost the same band gap energy. While the positive conduction band level of WO₃ (around 0.37 V vs NHE) might limit its use as a photocatalyst in terms of the oxidative degradation of organic compounds (Scaife, 1980), the addition of H₂O₂ to the system may exert a positive effect on the LNR decay by acting as an electron acceptor because the potential for the single-electron reduction of H₂O₂ was reported to be 0.32V vs NHE ($\text{H}_2\text{O}_2 + \text{e}^- \rightarrow \text{OH}^- + \text{HO}^\bullet$, 0.32 V vs NHE) (Castagna et al., 2008).

The profile of LNR decomposition in the suspension of the above three semiconductors under a variety of conditions is shown in Figure 6-4. It can be seen that purging O₂ led to a significant increase on the reaction rate in all cases. However, the mechanisms for the positive effect which O₂ exerts are different for the three semiconductors. In the case of TiO₂-P25 and ZnO, O₂ acts as an electron acceptor through single-electron reduction to prevent the recombination of photoinduced charges due to their conduction band level (-0.31V and -0.29 V vs NHE for ZnO and TiO₂, respectively) (Xu and Schoonen, 2000) were more negative than the potential for single-electron reduction of O₂ ($\text{O}_2 + \text{e}^- = \text{O}_2^-$, -0.284V vs NHE). In the presence of WO₃, however, the O₂ accepts electrons through multielectron reduction ($\text{O}_2 + 2\text{H}^+ + 2\text{e}^- = \text{H}_2\text{O}_2$, + 0.682V vs NHE; $\text{O}_2 + 4\text{H}^+ + 4\text{e}^- = 2\text{H}_2\text{O}$, +1.23V vs NHE) (Abe et al., 2008). Figure 6-4 also shows the addition of H₂O₂ resulted in a significant improvement on the LNR decay in the cases of P25 and WO₃, while no positive effect was observed for ZnO. This is likely due to the amount of H₂O₂ adsorbed onto

the surface of ZnO is negligible in comparison with that in the case of TiO₂ and WO₃ (Kormann et al., 1988; Evgenidou et al., 2005).

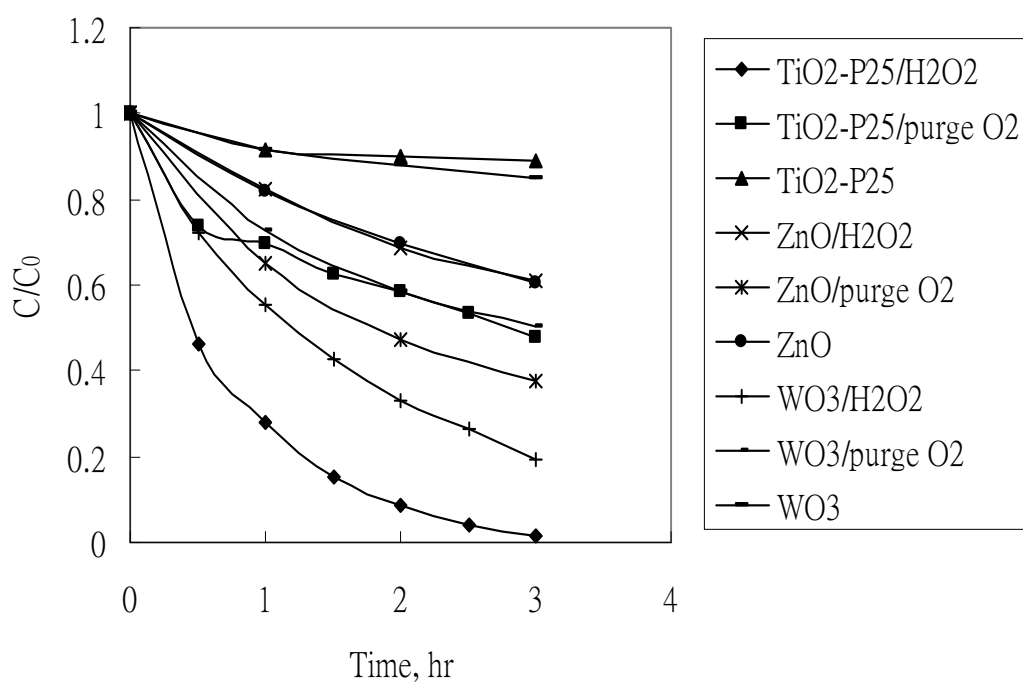


Figure 6-4: The performance of various semiconductors under different reaction conditions. (Notes: initial LNR concentration is 0.1 mM, semiconductor loading is 0.6 g/L, the initial concentration of H₂O₂ is 10 mM, initial pH value is 6.0)

6.2.4 Effect of TiO₂-P25 dosage

Because TiO₂-P25 has exhibited the best performance comparing to other combinations as described above, it was chosen as the exclusive photocatalyst for the detail study. The influence of TiO₂-P25 dosage (ranged from 0.05 to 1.0 g/L) on the LNR degradation was investigated with the concentration of H₂O₂ and LNR fixed at 10 and 0.1 mM, respectively, and the results were illustrated in Figure 6-5. It can be observed that the decay rate of LNR increases with the increment of TiO₂ dosage. It is also interesting to perceive that the pseudo first-order decay rate constants

increased linearly with the increment of TiO₂ dosage, but could be clearly divided into two stages with a breakpoint of 0.4 g/L dosage (Figure 6-5b). This suggested that the LNR decay was gradually retarded when TiO₂ dosage was increased over 0.4 g/L. This is because the increase in the opacity of the suspension with the abundance of TiO₂ particles resulted in a reduction in the light penetration (Inel and Okte, 1996). The most cost-efficient dose of 0.4 g/L TiO₂, therefore was employed in the following studies.

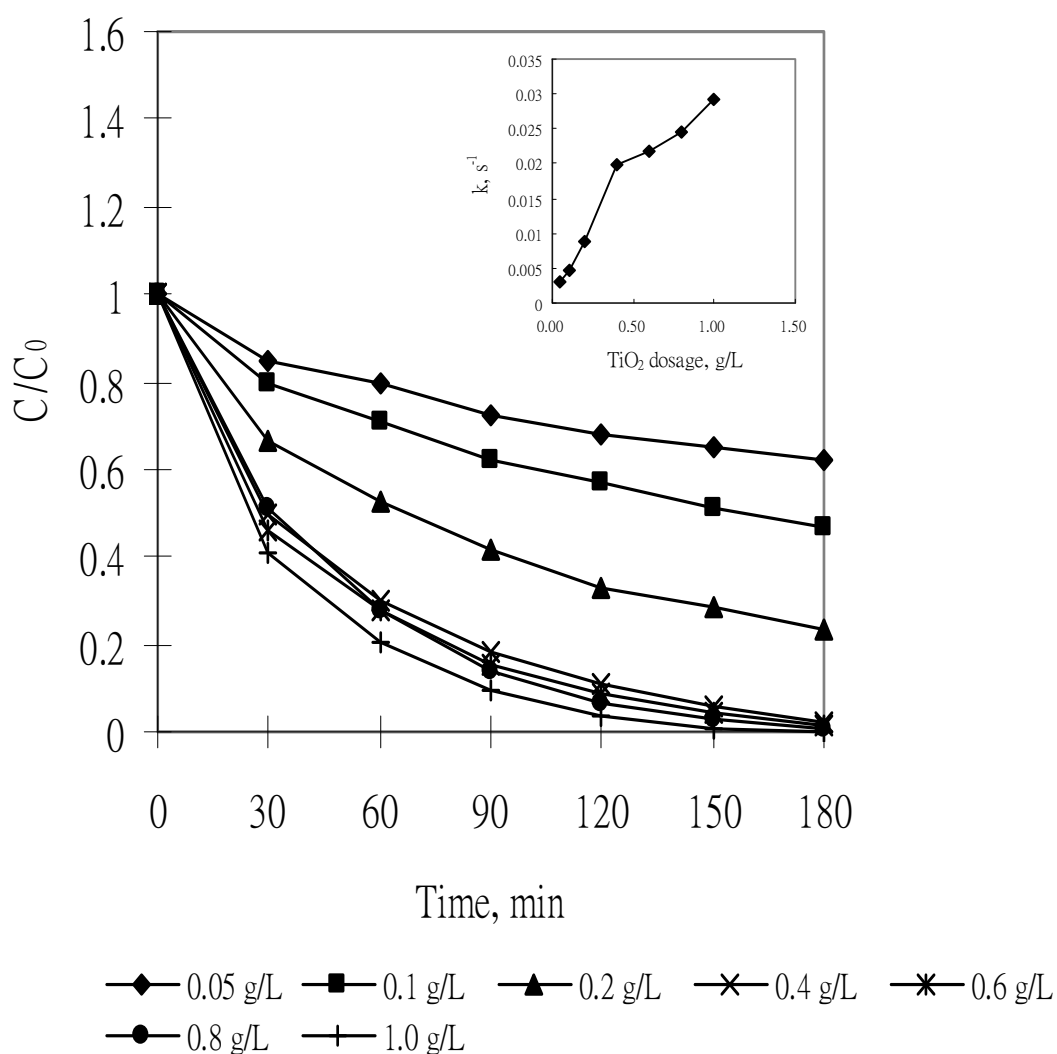


Figure 6-5: The effect of TiO₂-P25 dosage on the LNR decay rate (initial LNR concentration is 0.1 mM, the initial concentration of H₂O₂ is 10 mM, initial pH value is 6.0)

6.2.5 Effect of H₂O₂ concentration

As described previously, hydroxyl radicals play a key role in the LNR decomposition in TiO₂/H₂O₂ system under the irradiation of visible light. However, if the H₂O₂ is in excess, H₂O₂ may compete for HO• with the organic compound (Eqn. 6-4) and results in a negative effect. The determination of an optimum concentration of H₂O₂, thus, is critical for this system in any practical application.



The LNR degradation at 0.4 g/L TiO₂ with H₂O₂ concentration varying from 1 to 20 mM is indicated in Figure 6-6. It is interesting to observe that the increase of H₂O₂ concentration did not accelerate the LNR decay significantly, even at the low H₂O₂ concentrations. This result is different from the results by using UV as the light source (Choy and Chu, 2005; Kaniou et al., 2005). A possible explanation is that the total available electrons produced from the direct excitation from the valence band to the conduction band of TiO₂ and the transfer from surface complexes to the conduction band of TiO₂ under visible light are much less than the number available under UV irradiation, making the amount of the available electrons (but not the H₂O₂ concentration) a rate-limiting factor in the production of hydroxyl radicals.

As also demonstrated in Figure 6-6, the decay rate of LNR with 1 mM H₂O₂ and 2 mM H₂O₂ was retarded after 60 minutes and 150 minutes, respectively, which occurred as the H₂O₂ concentration reduced to around 0.1 mM in the solution as shown in Figure 6-6b. This indicates that the H₂O₂ concentration might become a rate-limiting factor when it was below 0.1 mM in the solution.

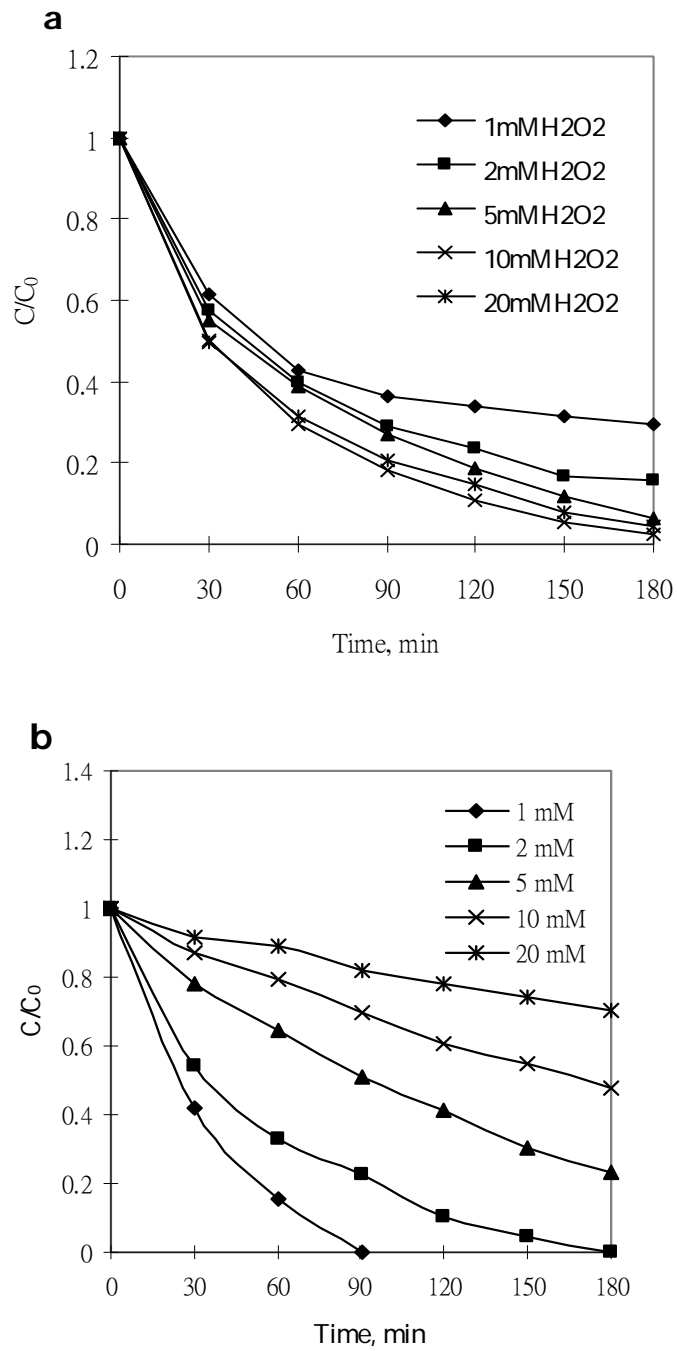


Figure 6-6: (a) The effect of H₂O₂ concentration on the LNR degradation; (b) The variation of H₂O₂ concentration during the reaction. (Notes: initial LNR concentration is 0.1 mM, TiO₂-P25 dosage is 0.4 g/L, initial pH value is 6.0)

6.2.6 Effect of pH level

The effect of initial pH on LNR decay with the addition of 5 mM H_2O_2 and 0.4 g/L TiO_2 was then examined as shown in Figure 6-7a. Under extremely acidic (pH 2.0) and basic conditions (pH 9 and 11), LNR degradation rate was significantly retarded and an optimal pH was found at 6 (see Figure 6-7b). Since H_2O_2 , as a dominant resource of hydroxyl radicals, play a major role in this system under visible light, the simultaneous decomposition of H_2O_2 in this system was also examined. Figure 6-7c shows the decay of H_2O_2 was noticeably inhibited at pH 2. At pH 2, H_2O_2 exists in the form of H_3O_2^+ and TiO_2 carries positive charges since the point of the zero charge (pzc) of TiO_2 is around pH 6. The positive charges on the surface of TiO_2 may hamper the adsorption of H_3O_2^+ on the surface of TiO_2 due to electrostatic repulsion, leading to the retardation of the formation of Titanium peroxide complex and the decomposition of H_2O_2 on the surface of TiO_2 . On the other hand, it is well known that H_2O_2 is unstable in an alkaline medium and breaks down rapidly into water and oxygen as demonstrated in Figure 6-7c, indicating less H_2O_2 molecules are available for the reactions that can produce hydroxyl radicals. Another minor possible reason for low LNR decay rate under basic condition is the dissolution of CO_2 from the air during the mixing and from the end product of LNR decay. The first and second pKa of H_2CO_3 are 6.4 and 10.3, respectively; when the pH level is higher than 6.4, the predominant species of a carbonate system will either be bicarbonate or carbonate ions. Since both of them are radical scavengers, these ions may compete with LNR for hydroxyl radicals (Wong and Chu, 2003).

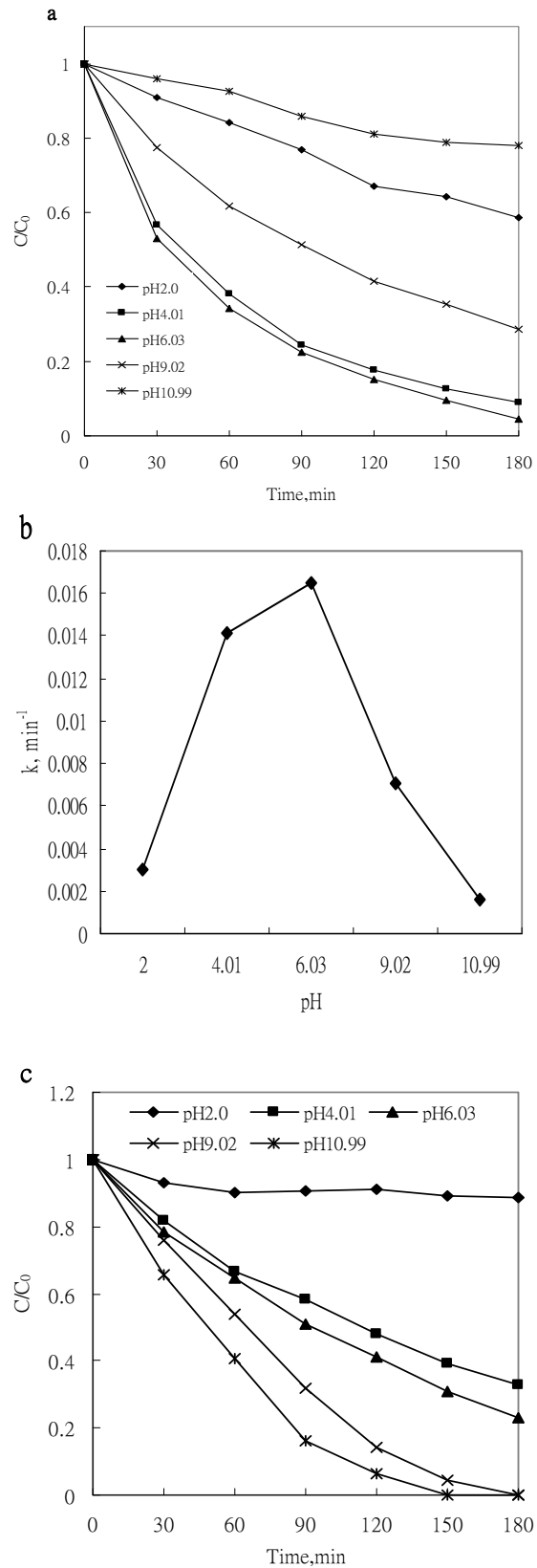


Figure 6-7: (a) LNR decomposition at different pH levels; (b) Observed rate constant at different pH levels; (c) H₂O₂ decomposition at different pH levels.

(Notes: initial LNR concentration is 0.1 mM, TiO₂-P25 dosage is 0.4 g/L, the initial concentration of H₂O₂ is 5 mM.)

6.2.7 Effect of initial concentration of LNR

LNR concentration in waters from various sources may range considerably (Caux et al., 1998), which makes the investigation on the effect of initial LNR concentration on the degradation rate of LNR interesting for the real application. The decay rate of LNR was tested with varied initial LNR concentrations by TiO₂/H₂O₂/vis system as shown in Figure 6-8a. The decay of LNR in TiO₂/H₂O₂/vis system was found to follow pseudo first-order kinetics. As also demonstrated in Figure 6-8, higher initial LNR concentration results in lower decay rate under the same reaction conditions.

The Langmuir-Hinshelwood (LH) kinetics is usually applied to quantitatively delineate such surface reactions. It is also possible to use the LH kinetics in heterogeneous photocatalysis systems only when homogeneous reaction is assumed to be insignificant (Fox and Dulay, 1993). The initial rate for the first 90 min, r_0 , can be expressed as:

$$r_0 = -\frac{d[LNR]_0}{dt} = \frac{kK[LNR]_0}{1 + K[LNR]_0} \quad (6-5)$$

where K is the equilibrium absorption constant of LNR on the surface of catalyst (mM⁻¹) and k represents the limiting reaction rate at maximum coverage (mM min⁻¹). For pseudo first-order kinetics, the incorporation of $-d[LNR]_0/dt = k_{\text{observed}}[LNR]_0$ into Eqn 6-5 gives

$$k_{\text{observed}}[LNR]_0 = \frac{kK[LNR]_0}{1 + K[LNR]_0} \quad (6-6)$$

The linearization of Eqn 6-6 gives

$$\frac{1}{k_{observed}} = \frac{1}{k}[LNR]_0 + \frac{1}{kK} \quad (6-7)$$

with an intercept of $1/kK$ and slope of $1/k$.

$1/k_{observed}$ versus $[LNR]_0$ was plotted in Figure 6-8b. The degradation of LNR at various initial concentrations fits well to the LH model with a linear regression (r^2) of 0.9873. The two constants, k and K , were calculated to be $0.00213 \text{ mM min}^{-1}$ and 59.50 mM^{-1} from the slope and intercept, respectively. The good correlation may indicate the degradation reaction of LNR in $\text{TiO}_2/\text{H}_2\text{O}_2/\text{vis}$ system dominantly occurs on the surface of TiO_2 while homogeneous reaction is insignificant.

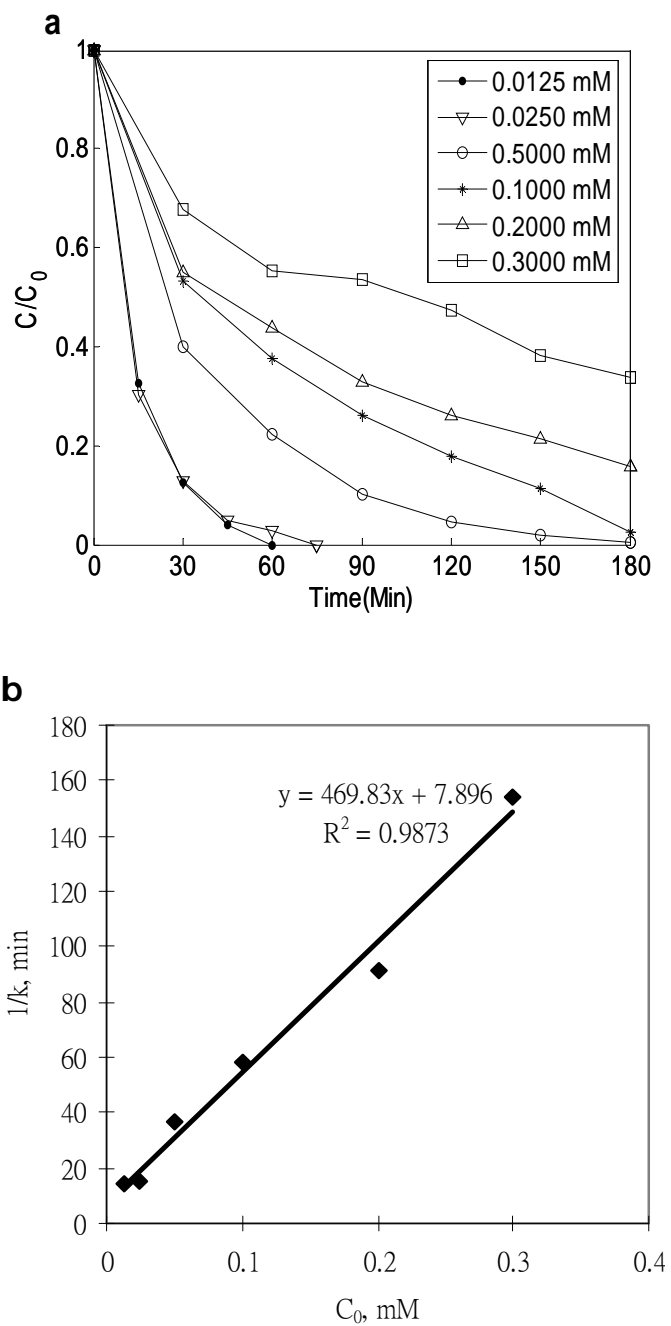


Figure 6-8: (a) Degradation of LNR at different initial concentrations; (b) L-H plot of LNR decay (Notes: $\text{TiO}_2\text{-P25}$ dosage is 0.4 g/L, the initial concentration of H_2O_2 is 5 mM, initial pH is 6.0)

6.3 Summary

The degradation of LNR in TiO₂ suspension with and without H₂O₂ was investigated under the irradiation of visible light. When no H₂O₂ involved, only 10% removal of LNR was observed. However the removal can be significantly increased to nearly 100% upon the addition of H₂O₂ to the process. In the absence of H₂O₂, anatase exhibited higher photocatalytic activities than TiO₂-P25 and no LNR decay was observed in rutile suspension; while in the presence of H₂O₂, TiO₂-P25 demonstrated the best performance and rutile showed higher activities than anatase.

The performance of various semiconductors under varied conditions was also investigated. ZnO showed the highest photocatalytic activities under visible light without using H₂O₂. The addition of H₂O₂ led to a considerable enhancement on the decay rate of LNR in the cases of TiO₂-P25 and WO₃, while no positive effect was observed for ZnO.

The process is optimized by examining the reaction rate under various reaction conditions. The decay rate of LNR, generally, increased with the increment of TiO₂ dosage. However, the LNR degradation could be gradually retarded when TiO₂ was overdosed (above 0.4 g/L) due to the reduction of light penetration.

The H₂O₂ concentration of the tested range (1 to 20 mM) did not show a significant influence on the LNR decay. This is likely due to the amount of the available electrons on the TiO₂ surface is much less than the H₂O₂ dosage in the solution, the former therefore becomes the rate-limiting factor rather than the concentration of H₂O₂. However, if the initial H₂O₂ is at low end (e.g. 1 or 2 mM) the retardation of

LNR decay will be observed as the remaining H_2O_2 in the solution reduced (consumed) to 0.1 mM. The optimal pH level for the H_2O_2 -assisted photocatalysis under visible light was found at neutral range, which is beneficial for the purpose of application. Furthermore, it was found that the Langmuir-Hinshelwood kinetics fitted well to the degradation of LNR throughout the examined concentration range of LNR, implying that surface reaction is dominant while homogeneous reaction is insignificant in this system.

Chapter 7 Reaction Mechanism of LNR Degradation in TiO₂ Suspension under Visible Light Irradiation with the Assistance of H₂O₂

7.1 Introduction

TiO₂-induced photocatalysis has attracted intensive attention as a water and wastewater treatment technology to eliminate toxic and recalcitrant organic compounds over the past decades due to its particularly optical properties, innocuity, low cost and enduring stability in terms of photo and chemical corrosion (Augugliaro et al., 1995, Hoffmann et al., 1995a). The widespread use of TiO₂ as an effective photocatalyst in practical application, however, has been curbed by its optical property that TiO₂ is only sensitive to UV light (Ding et al., 2000). The sun can furnish an abundance of photons; however, UV light only accounts for a small portion (~5%) of the sun spectrum in comparison to the visible region (~45%). Therefore, efforts have been devoted to shift the optical response of TiO₂ from the UV to the visible spectral range in order to make an effective utilization of solar energy. In recent years, doping (transmit metal and nonmetal) and dye-sensitization technologies have demonstrated successful performance in either narrowing the band gap of TiO₂ or sensitizing photocatalytic properties of TiO₂ towards visible light irradiation (Asahi et al., 2001, Cho et al., 2001, Huang et al., 2006, Lin et al., 1999, Zaleska et al., 2008). It has also been reported that the oxidation reaction of organic compounds occurs even under irradiation of visible light when TiO₂ particles are used as photocatalyst with the addition of H₂O₂ (Li et al., 2001, Ogino et al., 2008,

Ohno et al., 2001). It is known that the chemisorption of H_2O_2 on the surface of TiO_2 can result in the formation of yellow complex “Titanium peroxide” (Boonstra and Mutsaers, 1975). Ohno et al. proposed that the epoxidation reaction of 1-decene could be initiated by a photochemical reaction of $\text{Ti-}\eta^2\text{-peroxide}$ with 1-decene (Ohno et al., 2001). On the other hand, the formation of active hydroxyl radicals was proven in $\text{TiO}_2/\text{H}_2\text{O}_2$ suspension under visible light irradiation in the work of Li et al. (Li et al., 2001). They proposed a possible mechanism of the generation of hydroxyl radicals in this system. Titanium peroxide complex formed on the TiO_2 surface could extend the photoresponse to the visible region and can be excited by visible light. The excited surface complex injects an electron to the conduction band of TiO_2 . The electrons on the conduction band of TiO_2 , then, further initiate the decomposition of H_2O_2 to produce hydroxyl radicals. It was also reported that the water-oxide interface can lower the energy barrier for the H_2O_2 decomposition (Hiroki and LaVerne, 2005). As a result, hydroxyl radicals might be produced by the breakdown of H_2O_2 on the surface of TiO_2 under the irradiation of visible light ($\text{H}_2\text{O}_2 + \text{TiO}_2 + \text{vis} \rightarrow 2\text{HO}\cdot$). Although the interaction between H_2O_2 and TiO_2 is well-documented, the oxidation mechanism of organic compounds in the $\text{TiO}_2/\text{H}_2\text{O}_2$ system under visible light irradiation is not well-understood.

LNR was also chosen as a probe compound in this chapter. The degradation kinetics of LNR and the influence of varied parameters such as TiO_2 dosage, H_2O_2 concentration, pH level and LNR initial concentration on the performance of $\text{TiO}_2/\text{H}_2\text{O}_2/\text{vis}$ system have been investigated in chapter 6. This chapter will focus on the photocatalytic decomposition mechanism of LNR under visible range irradiation with the assistance of H_2O_2 .

7.2 Results and Discussion

7.2.1 LNR Degradation in Various Systems

Many studies have demonstrated that, under UV irradiation, H_2O_2 plays a dual role in enhancing the TiO_2 -based photocatalytic degradation of organic compounds by acting either as an electron scavenger to prevent the recombination of e^- and h^+ or as a direct source of hydroxyl radicals (Poulios et al., 2003; Wong and Chu, 2003; Kaniou et al., 2005; Nienow et al., 2008). However, under visible light, the mechanism behind the degradation of organic compounds in the system of $\text{TiO}_2/\text{H}_2\text{O}_2$ is still not well-defined.

In this section, the degradation of LNR was investigated under various conditions including the presence or absence of TiO_2 , the processes with or without H_2O_2 , and the use of visible light irradiation or in the dark. As shown in Figure 7-1, it is interesting to note that no decay of LNR was observed in the systems of $\text{TiO}_2/\text{H}_2\text{O}_2$ (in the dark), TiO_2 with or without purging O_2 under the irradiation of visible light (420 nm) and $\text{Vis}/\text{H}_2\text{O}_2$ after 5 hr of reaction. However, in the system of $\text{TiO}_2/\text{H}_2\text{O}_2$ under visible light (420 nm), more than 70% decay of LNR was observed.

No LNR decay was observed in TiO_2 suspension under the irradiation of visible light even with the purge of O_2 (a well-known electron acceptor) indicating no electron-hole pairs are generated and no trace of UV light leaking into the reactor in this system. It is expected that no LNR degradation was achieved in the system of $\text{H}_2\text{O}_2/\text{Vis}$ because direct dissociation of H_2O_2 to HO^\bullet can be attained only through absorbing UV light ($\lambda < 320$ nm). It has been reported that the degradation of

methylene blue can be accomplished in the presence of H_2O_2 -pretreated TiO_2 in the dark, which was ascribed to the formation of a stable oxidant - titanium peroxide on the surface of TiO_2 particles (Ogino et al., 2008). In the presence of H_2O_2 , the $-\text{OOH}$ groups of H_2O_2 substitute for the $-\text{OH}$ groups of basic $\equiv\text{TiOH}$, leading to the generation of a yellow surface complex--titanium peroxide (Boonstra and Mutsaers, 1975; Ohno et al., 2001). It has also been reported that the interaction between H_2O_2 and rutile TiO_2 can form surface O_2^- anions and $S = 1$ triplet radical anion pairs (Murphy et al., 1997). However, no LNR decay was observed in the $\text{TiO}_2/\text{H}_2\text{O}_2$ system in the dark in this study. This may suggest that the oxidizing power of both titanium peroxide and radical anions is too weak to effectively oxidize LNR.

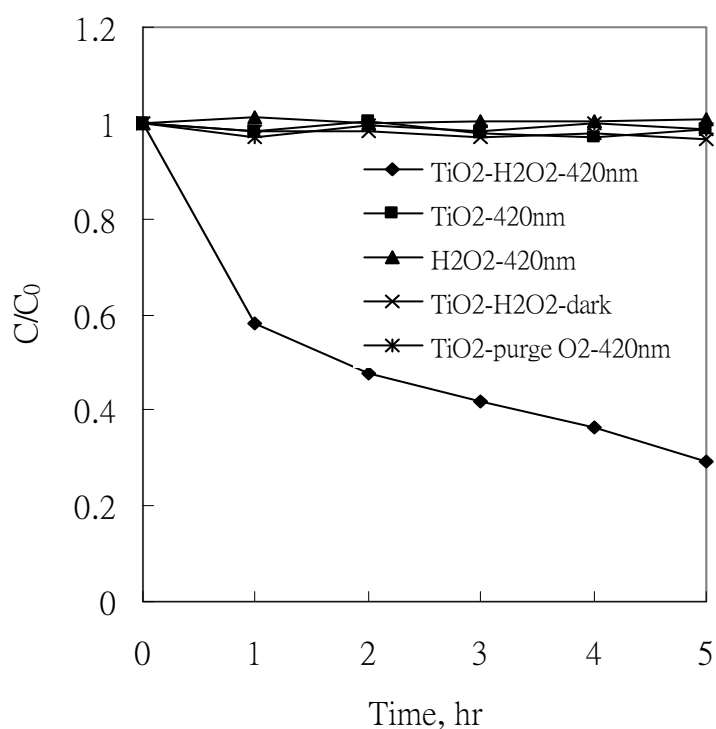


Figure 7-1: LNR degradation under different reaction conditions (Notes: initial LNR concentration is 0.1 mM, TiO_2 loading is 0.6 g/L, the initial concentration of H_2O_2 is 10 mM, initial pH value is 6.0).

7.2.2 Photocatalytic Degradation Mechanism of LNR under Visible Light

It was interesting to observe a synergistic effect in the system of TiO₂/H₂O₂/Vis for the decomposition of LNR. This synergistic effect may be rationalized by: (1) The interaction between H₂O₂ and TiO₂ leads to the formation of titanium peroxide complex and various radical anions on the TiO₂ surface which may act as oxidizing species with the assistance of visible light (Ohno et al., 2001); (2) Titanium peroxide complex on the TiO₂ surface extend the photoresponse of TiO₂ to the visible region, leading to the visible-light-induced surface electron transfer from surface complexes to the conduction band of TiO₂. The electrons on the conduction band of TiO₂ initiate the decomposition of H₂O₂, which gives rise to the generation of hydroxyl radicals (Eqn. 7-1) (Li et al., 2001); and (3) It was reported that the water-oxide interface can lower the energy barrier for the H₂O₂ decomposition (the presence of oxides leads to the activation energy of the cleavage of the O – O bond in H₂O₂ being decreased from 210 kJ/mol to 40 kJ/mol)(Hiroki and LaVerne, 2005). As a result, additional hydroxyl radicals might be produced by breaking down H₂O₂ on the surface of TiO₂ under the irradiation of visible light (Eqn. 7-2).



where e_{transfer}^- is the electron transferred from surface complexes to the conduction band of TiO₂.

In order to investigate the photodegradation mechanism of LNR, three selective radical scavengers were utilized to assess the contribution of various radicals or other oxidizing species to the LNR decay. Bicarbonate and tert-butanol selectively quench

hydroxyl radical while azide reacts with both singlet oxygen and hydroxyl radical (Xu et al., 2008). The addition of 100 mg/L bicarbonate and azide almost inhibited the LNR degradation completely in this process; 100 mg/L tert-butanol caused a significant reduction in the LNR removal (decrease from 64% to 28% at 4th hour after using the quencher) while 3 g/L tert-butanol completely hinders the LNR degradation (See Figure 7-2), indicating that the LNR decay is likely dominated by the oxidation of hydroxyl radicals. It is interesting to note the addition of 100 mg/L bicarbonate retards the LNR degradation more effectively than 100 mg/L tert-butanol does although tert-butanol is more reactive toward OH radicals than bicarbonate. This may be because bicarbonate can not only compete for hydroxyl radicals with LNR but also compete for the adsorption sites on the TiO₂ surface with H₂O₂ and LNR. It has been reported that the anions exerted an inhibiting effect on the photocatalytic degradation of organic pollutants due to the occurrence of the competitive adsorption (Liang et al., 2008).

It was reported that the water-oxide interface could lower the energy barrier for the H₂O₂ decomposition and the activation energy was around 42 kJ/mol for the decomposition of H₂O₂ (independent on the type of oxide) (Hiroki and LaVerne, 2005). Therefore, it may be interesting to examine both the H₂O₂ and LNR decay in the suspension of other metal oxides under the irradiation of visible light. Alumina (Al₂O₃), silica (SiO₂), and Gallium oxide (Ga₂O₃), known to be insensitive to visible light nor producing electron-hole pairs, were therefore selected as probe oxides. It has been proven that, in the presence of Al₂O₃ or SiO₂, the decomposition of H₂O₂ can be achieved at 80°C (Hiroki and LaVerne, 2005). However, no H₂O₂ and LNR decomposition was observed under visible light in the presence of these additionally

tested oxides. Only TiO_2 can initiate the reaction as shown in Figure 7-3. This is likely because the visible light from 300 W Xe lamp cannot furnish enough energy (42 kJ/mol) for the cleavage of O – O bond in H_2O_2 to produce hydroxyl radicals.

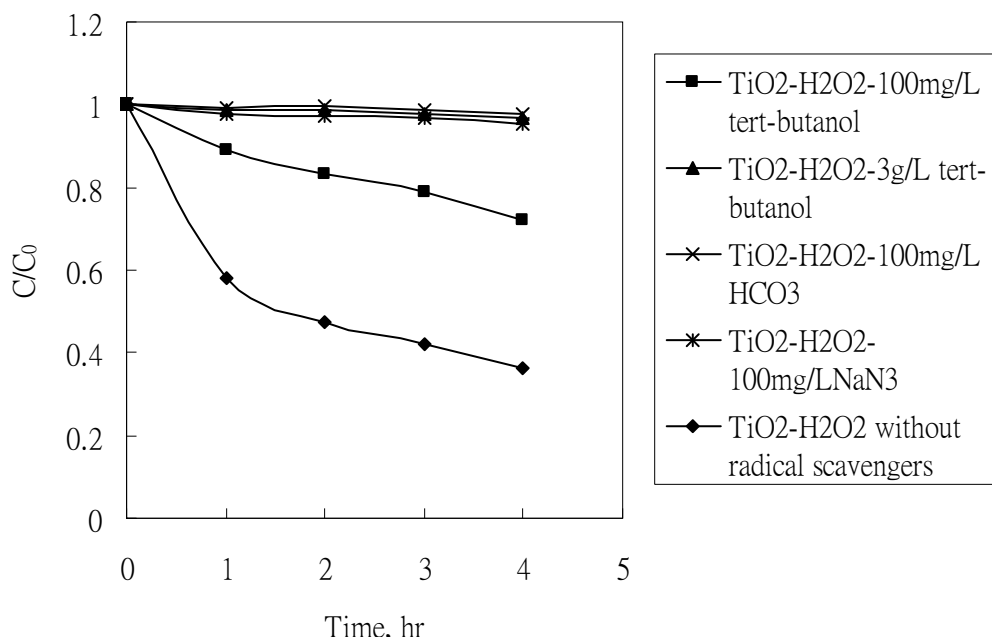


Figure 7-2: Effect of radical scavengers on visible-light photocatalysis of LNR with the assistance of H_2O_2 . (Notes: initial LNR concentration is 0.1 mM, TiO_2 loading is 0.6 g/L, the initial concentration of H_2O_2 is 10 mM, initial pH value is 6.0)

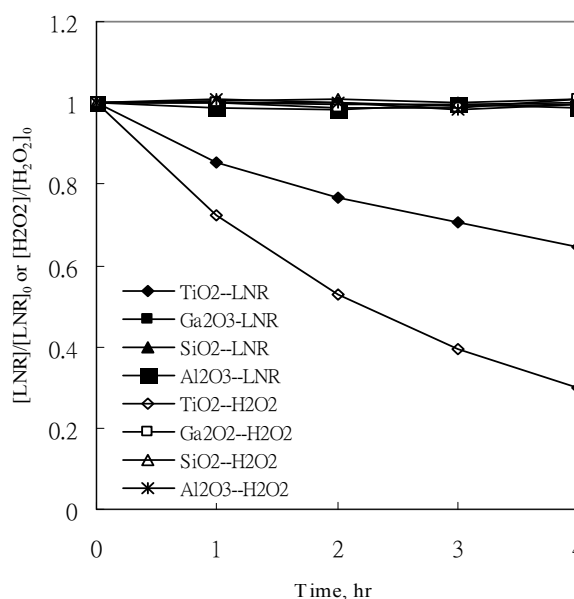


Figure 7-3: LNR and H₂O₂ decomposition in various oxides suspension under visible light irradiation (Notes: initial LNR concentration is 0.1 mM, all oxides loading is 0.6 g/L, the initial concentration of H₂O₂ is 1 mM, initial pH value is 6.0).

It was proposed that the titanium peroxide complex formed on the surface of TiO₂ can be excited by visible light to produce electrons which can be transferred to the conduction band of TiO₂ and subsequently initiate the decomposition of H₂O₂ to produce hydroxyl radicals in the study of Li et al. (Li et al., 2001). However, the production of electrons was not confirmed in their study. Thus, in order to investigate if electrons can be generated in this system, photocurrent generation was monitored from a TiO₂/ITO electrode immersed in aqueous 0.03 M H₂O₂ solution or DDW. The time profiles of photocurrents generated under visible light ($\lambda = 420 \pm 10$ nm) irradiation are demonstrated in Figure 7-4. When the visible light is on, the generation of around 410 nA photocurrent can be observed in aqueous H₂O₂ solution while no photocurrent is produced in DDW, indicating only the surface complex can

be excited by visible light to generate an electron which is transferred to the electrode to generate visible-light-induced current (I_{ph}).

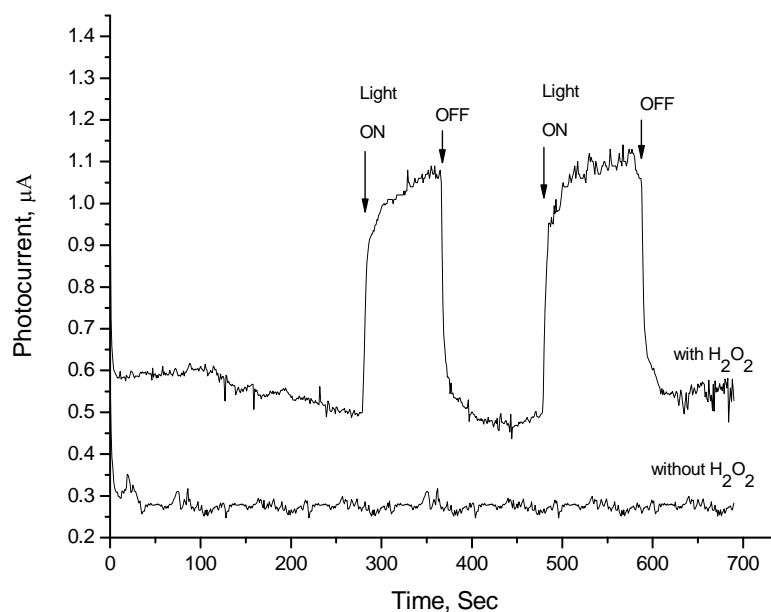
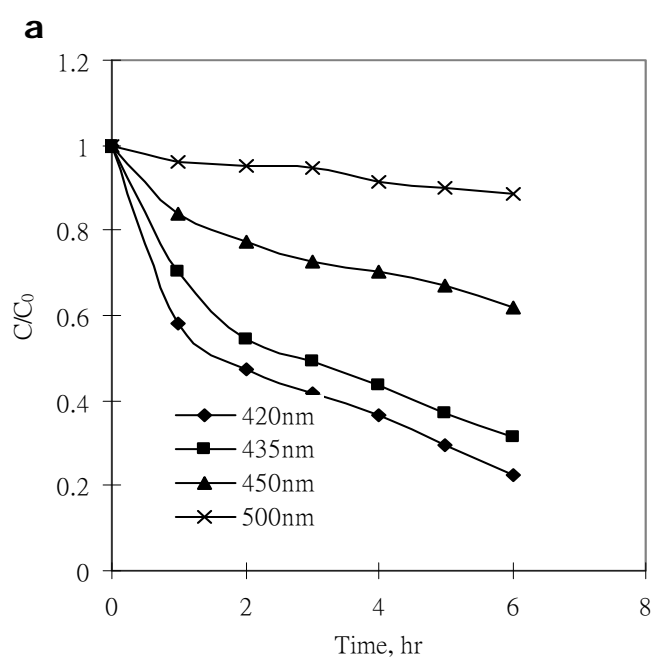


Figure 7-4: Visible-light-induced current (I_{ph}) generation on a TiO_2/ITO electrode in water with or without H_2O_2 (Notes: the concentration of H_2O_2 solution is 0.03 M).

7.2.3 Effect of Wavelength

The effect of wavelength of visible light on the LNR decay rate and the generation of photocurrent was also examined (See Figure 7-5). Figure 7-5a shows that the degradation rate of LNR decreased with the increment of irradiation wavelength, where less than 12% LNR was removed by using 500 nm light after 6-hour of irradiation. Figure 7-5b demonstrates the generated photocurrent and the consumption of H_2O_2 after 6 hours of reaction in the presence of H_2O_2 under different wavelength irradiations. It can be seen that the correlation between the generated photocurrent and the consumed H_2O_2 is well established under various wavelengths; shorter the wavelength (i.e. higher the energy), higher the photocurrent,

and subsequently faster the consumption of H_2O_2 . This suggests the electrons initiate the decomposition of H_2O_2 . However, it is interesting to note that no photocurrent was generated under the irradiation of 500 nm visible light, although the formation of TiO_2 surface complexes could be extended to 550 nm visible light (Li et al., 2001), and $3.6 \mu\text{mol H}_2\text{O}_2$ was consumed after 6 hours by 500 nm irradiation (from this study). This is likely because the signal of photocurrent produced is too weak to be detected by the potentiostat used in this study. In addition, the light intensity has also been measured in this study. The photo intensity at different wavelength is 178.6, 164.3, 167.8 and 203.6 Wm^{-2} for 420, 435, 450 and 500 nm, respectively. Although the photo intensity is the highest at 500 nm, the weak absorbance of titanium peroxide complex at 500 nm (Li et al., 2001) results in its weak response to light at this wavelength.



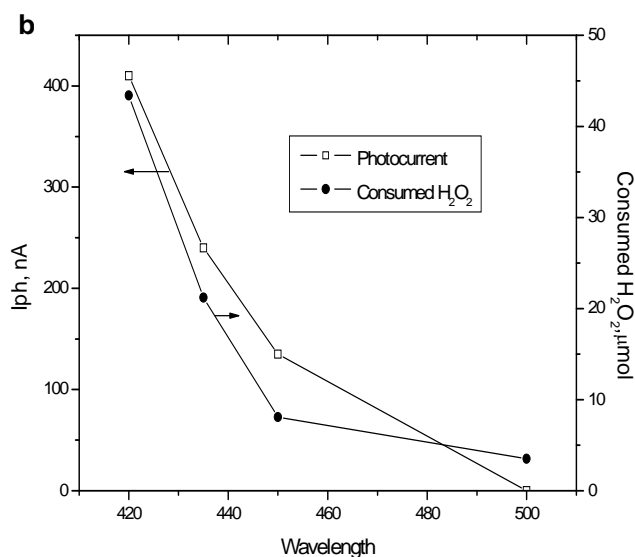


Figure 7-5: (a) The effect of wavelength of visible light on the LNR decay rate; (b) I_{ph} and the H_2O_2 consumption are compared as a function of the wavelength (Notes: initial LNR concentration is 0.1 mM, TiO_2 loading is 0.6 g/L, the initial concentration of H_2O_2 is 10 mM, initial pH value is 6.0).

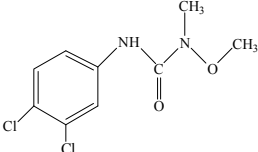
7.2.4 Photocatalytic Degradation Pathway of LNR under Visible Light or UV

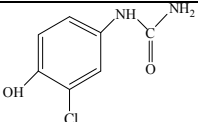
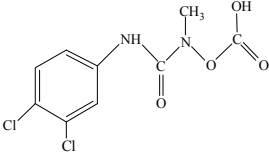
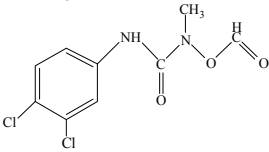
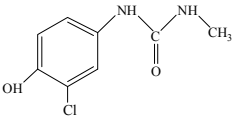
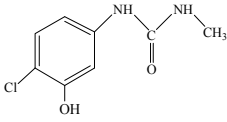
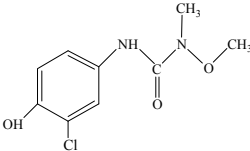
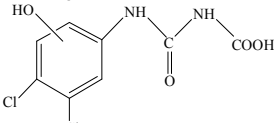
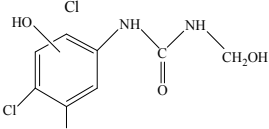
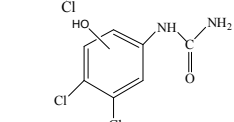
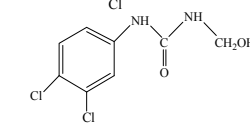
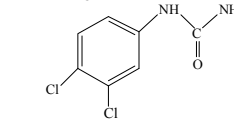
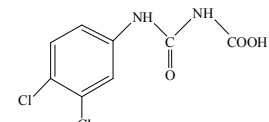
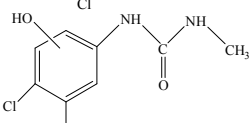
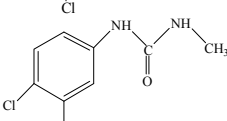
Irradiation

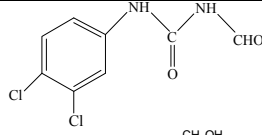
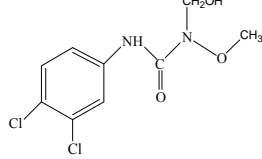
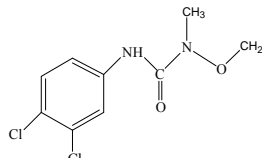
It is believed that hydroxyl radicals play a key role in the decomposition of organic compounds by UV/ TiO_2 process. The investigation on the transformation products of LNR produced both in visible light and UV-induced photocatalytic process may cast a bright light on the degradation mechanism of LNR by $TiO_2/H_2O_2/Vis$ process. The same concentration of LNR was degraded under irradiation of UV or visible light, where 16 and 17 intermediates were identified during the process on the basis of the molecular ions and mass fragment ions detected by MS spectrum for UV and visible light, respectively. The information on the intermediates including the mass of

deprotonated ion ($[M - H]^+$) of the daughter compounds, the proposed molecular structure, the relative abundances, and the proposed fragments is summarized (See Table 7-1). Actually, $[M + \text{acetate}]^-$ ions were obtained as a base peak of the mass spectra for most intermediates and LNR (See Appendix II) due to 5 mM ammonium acetate being used as mobile phase and negative-ion mode being employed in this study (Barcelo and Albaiges, 1989). The evolution profiles of major intermediates were organized and shown in Figure 7-6a and 7-6b (trace intermediates not included). As indicated in Figure 7-6, the formation/degradation profiles of the intermediates generated during these two processes are quite similar. It was also found that the decay of LNR was involved with *N*-demethoxylation and *N*-demethylation through alkylic-oxidation, dechlorination (hydroxylation at the chlorine site), and hydroxylation of the benzene ring in both processes. Direct dechlorination (no hydroxylation at the chlorine site) reported by other researchers (Lopez et al., 2005) was not observed in this study. Until now, it is believed that hydroxyl radicals also play a predominant role in Vis/TiO₂/H₂O₂ process similar to that in UV/TiO₂ process for the LNR decay. It can also be believed LNR suffers the same decay pathway by both Vis/TiO₂/H₂O₂ and UV/TiO₂ process.

Table 7-1: Identified degradation products and their main fragments determined by LC/ESI-MS

Compound	Retention time	Molecular weight	Molecular ion and main fragments	Structural formula	Detected in	
					UV	Vis
LNR	20.93	248	247, 217, 188, 160, 109		√	√

1	8.96	186	185,165,141,119		√	√
2	9.49	278	277, 250, 233, 217,119		√	√
3	10.02	262	261, 156, 119,109			√
4	10.65	200	199, 42,137,119		√	√
5	12.62	200	199, 137, 119		√	√
6	13.90	230	229, 37,119,109		√	√
7	14.61	264	263,176,119,109		√	√
8	14.83	250	249,219,202,176, 137,119,109		√	√
9	15.44, 15.56	220	219,203,176, 137 119,109		√	√
10	15.68	234	233,203,160, 137,119,109		√	√
11	16.31	204	203, 160, 137,119,109		√	√
12	16.69	248	247,203,88,160, 137,119,109		√	√
13	16.93	234	233, 202,176, 137,119,109		√	√
14	17.46	218	217, 160, 137,119,109		√	√

15	18.93	232	231,202,188 160, 137,119.109	 <chem>CC(=O)Nc1ccc(Cl)c(Cl)c1</chem>	√	√	
16 and 17	19.30, 19.72	264	263, 233, 217, 202,188,156,119, 109	 <chem>CN(C)C(=O)Nc1ccc(Cl)c(Cl)c1</chem>  <chem>CN(CO)C(=O)Nc1ccc(Cl)c(Cl)c1</chem>	OT	√	√

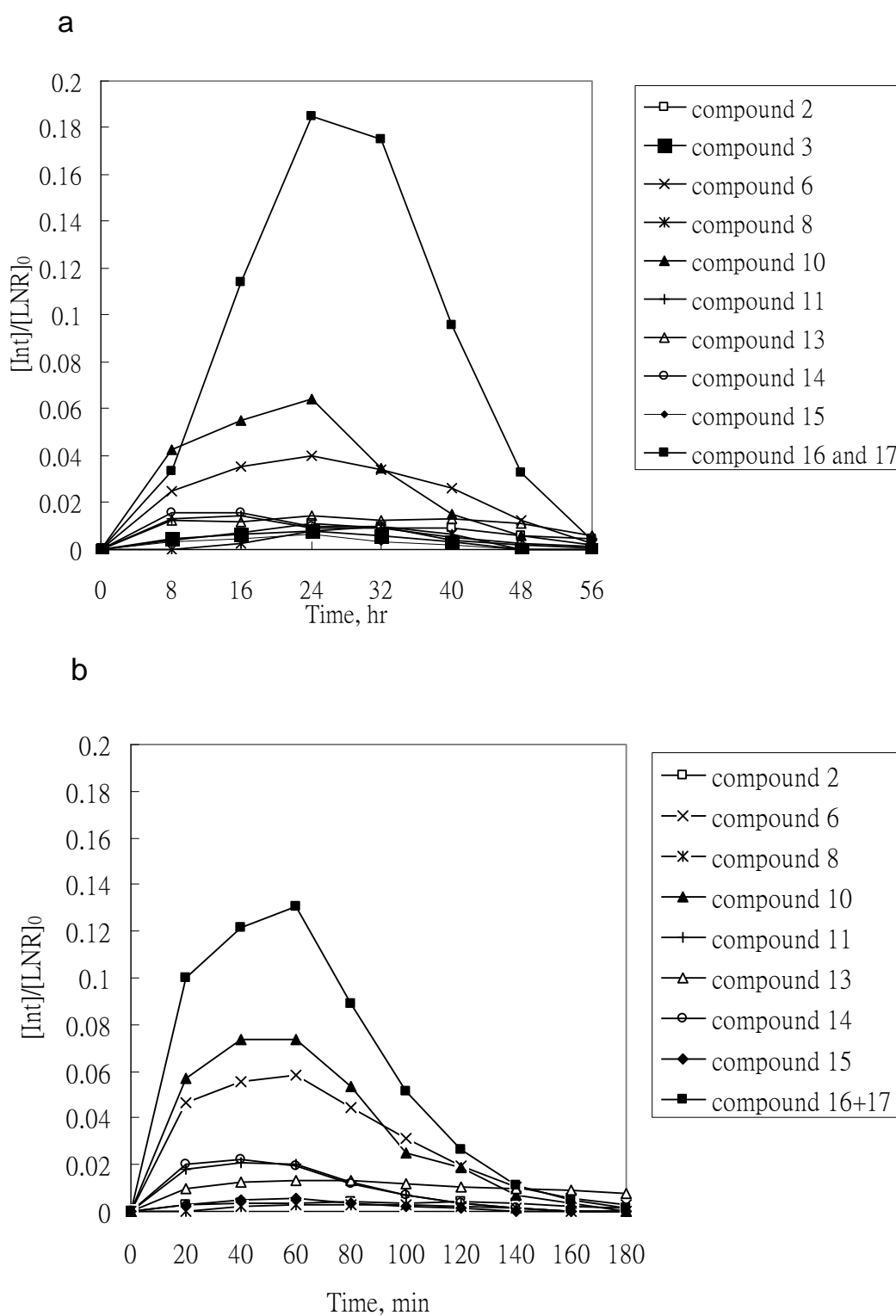


Figure 7-6: (a). The evolution profiles of generated intermediates in Vis/TiO₂/H₂O₂; (b).

The evolution profiles of intermediates in UV/TiO₂ system. (Notes: The initial concentration of LNR is 0.25 mM, the initial concentration of H₂O₂

is 10 mM, initial pH value is 6.0; for UV/TiO₂ system, six 350 nm UV lamps were used)

Therefore, the degradation pathway of LNR by Vis/TiO₂/H₂O₂ or UV/TiO₂ process was proposed on the basis of the profile analysis as illustrated in Figure 7-7. The decomposition of LNR was initiated by the attack of HO• on the chlorine site of the benzene ring, *N*-terminus methyl, and methoxyl groups, leading to the generation of compounds 6, 16 and 17, respectively at the first step. The emergence of compound 6 was accompanied by the release of chlorine at the beginning of the reaction, which has been quantified (See Figure 7-9). The oxidation of *N*-terminus methoxyl group of compound 16 led to the formation of compounds 2, 3 and 14 through dealkylation (alkylic side chain cleavage). The direct demethoxylation of compounds 6 and 17 resulted in the generation of compound 4 or 5 and 10, respectively. Compound 10 is believed to have another source (the oxidation of *N*-terminus methyl of compound 14), which gives rise to high yield of compound 10 at the beginning of the reaction as demonstrated in Figure 7-6. In addition, dechlorination of compound 14 (hydroxylation at the chlorine site) also could form compounds 4 or 5, which was confirmed by an individual test using the standard of compound 14 as the initial probe in Vis/TiO₂/H₂O₂ system. This individual test also verified that 13.6% of compound 14 was transformed into compound 13 while 4.2% of compound 14 was converted to compound 4 and 5 after 7 hours of reaction by Vis/TiO₂/H₂O₂ process (data not shown), which may rationalize higher yield of compound 13 than compounds 4 and 5 although compound 14 is the only possible source of compound 13. The further *N*-terminus oxidation of compound 10 produced compounds 15, 12 and 11 while the *N*-terminus oxidation of compound 13 caused the generation of compounds 8, 7 and 9. Compound 1 is believed to come from the *N*-terminus

demethylation of compound 4. It should be noted that Compound 13 may not be the only source responsible for the formation of compound 9, while compound 4 may not be the only source contributed to the production of compound 1. Compound 11 can also make contribution to the yield of compound 1 and 9 through dechlorination (hydroxylation at the chlorine site on the benzene ring) and direct hydroxylation on the benzene ring without dechlorination, respectively, which was confirmed by an additional test using the compound 11 as the initial probe compound in this process. It was believed that 2,3-dichloroaniline was the terminal product of LNR decomposition (Farre et al., 2007). However, it was not detected in this study.

All intermediates were categorized into alkylic-oxidation derivatives (AOD), dechlorination-hydroxylation derivatives (DHD) and derivatives from the hydroxylation of benzene ring (HBD). In order to elucidate the major mechanism involved in these two processes, the transformation of LNR, the intermediates (in terms of AODs, DHDs and HBDs), and the mass balance of benzene ring were reorganized and incorporated in Figures 7-8a and 7-8b. Figure 7-8 shows the concentration of AODs is much higher than that of DHDs and HBDs, indicating alkylic-oxidation is a dominant degradation mechanism while dechlorination (hydroxylation at the chlorine site) and hydroxylation of the aromatic ring are minor in terms of LNR decay in both UV/TiO₂ and Vis/TiO₂/H₂O₂ processes. This can be rationalized by the following: the di-substitution of the phenyl ring by chlorine atoms lowers its susceptibility towards any electrophilic or radical attack due to electron-drawing property of chlorine leading to the lower electron density on the benzene ring, resulting in the attack on the urea N-terminus group more competitive.

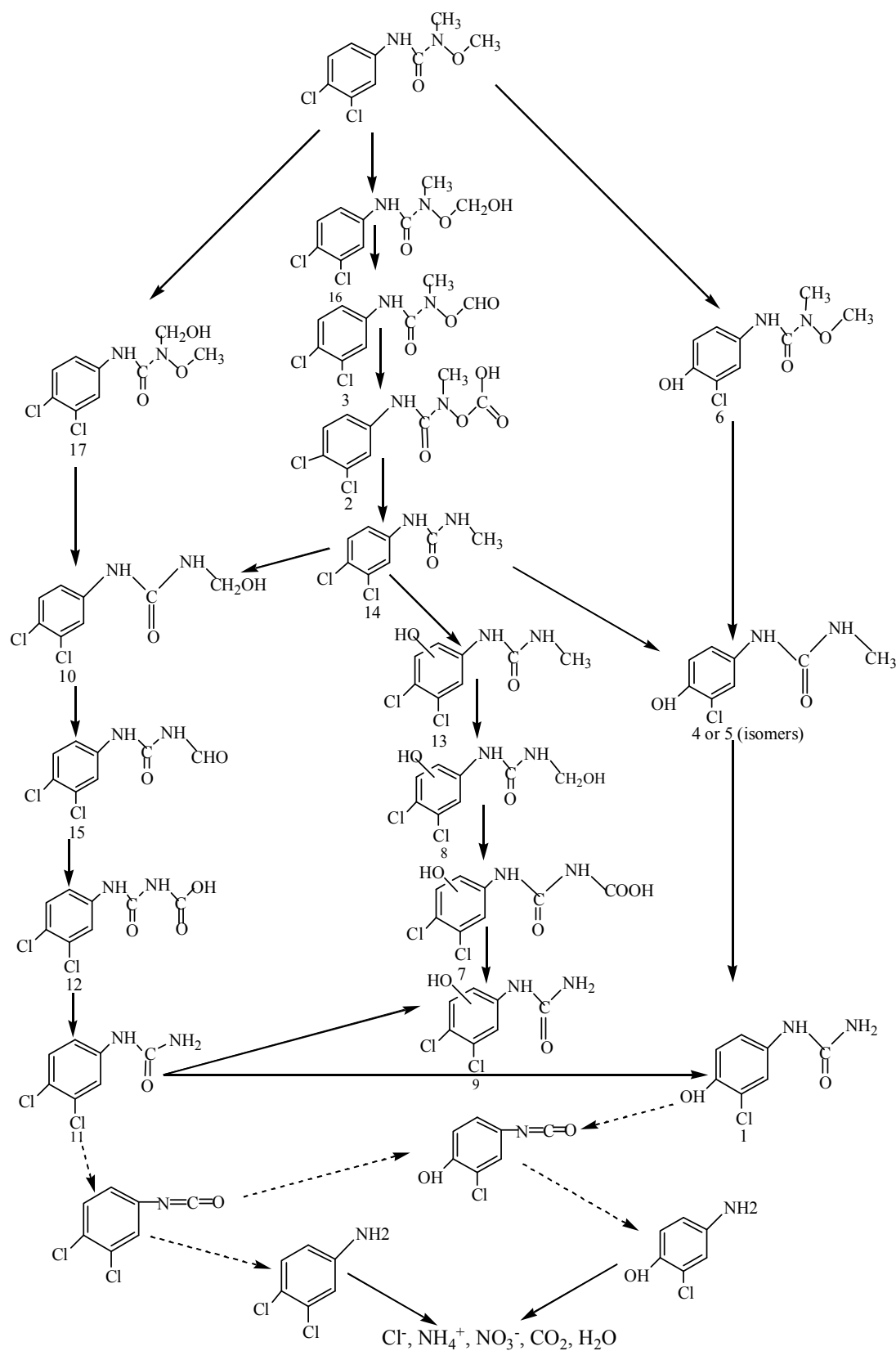


Figure 7-7: Degradation pathways of LNR for both Vis/TiO₂/H₂O₂ and UV/TiO₂ processes.

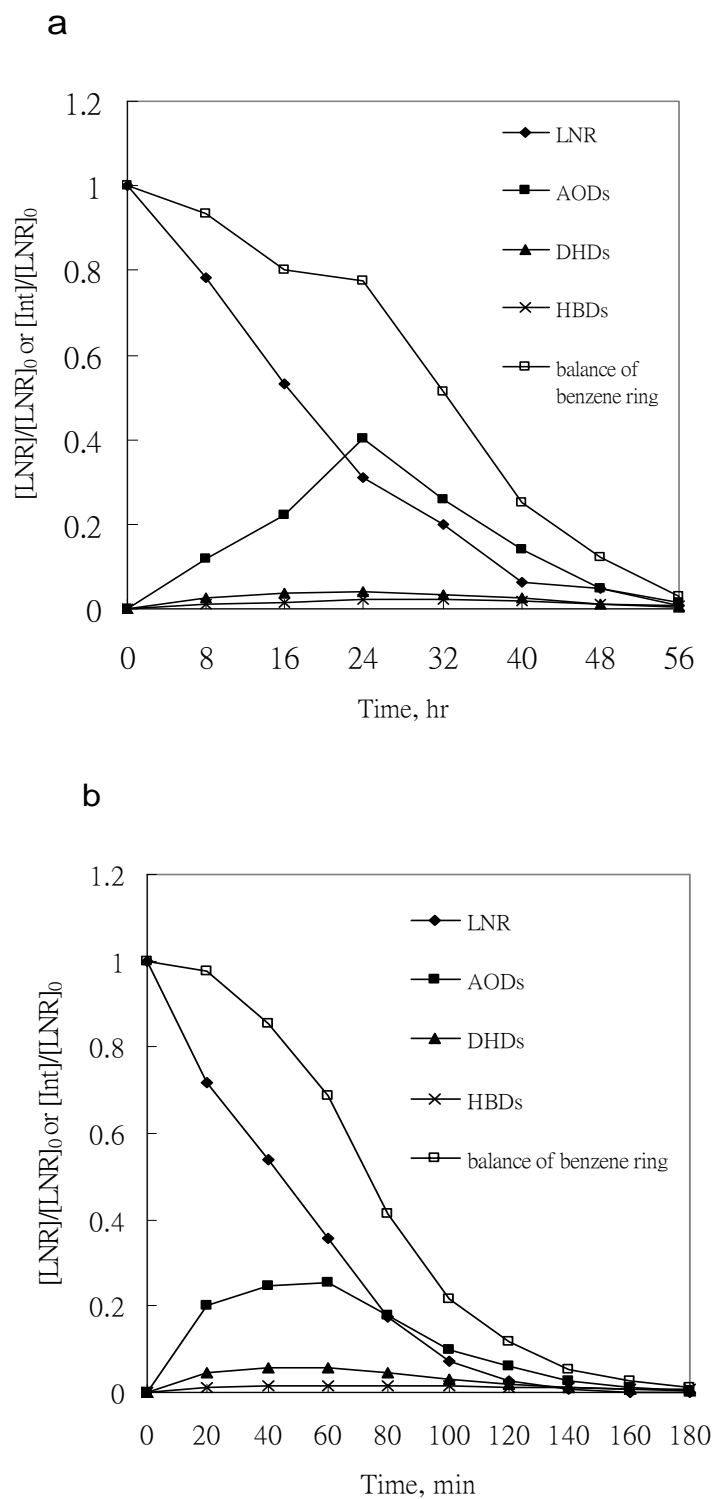


Figure 7-8: (a) Process summary of Vis/TiO₂/H₂O₂ (where [Int] stands for the concentration of intermediates); (b) Process summary of UV/TiO₂ (where [Int] stands for the concentration of intermediates)

The evolution of chloride, ammonium, nitrate and TOC was also monitored during the LNR decay reaction by Vis/TiO₂/H₂O₂ process (see Figure 7-9). Nearly 70% chlorine and 37% nitrogen were released after 56 hours of reaction as shown in Figure 7-9. Judging from the mass balance of benzene ring in Figure 7-8, ring opening was completed at the end of the reaction. However, only around 32% TOC was removed (see Figure 7-9). This suggests all aromatic compounds were broken down into simple aliphatic acids, which account for the dominating part of TOC. Furthermore, it is interesting to note that the TiO₂ particles sunk down to the bottom of the reactor automatically in 10 minutes right after the stirring was stopped. The release of chlorine due to dechlorination-hydroxylation and the generation of organic acid led to pH level dropping from 6.0 to 3.07. At pH 3.07, the TiO₂ surface is positively charged (Ti-OH₂)⁺, which may favor the adsorption of the anions released during the reaction. The anion adsorption may weaken the repulsion of TiO₂ particles positively charged and start the aggregation of TiO₂ particles.

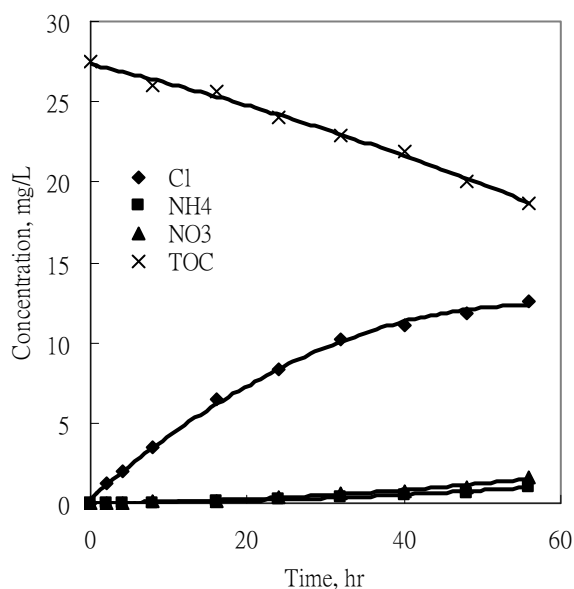


Figure 7-9: The evolution of TOC, chloride, ammonium and nitrate ions during the Vis-induced photocatalytic reaction (The initial concentration of LNR is

0.25 mM, the initial concentration of H₂O₂ is 10 mM, initial pH value is 6.0).

7.3 Summary

The application of TiO₂/H₂O₂/Vis (visible light) process for the aqueous degradation of linuron (LNR) has been investigated. in this chapter. The degradation mechanism of LNR by TiO₂/H₂O₂/Vis process has been verified through the investigation of the effects of various radical scavengers, monitoring the generation of photocurrent, examining the performance of other metal oxides in place of TiO₂ in this system, and comparing the intermediates and decay pathways of LNR by UV-TiO₂ and TiO₂/H₂O₂/Vis processes with 16 and 17 intermediates identified, respectively. It has been revealed that demethoxylation and demethylation through alkylic-oxidation is the major mechanism of LNR degradation while dechlorination (hydroxylation at the chlorine site) and direct hydroxylation on the benzene ring is minor in both processes.

It is believable that Vis/TiO₂/H₂O₂ process is cost efficient and practically applicable in the removal of persistent organic contaminants in natural waters since it can work under the irradiation of visible light which accounts for a much larger part of solar light than UV.

Chapter 8 Conclusion and Recommendation

8.1 Conclusion

The treatability of LNR has been investigated in depth by using various water treatment processes including continuous UV irradiation, ozonation, UV/ozonation, and TiO₂/H₂O₂/Vis (visible light). These findings based on lab-scale studies provide important information for engineers to design reactors or tackle specific problems they may encounter in real application, not confined to the effect of those critical parameters, but extended to the interference of intermediates and final products. In particular, the study on the mechanism of LNR degradation by TiO₂/H₂O₂/Vis process may perfect the theory about how TiO₂ work under the irradiation of visible light with the assistance of H₂O₂.

8.1.1 The Degradation of LNR by using UV, Ozonation, and UV/Ozone

The degradation for LNR by UV, O₃, and UV/O₃ processes were conducted under a wide range of conditions. The decay rate of LNR by UV/O₃ process was found to be around 3.5 times and 2.5 times faster than sole-UV and ozone-alone, respectively. No TOC removal was observed in sole UV process, and TOC removal was insignificant in ozonation process (about 15% mineralization after 100 minutes). However, nearly 80% mineralization was achieved by using UV/ozone process after 100 minutes. The overall rate constants increase exponentially with pH above 9.0 while the increase of rate constants with pH below 9 is insignificant in O₃ system. It was also observed that UV/ozone process was pH-dependent while UV photolysis was pH-independent in terms of LNR decay. The optimum synergistic effect of UV

combined with O₃ was found to be achieved at pH 9. The apparent photolysis rate constant of LNR is linearly increased with the increment of light intensity under the irradiation of UV at 254 nm. All predominating parameters such as quantum yield (Φ_{LNR}), k_{OOH} (rate constant for the formation of free radical HOO[•] from ozone decomposition at high pH), rate constant of linuron with ozone ($k_{o_3, LNR}$), rate constant of linuron with hydroxyl radical ($k_{OH, LNR}$), and α (the ratio of the production rate of HO[•] and the decay rate of ozone in UV/O₃ system), involved in these three processes were determined in the assistant of proposed linear models. The proposed models offer an accurate way to predict the LNR decomposition by the UV, O₃ and UV/O₃ processes under varied conditions.

In addition, the influence of various anions on the performance of ozonation has also been examined. Chloride ion was observed to significantly retard the degradation of LNR at pH 3 while it exerted no perceptible effect on the performance of ozonation at pH 7. The presence of phosphate ion led to the increase of LNR decay rate at pH 7 due to its buffer ability to keep pH stable and had no influence on the LNR degradation at pH 3. Both carbonate and sulfate ions were not observed to affect the performance of ozonation in terms of LNR decomposition.

The intermediates and end products generated during LNR decay by these three processes have been investigated in detail. Eight intermediates escaped from previous studies were detected in sole-UV system in this study. A new decay pathway of LNR was proposed on the basis of information about the identified intermediates during the LNR and DCPMU (a dominating intermediate generated during LNR decay) degradation by UV photolysis compared to previous studies.

Furthermore, *N*-terminus demethoxylation, photohydrolysis with dechlorination, and *N*-terminus demethylation were found to be the major mechanisms in the LNR decay while hydroxylation on benzene ring might make a minor contribution to LNR removal under the irradiation of UV at 254 nm. *N*-terminus demethoxylation, dechlorination and hydroxylation on benzene ring were observed to be involved in the ozonation process. It was observed that around 98% of chlorine on the benzene ring was released after 4 hr and trace amount of NH_4^+ and NO_3^- was detected, indicating de-nitrogenation could be achieved in the photolytic degradation of LNR by UV at 254 nm. For ozonation process, around 80% of chlorine and 13% of nitrogen were found to be released to the solution as chloride, nitrate and ammonia ions, respectively after 120 min. Among these three treatment processes, UV/ O_3 process has exhibited the best overall performance in terms of LNR removal, mineralization, de-chlorination and de-nitrogenation (Complete release of chlorine was achieved after 80 min and around 56% of nitrogen was released as ammonia and nitrate ions after 120 min).

8.1.2 The Degradation of LNR by $\text{TiO}_2/\text{H}_2\text{O}_2/\text{Vis}$ (visible light) process

The degradation of LNR in TiO_2 suspension with and without H_2O_2 was investigated under the irradiation of visible light (420 nm lamps were used as light source). When no H_2O_2 involved, only 10% removal of LNR was observed. However the removal can be significantly increased to nearly 100% upon the addition of H_2O_2 to the process after 3 hr of reaction. We also examined the effect of TiO_2 phase composition on the performance of this system. In the absence of H_2O_2 , anatase exhibited higher photocatalytic activities than TiO_2 -P25 and no LNR decay was

observed in rutile suspension; while in the presence of H₂O₂, TiO₂-P25 demonstrated the best performance and rutile showed higher activities than anatase.

The performance of various semiconductors under varied conditions was also investigated. ZnO showed the highest photocatalytic activities under visible light without using H₂O₂. The addition of H₂O₂ led to a considerable enhancement on the decay rate of LNR in the cases of TiO₂-P25 and WO₃, while no positive effect was observed for ZnO.

The process is optimized by examining the reaction rate under various reaction conditions. The decay rate of LNR, generally, increased with the increment of TiO₂ dosage. However, the LNR degradation could be gradually retarded when TiO₂ was overdosed (above 0.4 g/L) due to the reduction of light penetration.

The H₂O₂ concentration of the tested range (1 to 20 mM) did not show a significant influence on the LNR decay. However, if the initial H₂O₂ is at low end (e.g. 1 or 2 mM) the retardation of LNR decay will be observed as the remaining H₂O₂ in the solution reduced (consumed) to 0.1 mM. The optimal pH level for the H₂O₂-assisted photocatalysis under visible light was found at neutral range, which is beneficial for the purpose of application.

Furthermore, it was found that the Langmuir-Hinshelwood kinetics fitted well to the degradation of LNR throughout the examined concentration range of LNR, implying that surface reaction is dominant while homogeneous reaction is insignificant in this system.

The reaction mechanism of LNR degradation by $\text{TiO}_2/\text{H}_2\text{O}_2/\text{Vis}$ process using Xe lamp as the light source has been verified through the investigation of the effects of various radical scavengers, monitoring the generation of photocurrent, examining the performance of other metal oxides in place of TiO_2 in this system, and comparing the intermediates and decay pathways of LNR by UV- TiO_2 and $\text{TiO}_2/\text{H}_2\text{O}_2/\text{Vis}$ processes. Hydroxyl radicals are believed to play a dominant role in LNR degradation in $\text{Vis}/\text{TiO}_2/\text{H}_2\text{O}_2$ system, judging from LNR decay being completely hampered after the application of radical scavengers as well as the comparison of the identical intermediates and decay mechanism between $\text{Vis}/\text{TiO}_2/\text{H}_2\text{O}_2$ and UV/ TiO_2 processes. The generation of electrons was first confirmed by monitoring photocurrent while TiO_2 -coated ITO electrode was immersed in H_2O_2 solution. Subsequent reaction between electron and H_2O_2 can produce hydroxyl radicals.

It is believable that $\text{Vis}/\text{TiO}_2/\text{H}_2\text{O}_2$ process is cost efficient and practically applicable in the removal of persistent organic contaminants in natural waters since it can work under the irradiation of visible light which accounts for a much larger part of solar light than UV.

8.2 Limitation and Recommendation

In this study, all photochemical reactions were conducted in a batch reactor and the destruction of single target organics was focused. For practical application, it is suggested to examine the performance of UV/ O_3 and $\text{TiO}_2/\text{H}_2\text{O}_2/\text{Vis}$ systems in the presence of multiple organic pollutants. In the real treatment plant, influent are in flowing condition. The performance of these processes should be investigated in continuous flow reactor.

In addition, TiO₂ fine particles were used as photocatalyst in this study, which makes post-treatment necessary in real application. In order to overcome the disadvantages of the commercial TiO₂ fine powder, thus, coating TiO₂ on substrates such as glass beads, glass fiber, and activated carbon is recommended. The selection of substrates should be given special caution.

References:

- Abe, R., Takami, H., Murakami, N. and Ohtani, B. Pristine simple oxides as visible light driven photocatalysts: Highly efficient decomposition of organic compounds over platinum-loaded tungsten oxide. *Journal of the American Chemical Society* 2008, 130(25), 7780-7781.
- Acero, J.L., Stemmler, K. and Von Gunten, U. Degradation kinetics of atrazine and its degradation products with ozone and OH radicals: A predictive tool for drinking water treatment. *Environmental Science & Technology* 2000, 34(4), 591-597.
- Adams, C.D. and Randtke, S.J. Ozonation by-products of atrazine in synthetic and natural-waters. *Environmental Science & Technology* 1992, 26(11), 2218-2227.
- Adewuyi, Y.G. Sonochemistry in environmental remediation. 1. Combinative and hybrid sonophotochemical oxidation processes for the treatment of pollutants in water. *Environmental Science & Technology* 2005, 39(10), 3409-3420.
- Agrios, A.G., Gray, K.A. and Weitz, E. Narrow-band irradiation of a homologous series of chlorophenols on TiO₂: Charge-transfer complex formation and reactivity. *Langmuir* 2004, 20(14), 5911-5917.
- Al Momani, F., Smith, D.W. and El-Din, M.G. Degradation of cyanobacteria toxin by advanced oxidation processes. *Journal of Hazardous Materials* 2008, 150(2), 238-249.
- Asahi, R., Morikawa, T., Ohwaki, T., Aoki, K. and Taga, Y. Visible-light photocatalysis in nitrogen-doped titanium oxides. *Science* 2001, 293(5528), 269-271.
- Augugliaro, V., Loddo, V., Palmisano, L. and Schiavello, M. Performance of heterogeneous photocatalytic systems - Influence of operational variables on

- photoactivity of aqueous suspension of TiO₂. *Journal of Catalysis* 1995, 153(1), 32-40.
- Bahnemann, D. and Hart, E.J. Rate constants of the reaction of the hydrated electron and hydroxyl radical with ozone in aqueous solution. *Journal of Physical Chemistry* 1982, 86(2), 252-255.
- Barcelo, D. and Albaiges, J. Characterization of organo-phosphorus compounds and phenylurea herbicides by positive and negative-ion thermospray liquid-chromatography mass-spectrometry. *Journal of Chromatography* 1989, 474(1), 163-173.
- Beltran, F.J., Rivas, F.J. and Montero-de-Espinosa, R. Catalytic ozonation of oxalic acid in an aqueous TiO₂ slurry reactor. *Applied Catalysis B-Environmental* 2002, 39(3), 221-231.
- Beltran, F.J., Aguinaco, A. and Garcia-Araya, J.F. Mechanism and kinetics of sulfamethoxazole photocatalytic ozonation in water. *Water Research* 2009, 43(5), 1359-1369.
- Benitez, F.J., Beltranheredia, J. and Gonzalez, T. Degradation by ozone and UV-radiation of the herbicide cyanazine. *Ozone-Science & Engineering* 1994, 16(3), 213-234.
- Benitez, F.J., Real, F.J., Acero, J.L. and Garcia, C. Photochemical oxidation processes for the elimination of phenyl-urea herbicides in waters. *Journal of Hazardous Materials* 2006, 138(2), 278-287.
- Benitez, F.J., Real, F.J., Acero, J.L. and Garcia, C. Kinetics of the transformation of phenyl-urea herbicides during ozonation of natural waters: Rate constants and model predictions. *Water Research* 2007a, 41(18), 4073-4084.

- Benitez, F.J., Acero, J.L., Real, F.J. and Garcia, C. Removal of phenyl-urea herbicides in ultrapure water by ultrafiltration and nanofiltration processes. *Water Research* 2009, 43(2), 267-276.
- Benitez, F.J., Real, F.J., Real, J., Acero, J.L., Garcia, C. and Llanos, E.M. Kinetics of phenylurea herbicides oxidation by Fenton and photo-Fenton processes. *Journal of Chemical Technology and Biotechnology* 2007b, 82(1), 65-73.
- Bessekhouad, Y., Robert, D. and Weber, J.V. Photocatalytic activity of $\text{Cu}_2\text{O}/\text{TiO}_2$, $\text{Bi}_2\text{O}_3/\text{TiO}_2$ and $\text{ZnMn}_2\text{O}_4/\text{TiO}_2$ heterojunctions. *Catalysis Today* 2005, 101(3-4), 315-321.
- Bessekhouad, Y., Chaoui, N., Trzpit, M., Ghazzal, N., Robert, D. and Weber, J.V. UV-vis versus visible degradation of Acid Orange II in a coupled CdS/TiO_2 semiconductors suspension. *Journal of Photochemistry and Photobiology A-Chemistry* 2006, 183(1-2), 218-224.
- Bian, Z.F., Zhu, J., Wang, S.H., Cao, Y., Qian, X.F. and Li, H.X. Self-assembly of active $\text{Bi}_2\text{O}_3/\text{TiO}_2$ visible photocatalyst with ordered mesoporous structure and highly crystallized anatase. *Journal of Physical Chemistry C* 2008, 112(16), 6258-6262.
- Bin, A.K., Duczmal, B. and Machniewski, P., 2001 Hydrodynamics and ozone mass transfer in a tall bubble column, pp. 6233-6240, Melbourne, Australia.
- Boonstra, A.H. and Mutsaers, C. Adsorption of hydrogen-peroxide on surface of Titanium dioxide. *Journal of Physical Chemistry* 1975, 79(18), 1940-1943.
- Bouaifi, M.I. and Roustan, M. Bubble size and mass transfer coefficients in dual-impeller agitated reactors. *Canadian Journal of Chemical Engineering* 1998, 76(3), 390-397.

- Calvert, J.G. and Pitts, J.N.J., 1966. Photochemistry, John Wiley & Sons, Inc., New York, pp. 19-21.
- Canle, M., Rodriguez, S., Vazquez, L.F.R., Santaballa, J.A. and Steenken, S. First stages of photodegradation of the urea herbicides Fenuron, Monuron and Diuron. *Journal of Molecular Structure* 2001, 565, 133-139.
- Canton, C., Esplugas, S. and Casado, J. Mineralization of phenol in aqueous solution by ozonation using iron or copper salts and light. *Applied Catalysis B-Environmental* 2003, 43(2), 139-149.
- Cao, J., Sun, J.Z., Hong, J., Yang, X.G., Chen, H.Z. and Wang, M. Direct observation of microscopic photoinduced charge redistribution on TiO₂ film sensitized by chloroaluminum phthalocyanine and perylene diimide. *Applied Physics Letters* 2003, 83(9), 1896-1898.
- Castagna, R., Eiserich, J.P., Budamagunta, M.S., Stipa, P., Cross, C.E., Proietti, E., Voss, J.C. and Greci, L. Hydroxyl radical from the reaction between hypochlorite and hydrogen peroxide. *Atmospheric Environment* 2008, 42(26), 6551-6554.
- Caux, P.Y., Kent, R.A., Fan, G.T. and Grande, C. Canadian water quality guidelines for linuron. *Environmental Toxicology and Water Quality* 1998, 13(1), 1-41.
- Chai, S.Y., Kim, Y.J. and Lee, W.I. Photocatalytic WO₃/TiO₂ nanoparticles working under visible light. *Journal of Electroceramics* 2006, 17(2-4), 909-912.
- Chan, K.H. and Chu, W. Effect of humic acid on the photolysis of the pesticide atrazine in a surfactant-aided soil-washing system in acidic condition. *Water Research* 2005, 39(10), 2154-2166.
- Chen, W.R., Sharpless, C.M., Linden, K.G. and Suffet, I.H.M. Treatment of volatile organic chemicals on the EPA contaminant candidate list using ozonation and

- the O₃/H₂O₂ advanced oxidation process. *Environmental Science & Technology* 2006, 40(8), 2734-2739.
- Chen, W.R., Wu, C., Elovitz, M.S., Linden, K.G. and Suffet, I.H.M. Reactions of thiocarbamate, triazine and urea herbicides, RDX and benzenes on EPA Contaminant Candidate List with ozone and with hydroxyl radicals. *Water Research* 2008, 42(1-2), 137-144.
- Cho, Y.M., Choi, W.Y., Lee, C.H., Hyeon, T. and Lee, H.I. Visible light-induced degradation of carbon tetrachloride on dye-sensitized TiO₂. *Environmental Science & Technology* 2001, 35(5), 966-970.
- Choudhry, G.G. and Webster, G.R.B., 1987. Quantum yields of polychlorodibenzo-p-dioxins. In *Photochemistry of Environmental Aquatic Systems*, American Chemistry Society, Washington, DC, pp. 61-73.
- Choy, W.K. and Chu, W. Destruction of o-chloroaniline in UV/TiO₂ reaction with photosensitizing additives. *Industrial and Engineering Chemistry Research* 2005, 44(22), 8184-8189.
- Chu, W. Modeling the quantum yields of herbicide 2,4-D decay in UV/H₂O₂ process. *Chemosphere* 2001, 44(5), 935-941.
- Chu, W. and Tsui, S.M. Photo-sensitization of diazo disperse dye in aqueous acetone. *Chemosphere* 1999, 39(10), 1667-1677.
- Chu, W. and Ma, C.W. Quantitative prediction of direct and indirect dye ozonation kinetics. *Water Research* 2000, 34(12), 3153-3160.
- Chu, W. and Tsui, S.M. Modeling of photodecoloration of azo dye in a cocktail photolysis system. *Water Research* 2002, 36(13), 3350-3358.
- Chu, W. and Ching, M.H. Modeling the ozonation of 2,4-dichlorophoxyacetic acid through a kinetic approach. *Water Research* 2003, 37(1), 39-46.

- Chu, W. and Jia, J. The Photodegradation and Modeling of a Typical NAPL, Trichloroethene, by Monochromatic UV Irradiations. *Environmental Science & Technology* 2009, 43(5), 1455-1459.
- Chu, W., Chan, K.H., Kwan, C.Y. and Jafvert, C.T. Acceleration and quenching of the photolysis of PCB in the presence of surfactant and humic materials. *Environmental Science & Technology* 2005, 39(23), 9211-9216.
- Colborn, T., Saal, F.S.V. and Soto, A.M. Developmental effects of endocrine-disrupting chemicals in wildlife and humans. *Environmental Health Perspectives* 1993, 101(5), 378-384.
- Crosby, D.G. and Tang, C.S. Photodecomposition of 3-(p-Chlorophenyl)-1,1-Dimethylurea (Monuron). *Journal of Agricultural and Food Chemistry* 1969, 17(5), 1041-1044.
- Daam, M.A., Van den Brink, P.J. and Nogueira, A.J.A. Comparison of fate and ecological effects of the herbicide linuron in freshwater model ecosystems between tropical and temperate regions. *Ecotoxicology and Environmental Safety* 2009, 72(2), 424-433.
- de Moraes, S.G., Freire, R.S. and Duran, N. Degradation and toxicity reduction of textile effluent by combined photocatalytic and ozonation processes. *Chemosphere* 2000, 40(4), 369-373.
- Dejonghe, W., Berteloot, E., Goris, J., Boon, N., Crul, K., Maertens, S., Hofte, M., De Vos, P., Verstraete, W. and Top, E.M. Synergistic degradation of linuron by a bacterial consortium and isolation of a single linuron-degrading *Variovorax* strain. *Applied and Environmental Microbiology* 2003, 69(3), 1532-1541.

- DeLaat, J., MaoualaMakata, P. and Dore, M. Rate constants for reactions of ozone and hydroxyl radicals with several phenyl-ureas and acetamides. *Environmental Technology* 1996, 17(7), 707-716.
- Ding, Z., Lu, G.Q. and Greenfield, P.F. Role of the crystallite phase of TiO₂ in heterogeneous photocatalysis for phenol oxidation in water. *Journal of Physical Chemistry B* 2000, 104(19), 4815-4820.
- Dvoranov, D., Brezov, V., Milan, M. and Malati, M.A. Investigations of metal-doped titanium dioxide photocatalysts. *Applied Catalysis B-Environmental* 2002, 37(2), 91-105.
- Edhlund, B.L., Arnold, W.A. and McNeill, K. Aquatic photochemistry of nitrofurant antibiotics. *Environmental Science & Technology* 2006, 40(17), 5422-5427.
- EPA, U.S. Office of Pesticide Programs. Pesticide Fact Sheet for Linuron. 1984.
- Ernst, M., Lurot, F. and Schrotter, J.C. Catalytic ozonation of refractory organic model compounds in aqueous solution by aluminum oxide. *Applied Catalysis B-Environmental* 2004, 47(1), 15-25.
- Evgenidou, E., Fytianos, K. and Poulios, I. Semiconductor-sensitized photodegradation of dichlorvos in water using TiO₂ and ZnO as catalysts. *Applied Catalysis B-Environmental* 2005, 59(1-2), 81-89.
- Fan, X.X., Chen, X.Y., Zhu, S.P., Li, Z.S., Yu, T., Ye, J.H. and Zou, Z.G. The structural, physical and photocatalytic properties of the mesoporous Cr-doped TiO₂. *Journal of Molecular Catalysis A-Chemical* 2008, 284(1-2), 155-160.
- FAO, 2006 Statistical Database, <http://faostat.fao.org/> (Food and Agriculture Organization of the United Nations, Rome).

- Faria, P.C.C., Orfao, J.J.M. and Pereira, M.F.R. Activated carbon catalytic ozonation of oxamic and oxalic acids. *Applied Catalysis B-Environmental* 2008, 79(3), 237-243.
- Faria, P.C.C., Orfao, J.J.M. and Pereira, M.F.R. Activated carbon and ceria catalysts applied to the catalytic ozonation of dyes and textile effluents. *Applied Catalysis B-Environmental* 2009, 88(3-4), 341-350.
- Farre, M.J., Brosillon, S., Domenech, X. and Peral, J. Evaluation of the intermediates generated during the degradation of Diuron and Linuron herbicides by the photo-Fenton reaction. *Journal of Photochemistry and Photobiology A-Chemistry* 2007, 189(2-3), 364-373.
- Farre, M.J., Franch, M.I., Malato, S., Ayllon, J.A., Peral, J. and Domenech, X. Degradation of some biorecalcitrant pesticides by homogeneous and heterogeneous photocatalytic ozonation. *Chemosphere* 2005, 58(8), 1127-1133.
- Faure, V. and Boule, P. Phototransformation of linuron and chlorbromuron in aqueous solution. *Pesticide Science* 1997, 51(4), 413-418.
- Forni, L., Bahnemann, D. and Hart, E.J. Mechanism of the hydroxide ion initiated decomposition of ozone in aqueous solution. *Journal of Physical Chemistry* 1982, 86(2), 255-259.
- Fox, M.A. and Dulay, M.T. Heterogeneous Photocatalysis. *Chemical Reviews* 1993, 93(1), 341-357.
- Fryer, J.D. and Kirkland, K. Field Experiments to Investigate Long-Term Effects of Repeated Applications of MCPA, tri-allate, simazine and linuron: reports after 6 years. *Weed Research* 1970, 10(2), 133-158.

- Fu, H.B., Zhang, L.W., Yao, W.Q. and Zhu, Y.F. Photocatalytic properties of nanosized Bi₂WO₆ catalysts synthesized via a hydrothermal process. *Applied Catalysis B-Environmental* 2006, 66(1-2), 100-110.
- Fujishima, A. and Honda, K. Electrochemical Photolysis of Water at a Semiconductor Electrode. *Nature* 1972, 238(5358), 37-38.
- Funakoshi, Y., Nampo, T. and Enomoto, M. Photolysis Rate of The Herbicide Naproanilide Exposed to Sunlight in Water. *Journal of Pesticide Science* 1988, 13(2), 205-212.
- Fung, A.K.M., Chiu, B.K.W. and Lam, M.H.W. Surface modification of TiO₂ by a ruthenium(II) polypyridyl complex via silyl-linkage for the sensitized photocatalytic degradation of carbon tetrachloride by visible irradiation. *Water Research* 2003, 37(8), 1939-1947.
- Garcia-Lopez, E., Marci, G., Serpone, N. and Hidaka, H. Photoassisted oxidation of the recalcitrant cyanuric acid substrate in aqueous ZnO suspensions. *Journal of Physical Chemistry C* 2007, 111(49), 18025-18032.
- Garmouma, M., Blanchard, M., Chesterikoff, A., Ansart, P. and Chevreuil, M. Seasonal transport of herbicides (triazines and phenylureas) in a small stream draining an agricultural basin: Melarchez (France). *Water Research* 1997, 31(6), 1489-1503.
- Gilbert, E. Influence of ozone on the photocatalytic oxidation of organic compounds. *Ozone-Science & Engineering* 2002, 24(2), 75-82.
- Gimeno, O., Rivas, F.J., Beltran, F.J. and Carbajo, M. Photocatalytic ozonation of winery wastewaters. *Journal of Agricultural and Food Chemistry* 2007, 55, 9944-9950.

- Giraldez, I., Garcia-Araya, J.F. and Beltran, F.J. Activated carbon promoted ozonation of Polyphenol mixtures in water: comparison with single ozonation. *Industrial & Engineering Chemistry Research* 2007, 46, 8241-8247.
- Gong, J.L., Liu, Y.D. and Sun, X.B. O₃ and UV/O₃ oxidation of organic constituents of biotreated municipal wastewater. *Water Research* 2008, 42(4-5), 1238-1244.
- Graham, N., Chu, W. and Lau, C. Observations of 2,4,6-trichlorophenol degradation by ozone. *Chemosphere* 2003, 51(4), 237-243.
- Gurol, M.D. and Akata, A. Kinetics of ozone photolysis in aqueous solution. *AIChE Journal* 1996, 42(11), 3283-3292.
- Han, C.H., Li, Z.Y. and Shen, J.Y. Photocatalytic degradation of dodecylbenzenesulfonate over TiO₂-Cu₂O under visible irradiation. *Journal of Hazardous Materials* 2009, 168(1), 215-219.
- Hayase, Y. and Takahashi, T. Aceton-sensitized photolysis of the herbicide 3-(5-tert-butyl-3-isoxazolyl)-1,1-Dimethylurea (Isouron). *Journal of Pesticide Science* 1983, 8(4), 513-517.
- He, Z.Q., Song, S., Qiu, J.P., Yao, J., Cao, X.Y., Hu, Y.Q. and Chen, J.M. Decolorization of CI Reactive Yellow 84 in aqueous solution by electrocoagulation enhanced with ozone: Influence of operating conditions. *Environmental Technology* 2007a, 28(11), 1257-1263.
- He, Z.Q., Song, S., Xia, M., Qiu, J.P., Ying, H.P., Lu, B.S., Jiang, Y.F. and Chen, J.M. Mineralization of CI Reactive Yellow 84 in aqueous solution by sonolytic ozonation. *Chemosphere* 2007b, 69(2), 191-199.
- Hiroki, A. and LaVerne, J.A. Decomposition of hydrogen peroxide at water-ceramic oxide interfaces. *Journal of Physical Chemistry B* 2005, 109(8), 3364-3370.

- Hoffmann, M.R., Martin, S.T., Choi, W.Y. and Bahnemann, D.W. Environmental applications of semiconductor photocatalysis. *Chemical Reviews* 1995a, 95(1), 69-96.
- Hoffmann, M.R., Martin, S.T., Choi, W.Y. and Bahnemann, D.W. Environmental Applications of Semiconductor Photocatalysis. *Chemical Reviews* 1995b, 95(1), 69-96.
- Hoigne, J. and Bader, H. Rate constants of reactions of ozone with organic and inorganic-compounds in water. 1. Non-dissociating organic-compounds. *Water Research* 1983, 17(2), 173-183.
- Hossain, F.M., Sheppard, L., Nowotny, J. and Murch, G.E. Optical properties of anatase and rutile titanium dioxide: Ab initio calculations for pure and anion-doped material. *Journal of Physics and Chemistry of Solids* 2008, 69(7), 1820-1828.
- Huang, C.R. and Shu, H.Y. The reaction kinetics, decomposition pathways and intermediate formations of phenol in ozonation, UV/O₃ and UV/H₂O₂ processes. *Journal of Hazardous Materials* 1995, 41(1), 47-64.
- Huang, Y., Zheng, Z., Ai, Z.H., Zhang, L.Z., Fan, X.X. and Zou, Z.G. Core-shell microspherical Ti_{1-x}Zr_xO₂ solid solution photocatalysts directly from ultrasonic spray pyrolysis. *Journal of Physical Chemistry B* 2006, 110(39), 19323-19328.
- Inel, Y. and Okte, A.N. Photocatalytic degradation of malonic acid in aqueous suspensions of titanium dioxide: An initial kinetic investigation of CO₂ photogeneration. *Journal of Photochemistry and Photobiology A-Chemistry* 1996, 96(1-3), 175-180.

- Jin, F.M., Leitich, J. and vonSonntag, C. The photolysis ($\lambda=254$ nm) of tyrosine in aqueous solutions in the absence and presence of oxygen. The reaction of tyrosine with singlet oxygen. *Journal of Photochemistry and Photobiology A-Chemistry* 1995, 92(3), 147-153.
- Jing, L.Q., Li, S.D., Song, S., Xue, L.P. and Fu, H.G. Investigation on the electron transfer between anatase and rutile in nano-sized TiO₂ by means of surface photovoltage technique and its effects on the photocatalytic activity. *Solar Energy Materials and Solar Cells* 2008, 92(9), 1030-1036.
- Jirkovsky, J., Faure, V. and Boule, P. Photolysis of diuron. *Pesticide Science* 1997, 50(1), 42-52.
- Johnson, P.N. and Davis, R.A. Diffusivity of ozone in water. *Journal of Chemical and Engineering Data* 1996, 41(6), 1485-1487.
- Kaniou, S., Pitarakis, K., Barlagianni, I. and Poullos, I. Photocatalytic oxidation of sulfamethazine. *Chemosphere* 2005, 60(3), 372-380.
- Kaptijn, J.P. The Ecoclear(R) process. Results from full-scale installations. *Ozone-Science & Engineering* 1997, 19(4), 297-305.
- Kasprzyk-Hordern, B., Ziolk, M. and Nawrocki, J. Catalytic ozonation and methods of enhancing molecular ozone reactions in water treatment. *Applied Catalysis B-Environmental* 2003, 46(4), 639-669.
- Kasprzyk, B. and Nawrocki, J. Preliminary results on ozonation enhancement by a perfluorinated bonded alumina phase. *Ozone-Science & Engineering* 2002, 24(1), 63-68.
- Kastner, J.R., Ganagavaram, R., Kolar, P., Teja, A. and Xu, C.B. Catalytic ozonation of propanal using wood fly ash and metal oxide nanoparticle impregnated carbon. *Environmental Science & Technology* 2008, 42(2), 556-562.

- Katsumata, H., Kaneco, S., Suzuki, T., Ohta, K. and Yobiko, Y. Degradation of linuron in aqueous solution by the photo-Fenton reaction. *Chemical Engineering Journal* 2005, 108(3), 269-276.
- Kempsonjones, G.F. and Hance, R.J. Kinetics of Linuron and Metribuzin degradation in soil. *Pesticide Science* 1979, 10(6), 449-454.
- Khan, M.M.T., Bhardwaj, R.C. and Bhardwaj, C. Ru(bpy)₃(2+) photosensitized oxidation of ascorbic-acid and hydrogen evolution on TiO₂. *Inorganica Chimica Acta* 1987, 130(2), 153-154.
- Kim, I.H., Tanaka, H., Iwasaki, T., Takubo, T., Morioka, T. and Kato, Y. Classification of the degradability of 30 pharmaceuticals in water with ozone, UV and H₂O₂. *Water Science and Technology* 2008, 57(2), 195-200.
- Kishimoto, N., Yasuda, Y., Mizutani, H. and Ono, Y. Applicability of ozonation combined with electrolysis to 1,4-dioxane removal from wastewater containing radical scavengers. *Ozone-Science & Engineering* 2007, 29(1), 13-22.
- Kishimoto, N., Morita, Y., Tsuno, H., Oomura, T. and Mizutani, H. Advanced oxidation effect of ozonation combined with electrolysis. *Water Research* 2005, 39(19), 4661-4672.
- Kishimoto, N., Nakagawa, T., Asano, M., Abe, M., Yamada, M. and Ono, Y. Ozonation combined with electrolysis of 1,4-dioxane using a two-compartment electrolytic flow cell with solid electrolyte. *Water Research* 2008, 42(1-2), 379-385.
- Klare, M., Waldner, G., Bauer, R., Jacobs, H. and Broekaert, J.A.C. Degradation of nitrogen containing organic compounds by combined photocatalysis and ozonation. *Chemosphere* 1999, 38(9), 2013-2027.

- Klosek, S. and Raftery, D. Visible light driven V-doped TiO₂ photocatalyst and its photooxidation of ethanol. *Journal of Physical Chemistry B* 2001, 105(14), 2815-2819.
- Kormann, C., Bahnemann, D.W. and Hoffmann, M.R. Photocatalytic production of H₂O₂ and organic peroxides in aqueous suspensions of TiO₂, ZnO, and desert sand. *Environmental Science & Technology* 1988, 22(7), 798-806.
- Lall, R., Mutharasan, R., Shah, Y.T. and Dhurjati, P. Decolorization of the dye, reactive blue 19, using ozonation, ultrasound, and ultrasound-enhanced ozonation. *Water Environment Research* 2003, 75(2), 171-179.
- Lambright, C., Ostby, J., Bobseine, K., Wilson, V., Hotchkiss, A.K., Mann, P.C. and Gray, L.E. Cellular and molecular mechanisms of action of linuron: An antiandrogenic herbicide that produces reproductive malformations in male rats. *Toxicological Sciences* 2000, 56(2), 389-399.
- Lan, B.Y., Nigmatullin, R. and Puma, G.L. Ozonation kinetics of cork-processing water in a bubble column reactor. *Water Research* 2008, 42(10-11), 2473-2482.
- Lau, T.K., Chu, W. and Graham, N. The degradation of endocrine disruptor di-n-butyl phthalate by UV irradiation: A photolysis and product study. *Chemosphere* 2005, 60(8), 1045-1053.
- Lau, T.K., Chu, W. and Graham, N. Reaction pathways and kinetics of butylated hydroxyanisole with UV, ozonation, and UV/O₃ processes. *Water Research* 2007, 41(4), 765-774.
- Legube, B. and Leitner, N.K.V. Catalytic ozonation: a promising advanced oxidation technology for water treatment. *Catalysis Today* 1999, 53(1), 61-72.
- Li, X.K., Zhang, Q.Y., Tang, L.L., Lu, P., Sun, F.Q. and Li, L.S. Catalytic ozonation of p-chlorobenzoic acid by activated carbon and nickel supported activated

- carbon prepared from petroleum coke. *Journal of Hazardous Materials* 2009, 163(1), 115-120.
- Li, X.Z., Chen, C.C. and Zhao, J.C. Mechanism of photodecomposition of H₂O₂ on TiO₂ surfaces under visible light irradiation. *Langmuir* 2001, 17(13), 4118-4122.
- Liang, H.C., Li, X.Z., Yang, Y.H. and Sze, K.H. Effects of dissolved oxygen, pH, and anions on the 2,3-dichlorophenol degradation by photocatalytic reaction with anodic TiO₂ nanotube films. *Chemosphere* 2008, 73(5), 805-812.
- Lin, C.F., Wu, C.H. and Onn, Z.N. Degradation of 4-chlorophenol in TiO₂, WO₃, SnO₂, TiO₂/WO₃ and TiO₂/SnO₂ systems. *Journal of Hazardous Materials* 2008, 154(1-3), 1033-1039.
- Lin, J., Yu, J.C., Lo, D. and Lam, S.K. Photocatalytic activity of rutile Ti_{1-x}Sn_xO₂ solid solutions. *Journal of Catalysis* 1999, 183(2), 368-372.
- Lin, L., Lin, W., Zhu, Y.X., Zhao, B.Y. and Xie, Y.C. Phosphor-doped titania - a novel photocatalyst active in visible light. *Chemistry Letters* 2005, 34(3), 284-285.
- Linsebigler, A.L., Lu, G.Q. and Yates, J.T. Photocatalysis on TiO₂ Surfaces: Principles, Mechanisms, and Selected Results. *Chemical Reviews* 1995, 95(3), 735-758.
- Lintelmann, J., Katayama, A., Kurihara, N., Shore, L. and Wenzel, A. Endocrine disruptors in the environment - (IUPAC Technical Report). *Pure and Applied Chemistry* 2003, 75(5), 631-681.
- Liu, H.Y. and Gao, L. Preparation and properties of nanocrystalline alpha-Fe₂O₃-sensitized TiO₂ nanosheets as a visible light photocatalyst. *Journal of the American Ceramic Society* 2006, 89(1), 370-373.

- Liu, Y. and Sun, D.Z. Development of Fe₂O₃-CeO₂-TiO₂/gamma-Al₂O₃ as catalyst for catalytic wet air oxidation of methyl orange azo dye under room condition. *Applied Catalysis B-Environmental* 2007, 72(3-4), 205-211.
- Lo, S., King, I., Allera, A. and Klingmuller, D. Effects of various pesticides on human 5 alpha-reductase activity in prostate and LNCaP cells. *Toxicology In Vitro* 2007, 21(3), 502-508.
- Logemann, F.P. and Annee, J.H.J. Water treatment with a fixed bed catalytic ozonation process. *Water Science and Technology* 1997, 35(4), 353-360.
- Lopez, M.C., Fernandez, M.I., Rodriguez, S., Santaballa, J.A., Steenken, S. and Vulliet, E. Mechanisms of direct and TiO₂-photocatalysed UV degradation of phenylurea herbicides. *Chemphyschem* 2005, 6(10), 2064-2074.
- Ma, H.J., Wang, M., Pu, C.Y., Zhang, J., Zhao, S.F., Yao, S. and Xiong, J. Transient and steady-state photolysis of p-nitroaniline in aqueous solution. *Journal of Hazardous Materials* 2009, 165(1-3), 867-873.
- McIntyre, B.S., Barlow, N.J., Wallace, D.G., Maness, S.C., Gaido, K.W. and Foster, P.M.D. Effects of in utero exposure to linuron on androgen-dependent reproductive development in the male Crl : CD(SD)BR rat. *Toxicology and Applied Pharmacology* 2000, 167(2), 87-99.
- Murphy, D.M., Griffiths, E.W., Rowlands, C.C., Hancock, F.E. and Giamello, E. EPR study of the H₂O₂ interaction with TiO₂; evidence for a novel S=1 surface radical pair. *Chemical Communications* 1997, (22), 2177-2178.
- Ni, C.H. and Chen, J.N. Heterogeneous catalytic ozonation of 2-chlorophenol aqueous solution with alumina as a catalyst. *Water Science and Technology* 2001, 43(2), 213-220.

- Ni, C.H., Chen, J.N. and Yang, P.Y., 2003 Catalytic ozonation of 2-dichlorophenol by metallic ions, pp. 77-82, Singapore, Singapore.
- Nienow, A.M., Bezares-Cruz, J.C., Poyer, I.C., Hua, I. and Jafvert, C.T. Hydrogen peroxide-assisted UV photodegradation of Lindane. *Chemosphere* 2008, 72(11), 1700-1705.
- Niishiro, R., Konta, R., Kato, H., Chun, W.J., Asakura, K. and Kudo, A. Photocatalytic O₂ evolution of rhodium and antimony-codoped rutile-type TiO₂ under visible light irradiation. *Journal of Physical Chemistry C* 2007, 111, 17420-17426.
- Ogino, C., Dadjour, M.F., Iida, Y. and Shimizu, N. Decolorization of methylene blue in aqueous suspensions of titanium peroxide. *Journal of Hazardous Materials* 2008, 153(1-2), 551-556.
- Ohno, T., Masaki, Y., Hirayama, S. and Matsumura, M. TiO₂-photocatalyzed epoxidation of 1-decene by H₂O₂ under visible light. *Journal of Catalysis* 2001, 204(1), 163-168.
- Orton, F., Lutz, I., Kloas, W. and Routledge, E.J. Endocrine disrupting effects of herbicides and pentachlorophenol: In vitro and in vivo evidence. *Environmental Science & Technology* 2009, 43(6), 2144-2150.
- Pal, B., Sharon, M. and Nogami, G. Preparation and characterization of TiO₂/Fe₂O₃ binary mixed oxides and its photocatalytic properties. *Materials Chemistry and Physics* 1999, 59(3), 254-261.
- Patrick, B. and Kamat, P.V. Photoelectrochemistry in Semiconductor Particulate Systems.17. Photosensitization of Large-Bandgap Semiconductors - Charge Injection from Triplet Excited Thionine into ZnO Colloids. *Journal of Physical Chemistry* 1992, 96(3), 1423-1428.

- Paul, T., Miller, P.L. and Strathmann, T.J. Visible-light-mediated TiO₂ photocatalysis of fluoroquinolone antibacterial agents. *Environmental Science & Technology* 2007, 41(13), 4720-4727.
- Peyton, G.R. and Glaze, W.H. Destruction of pollutants in water with ozone in combination with ultraviolet-radiation.3. Photolysis of aqueous ozone. *Environmental Science & Technology* 1988, 22(7), 761-767.
- Piera, E., Tejedor-Tejedor, M.I., Zorn, M.E. and Anderson, M.A. Relationship concerning the nature and concentration of Fe(III) species on the surface of TiO₂ particles and photocatalytic activity of the catalyst. *Applied Catalysis B-Environmental* 2003, 46(4), 671-685.
- Pimentel, D. Amounts of pesticides reaching target pests - Environmental impacts and ethics. *Journal of Agricultural and Environmental Ethics* 1995, 8(1), 17-29.
- Pines, D.S. and Reckhow, D.A. Effect of dissolved cobalt(II) on the ozonation of oxalic acid. *Environmental Science & Technology* 2002, 36(19), 4046-4051.
- Poulios, I., Micropoulou, E., Panou, R. and Kostopoulou, E. Photooxidation of eosin Y in the presence of semiconducting oxides. *Applied Catalysis B-Environmental* 2003, 41(4), 345-355.
- Rabek, J.F., 1982. *Experimental Methods in Photochemistry and Photophysics Part 2*, John Wiley & Sons Ltd, pp. 854.
- Regazzoni, A.E., Mandelbaum, P., Matsuyoshi, M., Schiller, S., Bilmes, S.A. and Blesa, M.A. Adsorption and photooxidation of salicylic acid on titanium dioxide: A surface complexation description. *Langmuir* 1998, 14(4), 868-874.
- Rezaee, A., Ghaneian, M., Hashemian, S.J., Mosavi, G. and Hajizadeh, E. Enhanced decolorization of reactive blue 19 dye from synthetic textile wastewater

- through UV photolysis in alkaline conditions. *Environmental Engineering and Management Journal* 2008, 7(2), 119-123.
- Rodriguez-Cruz, M.S., Andrades, M.S., Parada, A.M. and Sanchez-Martin, M.J. Effect of different wood pretreatments on the sorption-desorption of linuron and metalaxyl by woods. *Journal of Agricultural and Food Chemistry* 2008, 56(16), 7339-7346.
- Sanchez, L., Peral, J. and Domenech, X. Aniline degradation by combined photocatalysis and ozonation. *Applied Catalysis B-Environmental* 1998, 19(1), 59-65.
- Scaife, D.E. Oxide semiconductors in photoelectrochemical conversion of solar energy. *Solar Energy* 1980, 25(1), 41-54.
- Schwarzenbach, R.P., Escher, B.I., Fenner, K., Hofstetter, T.B., Johnson, C.A., von Gunten, U. and Wehrli, B. The challenge of micropollutants in aquatic systems. *Science* 2006, 313(5790), 1072-1077.
- Serpone, N., Maruthamuthu, P., Pichat, P., Pelizzetti, E. and Hidaka, H. Exploiting the interparticle electron-transfer process in the photocatalyzed oxidation of phenol, 2-chlorophenol and pentachlorophenol - Chemical evidence for electron and hole transfer between coupled semiconductors. *Journal of Photochemistry and Photobiology A-Chemistry* 1995, 85(3), 247-255.
- Smith, A.E. and Emmond, G.S. Persistence of Linuron in Saskatchewan soils. *Canadian Journal of Soil Science* 1975, 55(2), 145-148.
- Solomons, T.W.G., Fryhle, C.B., 2006. Organic Chemistry, John Wiley & Sons, Inc., Jefferson, USA, pp. 650-661.
- Song, S., Xu, X., Xu, L.J., He, Z.Q., Ying, H.P., Chen, J.M. and Yan, B. Mineralization of CI reactive yellow 145 in aqueous solution by ultraviolet-

- enhanced ozonation. *Industrial & Engineering Chemistry Research* 2008, 47(5), 1386-1391.
- Sorensen, S.R., Rasmussen, J., Jacobsen, C.S., Jacobsen, O.S., Juhler, R.K. and Aamand, J. Elucidating the key member of a linuron-mineralizing bacterial community by PCR and reverse transcription-PCR denaturing gradient gel electrophoresis 16S rRNA gene fingerprinting and cultivation. *Applied and Environmental Microbiology* 2005, 71(7), 4144-4148.
- Spamer, A., Dube, T.I., Moodley, D.J., van Schalkwyk, C. and Botha, J.M. Application of a WO₃/SiO₂ catalyst in an industrial environment: part II. *Applied Catalysis A-General* 2003, 255(2), 133-142.
- Srinivasan, S.S., Wade, J. and Stefanakos, E.K. Visible light photocatalysis via CdS/TiO₂ nanocomposite materials. *Journal of Nanomaterials* 2006.
- Staehelin, J. and Hoigne, J. Decomposition of ozone in water: rate of initiation by hydroxide ions and hydrogen peroxide. *Environmental Science & Technology* 1982, 16(10), 676-681.
- Tachikawa, T., Tojo, S., Kawai, K., Endo, M., Fujitsuka, M., Ohno, T., Nishijima, K., Miyamoto, Z. and Majima, T. Photocatalytic oxidation reactivity of holes in the sulfur- and carbon-doped TiO₂ powders studied by time-resolved diffuse reflectance spectroscopy. *Journal of Physical Chemistry B* 2004, 108(50), 19299-19306.
- Tahmasseb, L.A., Nelieu, S., Kerhoas, L. and Einhorn, J. Ozonation of chlorophenylurea pesticides in water: reaction monitoring and degradation pathways. *Science of the Total Environment* 2002, 291(1-3), 33-44.

- Tanaka, K., Abe, K. and Hisanaga, T. Photocatalytic water treatment on immobilized TiO₂ combined with ozonation. *Journal of Photochemistry and Photobiology A-Chemistry* 1996, 101(1), 85-87.
- Thompson, T.L. and Yates, J.T. Surface science studies of the photoactivation of TiO₂-new photochemical processes. *Chemical Reviews* 2006, 106(10), 4428-4453.
- United Nations Educational, Scientific and Cultural Organization, 2003 Water for People, Water for Life-the United Nations World Water Development Report, Berghahn Books, Barcelona.
- van Schalkwyk, C., Spamer, A., Moodley, D.J., Dube, T., Reynhardt, J. and Botha, J.M. Application of a WO₃/SiO₂ catalyst in an industrial environment: Part I. *Applied Catalysis A-General* 2003, 255(2), 121-131.
- Wagner, S.L., 1983. *Clinical Toxicology of Agricultural Chemicals*, pp. 273-274.
- Wang, C., Li, J., Mele, G., Yang, G.M., Zhang, F.X., Palmisano, L. and Vasapollo, G. Efficient degradation of 4-nitrophenol by using functionalized porphyrin-TiO₂ photocatalysts under visible irradiation. *Applied Catalysis B-Environmental* 2007, 76, 218-226.
- Wang, S.P., Shiraishi, F. and Nakano, K. A synergistic effect of photocatalysis and ozonation on decomposition of formic acid in an aqueous solution. *Chemical Engineering Journal* 2002, 87(2), 261-271.
- Wayne, R.P., 1970. *Photochemistry*, Butterworth & Co (Publishers) Ltd, London, pp. 1.
- Wayne, R.P., 1988. *Principles and Applications of Photochemistry*, Oxford University Press, Walton Street, Oxford OX2 6DP, London, pp. 5-7.

- Weavers, L.K. and Hoffmann, M.R. Sonolytic decomposition of ozone in aqueous solution: Mass transfer effects. *Environmental Science & Technology* 1998, 32(24), 3941-3947.
- Wells, C.H.J., 1972. Introduction to Molecular Photochemistry, John Wiley & Sons, Inc., New York, pp. 88-115.
- Wilson, V.S., Lambright, C.R., Furr, J.R., Howdeshell, K.L. and Gray, L.E. The herbicide linuron reduces testosterone production from the fetal rat testis during both in utero and in vitro exposures. *Toxicology Letters* 2009, 186(2), 73-77.
- Winarno, E.K. and Getoff, N. Comparative studies on the degradation of aqueous 2-chloroaniline by O₃ as well as by UV-light and gamma-rays in the presence of ozone. *Radiation Physics and Chemistry* 2002, 65(4-5), 387-395.
- Wong, C.C. and Chu, W. The hydrogen peroxide-assisted photocatalytic degradation of alachlor in TiO₂ suspensions. *Environmental Science & Technology* 2003, 37(10), 2310-2316.
- Xiao, H., Liu, R.P., Zhao, X. and Qu, J.H. Effect of manganese ion on the mineralization of 2,4-dichlorophenol by ozone. *Chemosphere* 2008, 72(7), 1006-1012.
- Xu, Y. and Schoonen, M.A.A. The absolute energy positions of conduction and valence bands of selected semiconducting minerals. *American Mineralogist* 2000, 85(3-4), 543-556.
- Xu, Z.H., Jing, C.Y., Li, F.S. and Meng, X.G. Mechanisms of photocatalytic degradation of monomethylarsonic and dimethylarsinic acids using nanocrystalline titanium dioxide. *Environmental Science & Technology* 2008, 42(7), 2349-2354.

- Yao, C.C.D. and Haag, W.R. Rate constants for direct reactions of ozone with several drinking water contaminants. *Water Research* 1991, 25(7), 761-773.
- Yeatts, L.R.B. and Taube, H. The kinetics of the reaction of ozone and chloride ion in acid aqueous solution. *Journal of the American Chemical Society* 1949, 71(12), 4100-4105.
- Yu, J.C., Zhang, L.Z., Zheng, Z. and Zhao, J.C. Synthesis and characterization of phosphated mesoporous titanium dioxide with high photocatalytic activity. *Chemistry of Materials* 2003, 15(11), 2280-2286.
- Zaleska, A., Sobczak, J.W., Grabowska, E. and Hupka, J. Preparation and photocatalytic activity of boron-modified TiO₂ under UV and visible light. *Applied Catalysis B-Environmental* 2008, 78(1-2), 92-100.
- Zang, L. and Rodgers, M.A.J. Diffusion-controlled charge transfer from excited Ru(bpy)₃(2+) into nanosized TiO₂ colloids stabilized with EDTA. *Journal of Physical Chemistry B* 2000, 104(3), 468-474.
- Zhang, T. and Ma, J. Catalytic ozonation of trace nitrobenzene in water with synthetic goethite. *Journal of Molecular Catalysis A-Chemical* 2008, 279(1), 82-89.
- Zhao, L., Ma, J. and Sun, Z.Z. Oxidation products and pathway of ceramic honeycomb-catalyzed ozonation for the degradation of nitrobenzene in aqueous solution. *Applied Catalysis B-Environmental* 2008, 79(3), 244-253.
- Zhao, L., Sun, Z.Z., Ma, J. and Liu, H.L. Enhancement Mechanism of Heterogeneous Catalytic Ozonation by Cordierite-Supported Copper for the Degradation of Nitrobenzene in Aqueous Solution. *Environmental Science & Technology* 2009, 43(6), 2047-2053.

APPENDIX I: Experimental runs

Experiment No.	Compound	Initial Concentration	Parameters				
			<i>pH</i>	<i>O₃</i> (mM)	<i>UV</i> (nm)	<i>Intensity</i> (Einstein L ⁻¹ min ⁻¹)	<i>H₂O₂</i> (mM)
4-1	LNR	0.1 mM	6.0		254	3.0×10 ⁻⁶	
4-2	LNR	0.1 mM	6.0		254	6.0×10 ⁻⁶	
4-3	LNR	0.1 mM	6.0		254	9.0×10 ⁻⁶	
4-4	LNR	0.1 mM	6.0		254	1.2×10 ⁻⁵	
4-5	LNR	0.1 mM	3.0	0.0171			
4-6	LNR	0.1 mM	6.0	0.0171			
4-7	LNR	0.1 mM	9.0	0.0171			
4-8	LNR	0.1 mM	10.0	0.0171			
4-9	LNR	0.1 mM	10.7	0.0171			
4-10	LNR	0.1 mM	11.0	0.0171			
4-11	LNR	0.1 mM	9.0	0.00996			
4-12	LNR	0.1 mM	10.0	0.00996			
4-13	LNR	0.1 mM	10.7	0.00996			
4-14	LNR	0.1 mM	11.0	0.00996			
4-15	LNR	0.1 mM	9.0	0.0244			
4-16	LNR	0.1 mM	10.0	0.0244			
4-17	LNR	0.1 mM	10.7	0.0244			
4-18	LNR	0.1 mM	11.0	0.0244			
4-19	LNR	0.1 mM	9.0	0.0309			
4-20	LNR	0.1 mM	10.0	0.0309			

4-21	LNR	0.1 mM	10.7	0.0309			
4-22	LNR	0.1 mM	11.0	0.0309			
4-23	LNR and ATZ	10 μ M	6.0		254	3.0×10^{-6}	20
4-24	LNR	0.1 mM	4.0	0.0171	254	3.0×10^{-6}	
4-25	LNR	0.1 mM	4.0	0.0171	254	6.0×10^{-6}	
4-26	LNR	0.1 mM	4.0	0.0171	254	9.0×10^{-6}	
4-27	LNR	0.1 mM	4.0	0.0171	254	1.2×10^{-5}	
5-1	LNR	0.1 mM	3.0		254	6.0×10^{-6}	
5-2	LNR	0.1 mM	9.0		254	6.0×10^{-6}	
5-3	LNR	0.1 mM	10.0		254	6.0×10^{-6}	
5-4	LNR	0.1 mM	11.0		254	6.0×10^{-6}	
5-5	LNR	0.1 mM	3.0	0.0171	254	6.0×10^{-6}	
5-6	LNR	0.1 mM	6.0	0.0171	254	6.0×10^{-6}	
5-7	LNR	0.1 mM	9.0	0.0171	254	6.0×10^{-6}	
5-8	LNR	0.1 mM	10.0	0.0171	254	6.0×10^{-6}	
5-9	LNR	0.1 mM	11.0	0.0171	254	6.0×10^{-6}	
5-10	LNR	0.29 mM	6.0		254	9.0×10^{-6}	
5-11	LNR	0.29 mM (purge Argon)	6.0		254	9.0×10^{-6}	
5-12	DCPMU	0.18 mM	6.0		254	9.0×10^{-6}	
5-13	DCPU	0.20 mM	6.0		254	9.0×10^{-6}	
5-14	LNR	0.29 mM	6.0	0.0245			
5-15	DCPMU	0.18 mM	6.0	0.0245			
5-16	LNR	0.29 mM	6.0	0.0245	254	9.0×10^{-6}	

Experiment No.	Compound	Initial Concentration	Parameters					
			<i>pH</i>	<i>O₃</i> (mM)	<i>Cl</i> (M)	<i>SO₄²⁻</i> (M)	<i>CO₃²⁻</i> (M)	<i>HPO₄²⁻</i> (M)
5-17	LNR	0.1 mM	3.0	0.0171	0.01			
5-18	LNR	0.1 mM	3.0	0.0171		0.01		
5-19	LNR	0.1 mM	3.0	0.0171				0.01
5-20	LNR	0.1 mM	7.0	0.0245	0.01			
5-21	LNR	0.1 mM	7.0	0.0245		0.01		
5-22	LNR	0.1 mM	7.0	0.0245			0.01	
5-23	LNR	0.1 mM	7.0	0.0245				0.01
5-24	LNR	0.1 mM	7.0	0.0245				

Experiment No.	Compound	Initial Concentration	Parameters						
			<i>pH</i>	<i>TiO₂</i> (g/L)	<i>WO₃</i> (g/L)	<i>ZnO</i> (g/L)	<i>Hg lamp</i> (nm)	<i>DO</i> <i>mgL⁻¹</i>	<i>H₂O₂</i> (mM)
6-1	LNR	0.1 mM	6.0	0.6					10
6-2	LNR	0.1 mM	6.0	0.6			419		
6-3	LNR	0.1 mM	6.0				419		10
6-4	LNR	0.1 mM	6.0	0.6			419		10
6-5	LNR	0.1 mM (with quencher)	6.0	0.6			419		
6-6	LNR	0.1 mM (with quencher)	6.0	0.6			419		10
6-7	LNR	0.1 mM	6.0	0.6			419	31.2	
6-8	LNR	0.1 mM	6.0		0.6		419		
6-9	LNR	0.1 mM	6.0		0.6		419	30.8	
6-10	LNR	0.1 mM	6.0		0.6		419		10
6-11	LNR	0.1 mM	6.0			0.6	419		
6-12	LNR	0.1 mM	6.0			0.6	419	31.7	
6-13	LNR	0.1 mM	6.0			0.6	419		10
6-14	LNR	0.1 mM	6.0	0.05			419		10
6-15	LNR	0.1 mM	6.0	0.1			419		10
6-16	LNR	0.1 mM	6.0	0.2			419		10
6-17	LNR	0.1 mM	6.0	0.4			419		10
6-18	LNR	0.1 mM	6.0	0.8			419		10
6-19	LNR	0.1 mM	6.0	1.0			419		10
6-20	LNR	0.1 mM	6.0	0.4			419		1

6-21	LNR	0.1 mM	6.0	0.4			419		2
6-22	LNR	0.1 mM	6.0	0.4			419		5
6-23	LNR	0.1 mM	6.0	0.4			419		20
6-24	LNR	0.1 mM	2.0	0.4			419		5
6-25	LNR	0.1 mM	4.0	0.4			419		5
6-26	LNR	0.1 mM	9.0	0.4			419		5
6-27	LNR	0.1 mM	11.0	0.4			419		5
6-28	LNR	0.0125 mM	6.0	0.4			419		5
6-29	LNR	0.025 mM	6.0	0.4			419		5
6-30	LNR	0.05 mM	6.0	0.4			419		5
6-31	LNR	0.2 mM	6.0	0.4			419		5
6-32	LNR	0.3 mM	6.0	0.4			419		5

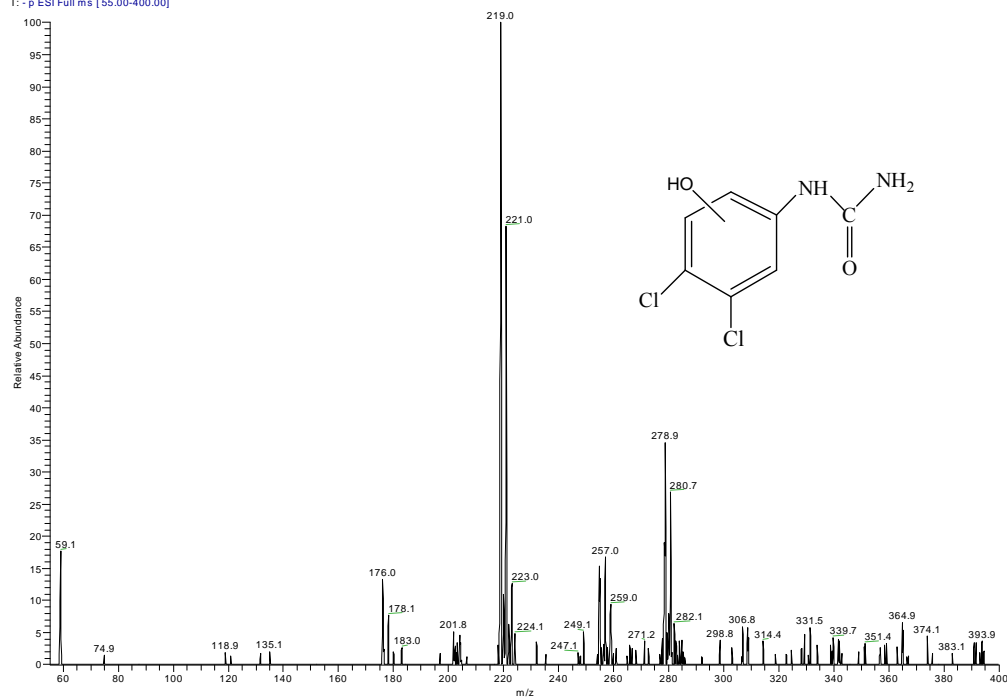
Experiment. No	Compound	Initial Concentration	Parameters					
			pH	Rutile (g/L)	Anatase (g/L)	Hg lamp (nm)	DO mgL^{-1}	H ₂ O ₂ (mM)
6-33	LNR	0.1 mM	6.0	0.6		419		
6-34	LNR	0.1 mM	6.0	0.6		419		10
6-35	LNR	0.1 mM	6.0		0.6	419		
6-36	LNR	0.1 mM	6.0		0.6	419		10

Experiment. No	Compound	Initial Concentration	Parameters					
			pH	TiO ₂ (g/L)	Hg lamp (nm)	Xe lamp (nm)	DO mgL ⁻¹	H ₂ O ₂ (mM)
7-1	LNR	0.1 mM	6.0	0.6		420	6.1	
7-2	LNR	0.1 mM	6.0			420	6.3	10
7-3	LNR	0.1 mM	6.0	0.6		420	39.3	
7-4	LNR	0.1 mM	6.0	0.6		420	5.9	10
7-5	LNR	0.1 mM	6.0	0.6		435	6.5	10
7-6	LNR	0.1 mM	6.0	0.6		450	6.4	10
7-7	LNR	0.1 mM	6.0	0.6		500	6.7	10
7-8	LNR (100 mg/L NaN ₃)	0.1 mM	6.0	0.6		435	6.1	10
7-9	LNR (100 mg/L HCO ₃)	0.1 mM	6.0	0.6		435	6.4	10
7-10	LNR (100 mg/L t-butanol)	0.1 mM	6.0	0.6		435	6.2	10
7-11	LNR (3 g/L t-butanol)	0.1 mM	6.0	0.6		435	6.1	10
7-12	LNR	0.29 mM	6.0	0.6		420	6.7	10
7-13	LNR	0.29 mM	6.0	0.1	350		6.5	
7-14	DCPMU	0.18 mM	6.0	0.6		420	6.4	10
7-15	DCPU	0.2 mM	6.0	0.6		420	6.3	10

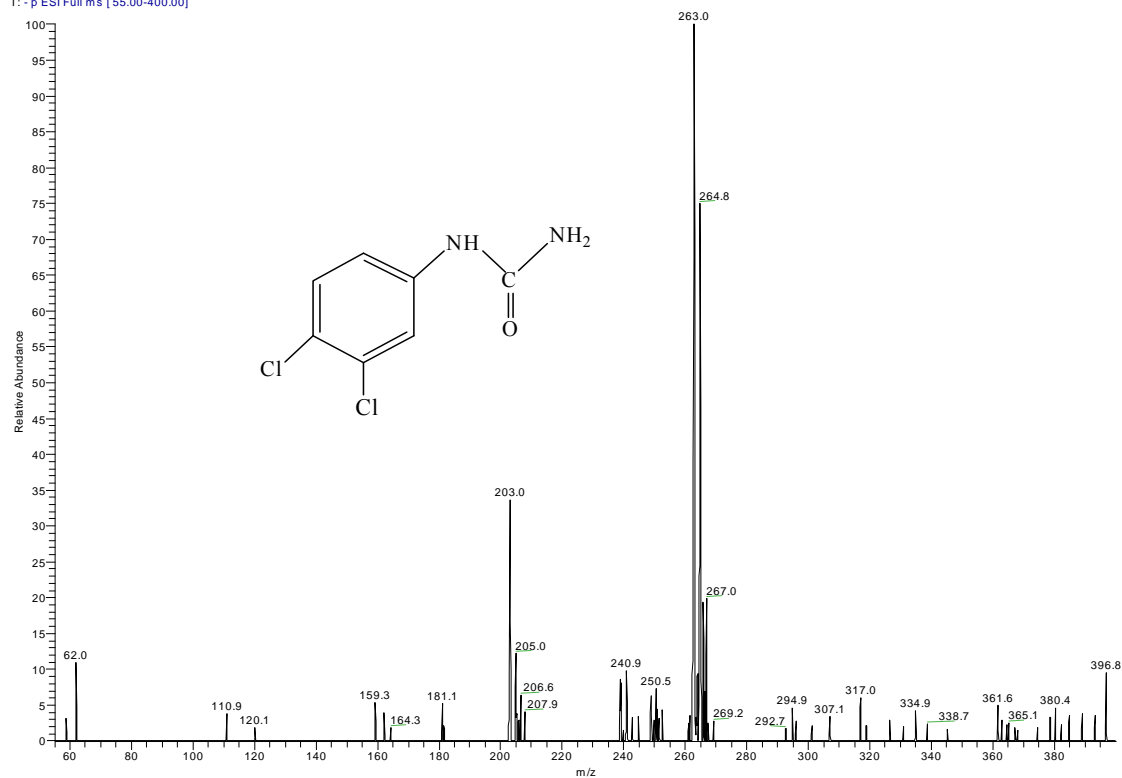
Experiment. No	Compound	Initial Concentration	Parameters					
			pH	Ga ₂ O ₃ (g/L)	SiO ₂ (g/L)	Al ₂ O ₃	Xe lamp (nm)	H ₂ O ₂ (mM)
7-16	LNR	0.1 mM	6.0	0.6			420	10
7-17	LNR	0.1 mM	6.0		0.6		420	10
7-18	LNR	0.1 mM	6.0			0.6	420	10

APPENDIX II: Mass spectrum of LNR and major intermediates

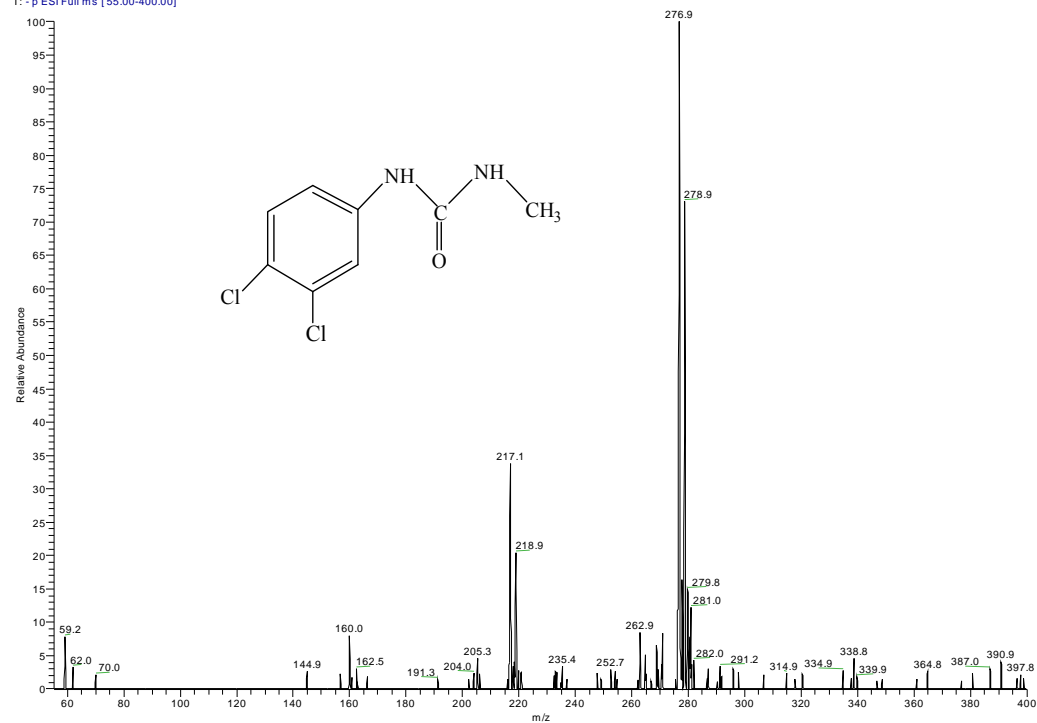
DCPU-P25-H2O2-420-4hr #1600 RT: 16.52 AV: 1 NL: 1.64E6
T: -p ESI Full ms [55.00-400.00]



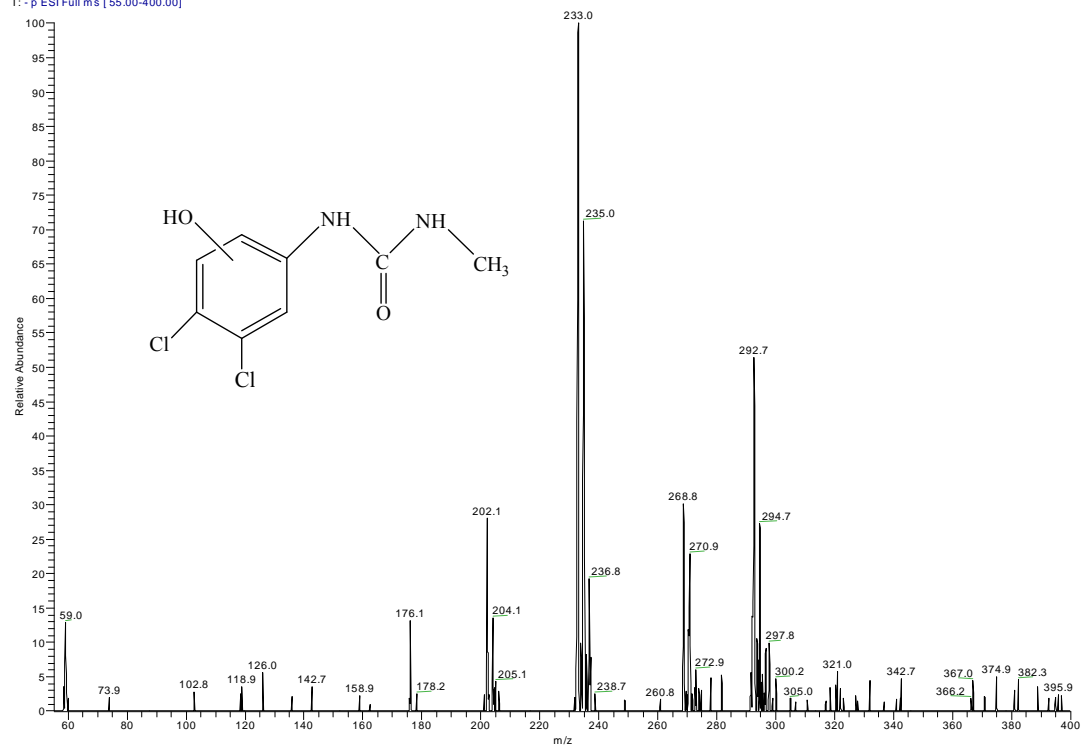
DCPU-P25-H2O2-420-8hr_090103162920 #1689 RT: 17.38 AV: 1 NL: 1.25E6
T: -p ESI Full ms [55.00-400.00]



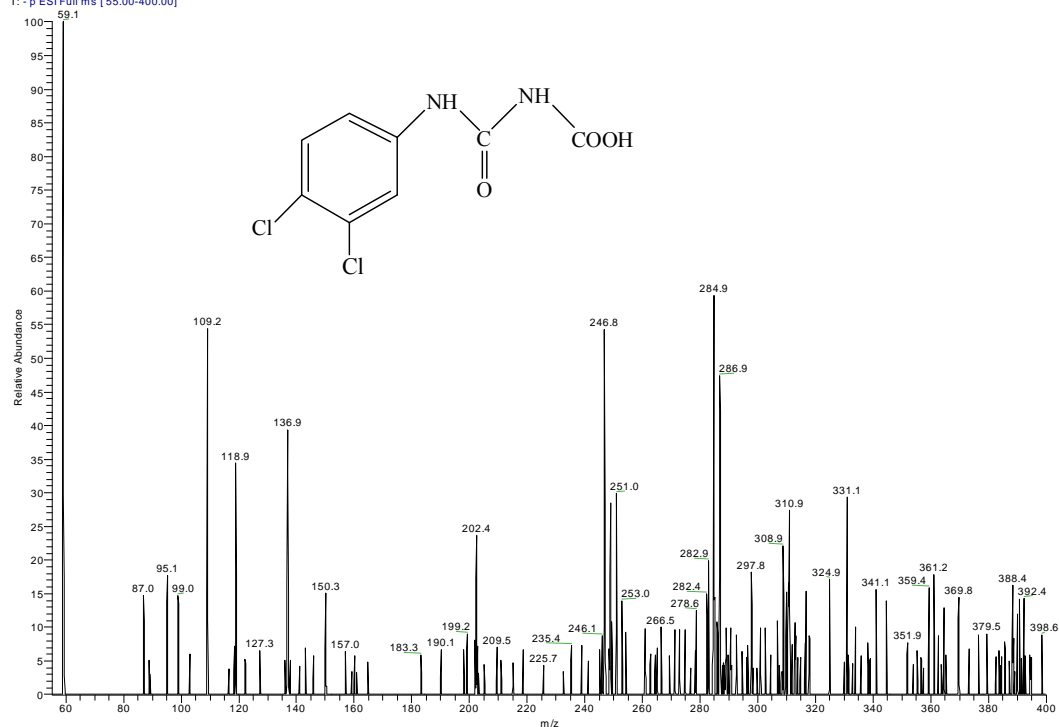
DCPMJ-P25-H2O2-7hr02 #1849 RT: 18.60 AV: 1 NL: 3.04E6
T: -p ESI Full ms [55.00-400.00]



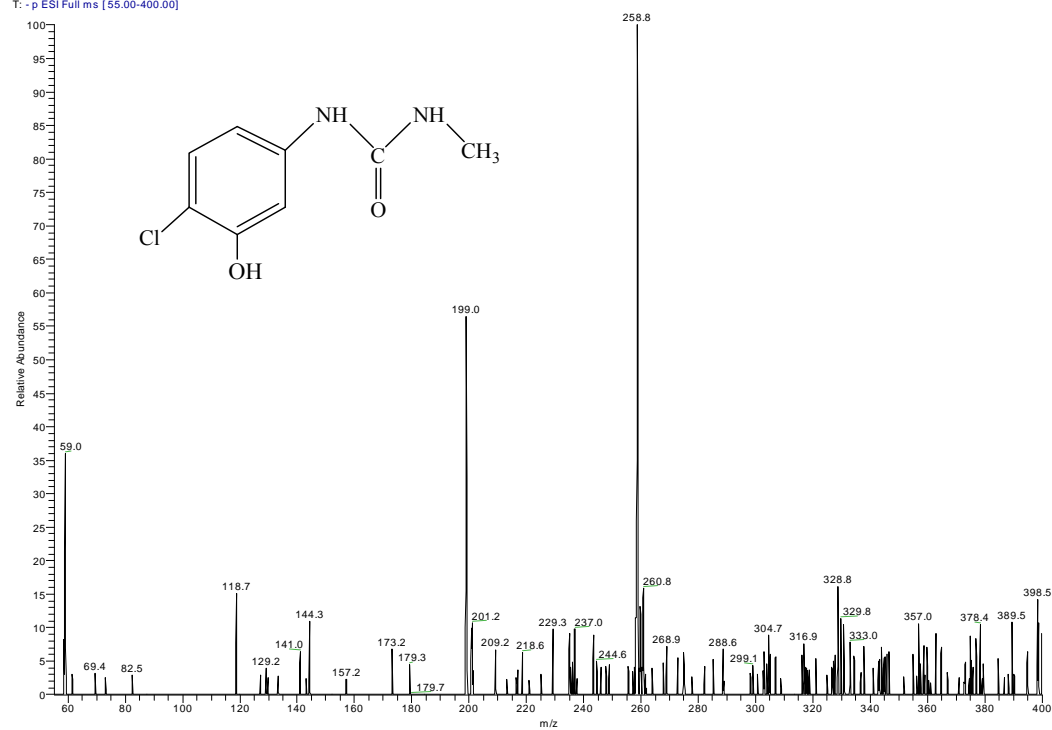
DCPMJ-P25-H2O2-7hr02 #1770 RT: 17.91 AV: 1 NL: 2.66E6
T: -p ESI Full ms [55.00-400.00]



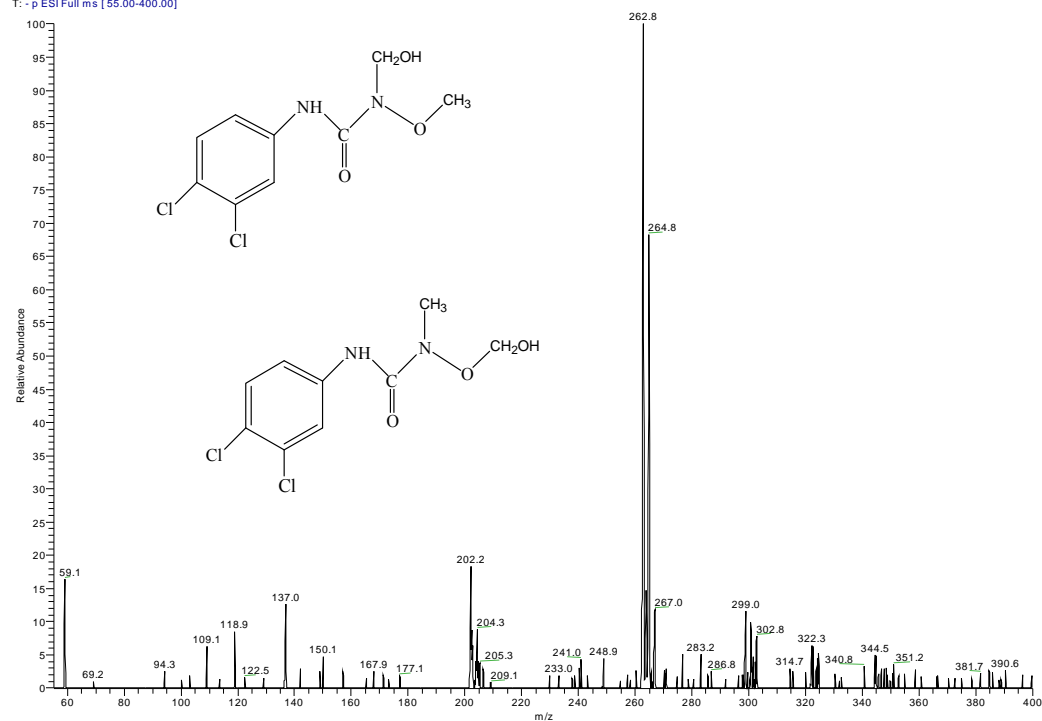
LNR-P25-H2O2-20hr #1678 RT: 16.71 AV: 1 NL: 3.15E5
T: -p ESI Full ms [55.00-400.00]



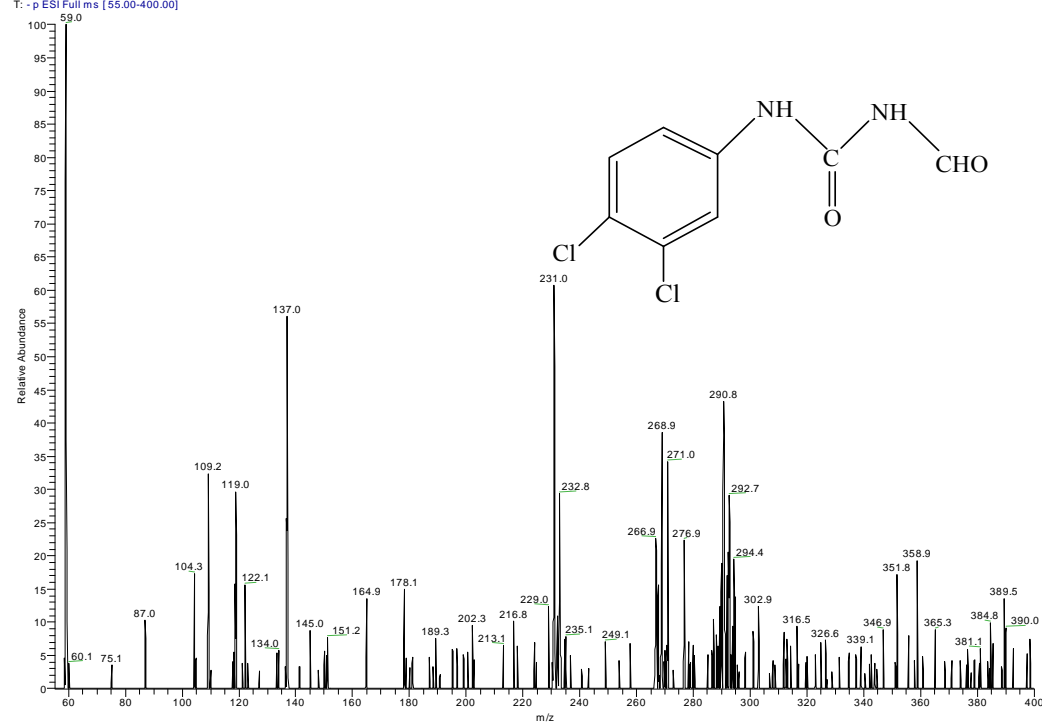
LNR-UV-1hr #1393 RT: 12.65 AV: 1 NL: 2.98E6
T: -p ESI Full ms [55.00-400.00]



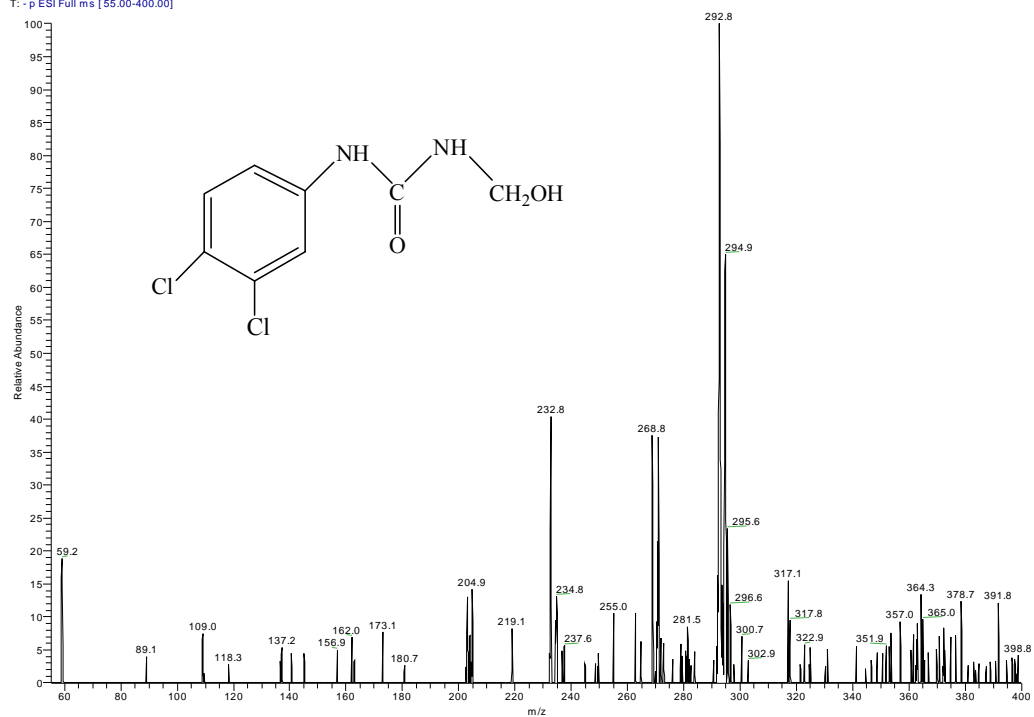
LNR-P25-H2O2-16hr #2028 RT: 19.83 AV: 1 NL: 2.52E6
T: -p ESI Full ms [55.00-400.00]



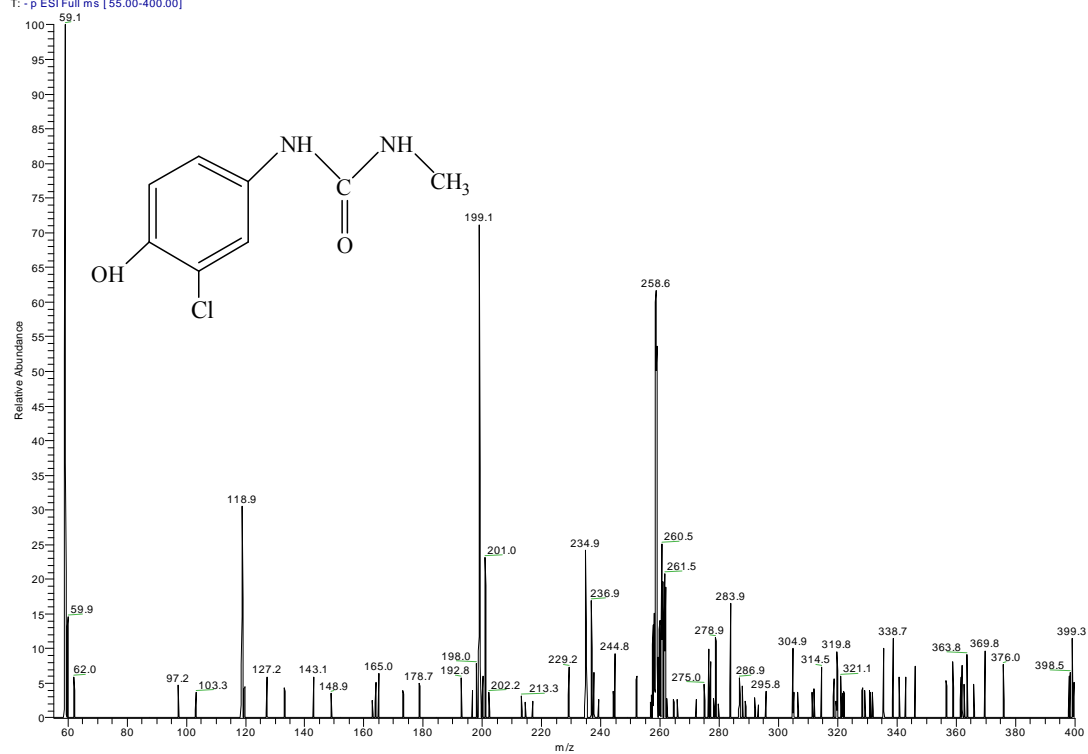
LNR-P25-H2O2-16hr #1915 RT: 18.83 AV: 1 NL: 5.35E5
T: -p ESI Full ms [55.00-400.00]



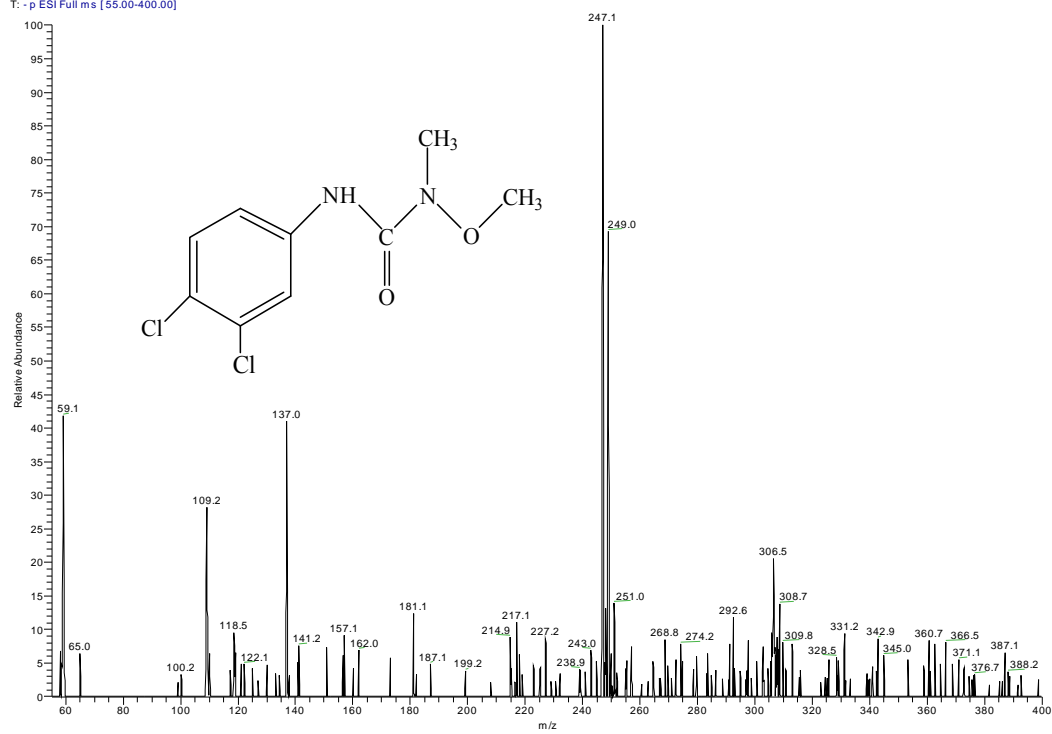
LNR-P25-H2O2-16hr #1570 RT: 15.75 AV: 1 NL: 1.07E6
T: -p ESI Full ms [55.00-400.00]



DCPMU-UV-20min #1040 RT: 10.41 AV: 1 NL: 6.27E5
T: -p ESI Full ms [55.00-400.00]



LNR-initial #2150 RT: 21.64 AV: 1 NL: 6.45E5
T: -p ESI Full ms [55.00-400.00]



APPENDIX III: Absorption spectrum of LNR

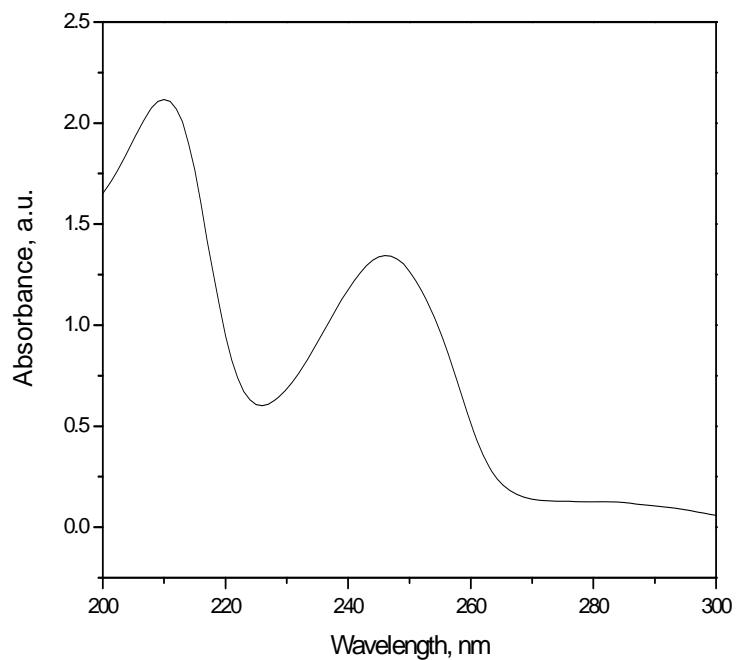


Figure A-1: Absorption spectrum of LNR at 0.295 mM

APPENDIX IV: Experimental Results

Expt No: 4-1

Probe cpd: LNR

System: sole-UV with 2 lamps at 254 nm

T (min)	R.T.	Area	C (mM)	C/C ₀	ln(C/C ₀)
0	6.298	1271214	0.0943	1	0
5	6.287	958668	0.0712	0.754136	-0.28218
10	6.301	709240	0.0526	0.557923	-0.58353
15	6.292	528882	0.0393	0.416045	-0.87696
20	6.295	379576	0.0282	0.298593	-1.20867
25	6.292	271125	0.0201	0.21328	-1.54515
30	6.302	190592	0.0141	0.149929	-1.89759

Expt No: 4-2

Probe cpd: LNR

System: sole-UV with 4 lamps at 254 nm

T (min)	R.T.	Area	C (mM)	C/C ₀	ln(C/C ₀)
0	6.275	1283471	0.0952	1	0
5	6.284	733668	0.0544	0.571628	-0.55927
10	6.281	412276	0.0306	0.32122	-1.13563
15	6.278	204317	0.0152	0.159191	-1.83765
20	6.287	94622	0.00702	0.073724	-2.60743
25	6.274	38846	0.00288	0.030267	-3.4977
30	6.271	11623	0.000862	0.009056	-4.70433

Expt No: 4-3

Probe cpd: LNR

System: sole-UV with 6 lamps at 254 nm

T (min)	R.T.	Area	C (mM)	C/C ₀	ln(C/C ₀)
0	6.245	1295864	0.0962	1	0
5	6.241	558656	0.0415	0.431107	-0.8414
10	6.243	211652	0.0157	0.163329	-1.81199
15	6.236	65241	0.00484	0.050346	-2.98884
20	6.248	13301	0.000987	0.010264	-4.57909

Expt No: 4-4

Probe cpd: LNR

System: sole-UV with 8 lamps at 254 nm

T (min)	R.T.	Area	C (mM)	C/C ₀	ln(C/C ₀)
0	6.330	1290147	0.0958	1	0
5	6.329	419101	0.0311	0.324848	-1.1244
10	6.326	107406	0.00798	0.083251	-2.4859
15	6.323	16688	0.00124	0.012935	-4.34782

Expt No: 4-5
 Probe cpd: LNR
 pH: 3
 System: sole-Ozone with [O₃] of 0.0171 mM

T (Sec)	R.T.	Area	C (mM)	C/C ₀	ln(C/C ₀)
0	6.256	1259883	0.0943	1	0
60	6.261	110211	0.0825	0.874772	-0.13379
120	6.257	982067	0.0735	0.779491	-0.24911
180	6.259	872436	0.0653	0.692474	-0.36748
240	6.263	792169	0.0593	0.628764	-0.464
300	6.260	721734	0.0540	0.572858	-0.55712

Expt No: 4-6
 Probe cpd: LNR
 pH: 6
 System: sole-Ozone with [O₃] of 0.0171 mM

T (Sec)	R.T.	Area	C (mM)	C/C ₀	ln(C/C ₀)
0	6.266	1278354	0.0949	1	0
30	6.261	1137173	0.0844	0.889561	-0.11703
60	6.267	1038597	0.0771	0.812449	-0.2077
120	6.270	919229	0.0682	0.719073	-0.32979
180	6.263	783383	0.0581	0.612806	-0.48971

Expt No: 4-7
 Probe cpd: LNR
 pH: 9
 System: sole-Ozone with [O₃] of 0.0171 mM

T (Sec)	R.T.	Area	C (mM)	C/C ₀	ln(C/C ₀)
0	6.310	1238976	0.0920	1	0
30	6.314	1065679	0.0791	0.860129	-0.15067
60	6.296	962484	0.0715	0.776839	-0.25252
90	6.318	857958	0.0637	0.692474	-0.36544
120	6.320	779023	0.0578	0.628764	-0.46623
180	6.294	709757	0.0527	0.572858	-0.71470

Expt No: 4-8
 Probe cpd: LNR
 pH: 10
 System: sole-Ozone with [O₃] of 0.0171 mM

T (Sec)	R.T.	Area	C (mM)	C/C ₀	ln(C/C ₀)
0	6.340	1348695	0.1002	1	0
15	6.391	1183251	0.0879	0.87733	-0.13087
30	6.395	1050198	0.0780	0.778677	-0.25016
45	6.397	990968	0.0736	0.734761	-0.30821
60	6.392	947194	0.0704	0.702304	-0.35339

Expt No: 4-9
 Probe cpd: LNR
 pH: 10.7
 System: sole-Ozone with [O₃] of 0.0171 mM

T (Sec)	R.T.	Area	C (mM)	C/C ₀	ln(C/C ₀)
0	6.253	1298849	0.0964	1	0
15	6.249	1098767	0.0815	0.845954	-0.16729
30	6.258	974902	0.0724	0.750589	-0.2869

45	6.251	832157	0.0617	<i>Cont'd</i> 0.640688	-0.44521
60	6.247	725760	0.0539	0.558772	-0.58201

Expt No: 4-10
Probe cpd: LNR
pH: 11
System: sole-Ozone with [O₃] of 0.0171 mM

T (Sec)	R.T.	Area	C (mM)	C/C ₀	ln(C/C ₀)
0	6.281	1313231	0.0975	1	0
15	6.285	998820	0.0742	0.760582	-0.27367
30	6.278	835310	0.0620	0.636072	-0.45244
45	6.290	699084	0.0519	0.532339	-0.63047
60	6.287	601564	0.0447	0.458079	-0.78071

Expt No: 4-11

Probe cpd: LNR

pH: 9

System: sole-Ozone with [O₃] of 0.00996 mM

T (Sec)	R.T.	Area	C (mM)	C/C ₀	ln(C/C ₀)
0	6.401	1248176	0.0927	1	0
60	6.396	1067541	0.0793	0.855281	-0.15633
120	6.393	932871	0.0693	0.747387	-0.29117
180	6.398	834165	0.0619	0.668307	-0.40301
240	6.404	730953	0.0543	0.585617	-0.53509

Expt No: 4-12

Probe cpd: LNR

pH: 10

System: sole-Ozone with [O₃] of 0.00996 mM

T (Sec)	R.T.	Area	C (mM)	C/C ₀	ln(C/C ₀)
0	6.335	1301892	0.0967	1	0
60	6.330	1037650	0.0770	0.797032	-0.22686
120	6.341	837124	0.0596	0.643006	-0.4426
180	6.339	720136	0.0535	0.553146	-0.59213
240	6.337	609842	0.0453	0.468427	-0.75837

Expt No: 4-13

Probe cpd: LNR

pH: 10.7

System: sole-Ozone with [O₃] of 0.00996 mM

T (Sec)	R.T.	Area	C (mM)	C/C ₀	ln(C/C ₀)
0	6.249	1286734	0.0955	1	0
60	6.254	936732	0.0695	0.727992	-0.31747
120	6.257	691208	0.0513	0.53718	-0.62142
180	6.246	547801	0.0406	0.42573	-0.85395
240	6.251	419872	0.0312	0.326308	-1.11991

Expt No: 4-14

Probe cpd: LNR

pH: 11

System: sole-Ozone with [O₃] of 0.00996 mM

T (Sec)	R.T.	Area	C (mM)	C/C ₀	ln(C/C ₀)
0	6.284	1331958	0.0989	1	0
				<i>Cont'd</i>	
15	6.290	1173124	0.0871	0.880751	-0.12698
30	6.281	1049816	0.0779	0.788175	-0.23804
45	6.287	968712	0.0719	0.727284	-0.31844
60	6.295	880412	0.0654	0.660991	-0.41402

Expt No: 4-15
 Probe cpd: LNR
 pH: 9
 System: sole-Ozone with [O₃] of 0.0244 mM

T (Sec)	R.T.	Area	C (mM)	C/C ₀	ln(C/C ₀)
0	6.312	1218721	0.0905	1	0
30	6.308	983793	0.0730	0.807234	-0.21414
60	6.297	860479	0.0639	0.706051	-0.34807
90	6.316	710575	0.0530	0.585305	-0.53562
120	6.305	616364	0.0458	0.505747	-0.68172

Expt No: 4-16
 Probe cpd: LNR
 pH: 10
 System: sole-Ozone with [O₃] of 0.0244 mM

T (Sec)	R.T.	Area	C (mM)	C/C ₀	ln(C/C ₀)
0	6.278	1346149	0.0999	1	0
30	6.271	961880	0.0658	0.714542	-0.33611
60	6.275	844058	0.0471	0.627017	-0.46678
90	6.269	703472	0.0360	0.522581	-0.64898
120	6.273	605678	0.0308	0.449934	-0.79865

Expt No: 4-17
 Probe cpd: LNR
 pH: 10.7
 System: sole-Ozone with [O₃] of 0.0244 mM

T (Sec)	R.T.	Area	C (mM)	C/C ₀	ln(C/C ₀)
0	6.267	1341142	0.0995	1	0
30	6.270	836128	0.0648	0.623445	-0.4725
60	6.263	663415	0.0499	0.494664	-0.70388
90	6.261	456137	0.0452	0.340111	-1.07848
120	6.265	317965	0.0388	0.237085	-1.43934

Expt No: 4-18
 Probe cpd: LNR
 pH: 11
 System: sole-Ozone with [O₃] of 0.0244 mM

T (Sec)	R.T.	Area	C (mM)	C/C ₀	ln(C/C ₀)
0	6.291	1325890	0.0984	1	0
15	6.287	956054	0.0710	0.721066	-0.32702
30	6.284	749062	0.0556	0.56495	-0.57102
45	6.281	623434	0.0463	0.47020	-0.7546
60	6.285	512592	0.0380	0.386602	-0.95036

Expt No: 4-19
 Probe cpd: LNR
 pH: 9
 System: sole-Ozone with [O₃] of 0.0309 mM

T (Sec)	R.T.	Area	C (mM)	C/C ₀	ln(C/C ₀)
0	6.310	1283732	0.0953	1	0
15	6.303	1026638	0.0762	0.799729	-0.22348
30	6.308	930386	0.0691	0.724751	-0.32193
45	6.298	858984	0.0638	0.66913	-0.40178
60	6.304	709144	0.0526	0.552408	-0.59347

Expt No: 4-20
 Probe cpd: LNR
 pH: 10
 System: sole-Ozone with [O₃] of 0.0309 mM

T (Sec)	R.T.	Area	C (mM)	C/C ₀	ln(C/C ₀)
0	6.275	1283732	0.0953	1	0
15	6.271	1004924	0.0746	0.782814	-0.24486
30	6.280	883612	0.0656	0.688315	-0.37351
45	6.278	790244	0.0587	0.615583	-0.48518
60	6.273	660548	0.0490	0.514553	-0.66446

Expt No: 4-21
 Probe cpd: LNR
 pH: 10.7
 System: sole-Ozone with [O₃] of 0.0309 mM

T (Sec)	R.T.	Area	C (mM)	C/C ₀	ln(C/C ₀)
0	6.312	1341918	0.0996	1	0
15	6.317	930796	0.0691	0.693631	-0.36582
30	6.320	775541	0.0576	0.577935	-0.54829
45	6.311	658433	0.0489	0.490666	-0.71199
60	6.323	532770	0.0395	0.397021	-0.92377

Expt No: 4-22
 Probe cpd: LNR
 pH: 11
 System: sole-Ozone with [O₃] of 0.0309 mM

T (Sec)	R.T.	Area	C (mM)	C/C ₀	ln(C/C ₀)
0	6.302	1324562	0.0983	1	0
15	6.308	840760	0.0624	0.634746	-0.45453
30	6.305	669373	0.0497	0.505354	-0.6825
45	6.310	533450	0.0396	0.402737	-0.90947
60	6.307	435708	0.0323	0.328945	-1.11187

Expt No: 4-23
 Probe cpd: LNR
 pH: 6
 System: UV/H₂O₂ with UV of 254 nm

T (Sec)	R.T.	Area	C (μM)	C ₀ /C	ln(C ₀ /C)
0	6.262	133648	9.92	1	0
5	6.265	131222	9.74	1.018488	0.018319

<i>Cont'd</i>					
10	6.267	122318	9.08	1.092627	0.088585
15	6.270	121197	8.99	1.102734	0.097792
20	6.263	117582	8.73	1.136637	0.128074
30	6.272	116879	8.68	1.143473	0.13407

Expt No: 4-23

Probe cpd: Atrazine (ATZ)

pH: 6

System: UV/H₂O₂ with UV of 254 nm

T (Sec)	R.T.	Area	C (μM)	C ₀ /C	ln(C ₀ /C)
0		208841	9.98	1	0
5		204362	9.76	1.021917	0.02168
10		191344	9.14	1.091443	0.0875
15		188876	9.02	1.105704	0.100482
20		184859	8.83	1.129731	0.12198
30		179327	8.57	1.164582	0.152362

Expt No: 4-24

Probe cpd: LNR

pH: 6

System: UV/O₃ with [O₃] of 0.0171 mM and 2 lamps at 254 nm

T (min)	R.T.	Area	C (mM)	C/C ₀	ln(C/C ₀)
0	6.308	1265710	0.0939	1	0
2	6.302	700180	0.0519	0.553192	-0.59205
4	6.311	454226	0.0337	0.358871	-1.02479
6	6.298	269483	0.0199	0.212911	-1.54688
8	6.305	124652	0.0092	0.098484	-2.31786
10	6.301	32263	0.0024	0.02549	-3.66947

Expt No: 4-25

Probe cpd: LNR

pH: 6

System: UV/O₃ with [O₃] of 0.0171 mM and 4 lamps at 254 nm

T (min)	R.T.	Area	C (mM)	C/C ₀	ln(C/C ₀)
0	6.324	1216178	0.0902	1	0
2	6.328	634652	0.0471	0.521841	-0.65039
4	6.320	331446	0.0246	0.272531	-1.3
6	6.329	146630	0.0108	0.120566	-2.11556
8	6.318	47378	0.0035	0.038956	-3.24531

Expt No: 4-26

Probe cpd: LNR

pH: 6

System: UV/O₃ with [O₃] of 0.0171 mM and 6 lamps at 254 nm

T (min)	R.T.	Area	C (mM)	C/C ₀	ln(C/C ₀)
0	6.290	1278120	0.0948	1	0
2	6.295	623285	0.0462	0.487658	-0.71814
4	6.302	231118	0.0171	0.180827	-1.71021
6	6.293	65954	0.00489	0.051603	-2.96418
8	6.297	14749	0.00109	0.01154	-4.46196

Expt No: 4-27

Probe cpd: LNR

pH: 6

System: UV/O₃ with [O₃] of 0.0171 mM and 8 lamps at 254 nm

T (min)	R.T.	Area	C (mM)	C/C ₀	ln(C/C ₀)
0	6.268	1283426	0.0952	1	0
1	6.271	629328	0.0467	0.490358	-0.71265
2	6.265	314670	0.0233	0.245180	-1.40578
3	6.263	167399	0.0124	0.130432	-2.0369
4	6.274	88243	0.0065	0.068756	-2.67719

Expt No: 5-1

Probe cpd: LNR

pH: 3

System: sole-UV with 4 lamps at 254 nm

T (min)	R.T.	Area	C (mM)	C/C ₀	ln(C/C ₀)
0	6.261	1261024	0.0935	1	0
5	6.258	654179	0.0485	0.518768	-0.6563
10	6.267	351539	0.0260	0.278773	-1.27736
15	6.263	180782	0.0134	0.143361	-1.94239
20	6.269	85235	0.00632	0.067592	-2.69427
25	6.271	29397	0.00218	0.023312	-3.75879
30	6.265	9971	0.000739	0.007907	-4.84

Expt No: 5-2

Probe cpd: LNR

pH: 9

System: sole-UV with 4 lamps at 254 nm

T (min)	R.T.	Area	C (mM)	C/C ₀	ln(C/C ₀)
0	6.312	1298647	0.0963	1	0
5	6.307	725502	0.0538	0.55866	-0.58221
10	6.303	378521	0.0281	0.291474	-1.23281
15	6.305	178339	0.0132	0.137327	-1.98539
20	6.297	86591	0.00642	0.066678	-2.70789
25	6.301	32669	0.00242	0.025156	-3.68266
30	6.311	7665	0.00057	0.005902	-5.13238

Expt No: 5-3

Probe cpd: LNR

pH: 10

System: sole-UV with 4 lamps at 254 nm

T (min)	R.T.	Area	C (mM)	C/C ₀	ln(C/C ₀)
0	6.283	1259608	0.0934	1	0
5	6.289	673934	0.0499	0.535035	-0.62542
10	6.293	351145	0.0260	0.278773	-1.27736
15	6.287	163909	0.0121	0.130127	-2.03925
20	6.281	74629	0.0055	0.059248	-2.82602
25	6.285	27681	0.0020	0.021976	-3.81782
30	6.290	6118	0.00045	0.004857	-5.3273

Expt No: 5-4
 Probe cpd: LNR
 pH: 11
 System: sole-UV with 4 lamps at 254 nm

T (min)	R.T.	Area	C (mM)	C/C ₀	ln(C/C ₀)
0	6.267	1309359	0.0971	1	0
5	6.278	767481	0.0569	0.58615	-0.53418
10	6.269	433230	0.0321	0.330872	-1.10602
15	6.273	244565	0.0181	0.186782	-1.67781
20	6.270	127017	0.0094	0.097007	-2.33297
25	6.269	61502	0.0045	0.046971	-3.05822
30	6.274	25643	0.0019	0.019584	-5.30549

Expt No: 5-5
 Probe cpd: LNR
 pH: 3
 System: UV/O₃ with 4 lamps at 254 nm

T (min)	R.T.	Area	C (mM)	C/C ₀	ln(C/C ₀)
0	6.350	1249870	0.0927	1	0
2.5	6.347	751688	0.0558	0.601413	-0.50847
5	6.352	575033	0.0426	0.460074	-0.77637
7.5	6.358	413557	0.0307	0.33088	-1.106
10	6.354	264614	0.0196	0.211713	-1.55252

Expt No: 5-6
 Probe cpd: LNR
 pH: 6
 System: UV/O₃ with 4 lamps at 254 nm

T (min)	R.T.	Area	C (mM)	C/C ₀	ln(C/C ₀)
0	6.281	1230198	0.0912	1	0
2	6.278	610157	0.0448	0.491395	-0.71051
4	6.285	301762	0.0224	0.245295	-1.40529
6	6.287	134612	0.0096	0.105816	-2.24605
8	6.283	35712	0.0026	0.029029	-3.53944

Expt No: 5-7
 Probe cpd: LNR
 pH: 9
 System: UV/O₃ with 4 lamps at 254 nm

T (min)	R.T.	Area	C (mM)	C/C ₀	ln(C/C ₀)
0	6.265	1274158	0.0945	1	0
0.5	6.269	910091	0.0675	0.714269	-0.3365
1	6.258	750550	0.0557	0.589056	-0.52923
1.5	6.261	556212	0.0412	0.436533	-0.82889
2	6.267	458106	0.0340	0.359536	-1.02294

Expt No: 5-8
 Probe cpd: LNR
 pH: 10
 System: UV/O₃ with 4 lamps at 254 nm

T (min)	R.T.	Area	C (mM)	C/C ₀	ln(C/C ₀)
0	6.313	1241701	0.0921	1	0

<i>Cont'd</i>					
0.5	6.309	841205	0.0624	0.677462	-0.3894
1	6.315	618401	0.0459	0.498027	-0.6971
1.5	6.311	412735	0.0306	0.332395	-1.10143
2	6.307	310928	0.0231	0.250405	-1.38468

Expt No: 5-9

Probe cpd: LNR

pH: 11

System: UV/O₃ with 4 lamps at 254 nm

T (min)	R.T.	Area	C (mM)	C/C ₀	ln(C/C ₀)
0	6.330	1254389	0.0930	1	0
0.5	6.337	654841	0.0485	0.52204	-0.65001
1	6.331	367632	0.0272	0.293077	-1.22732
1.5	6.328	209075	0.0155	0.166675	-1.79171
2	6.335	128548	0.0095	0.102479	-2.2781

Expt No: 5-17

Probe cpd: LNR

pH: 3

System: sole-Ozone with [O₃] at 0.0171 mM and [Cl⁻] at 0.01 M

T (min)	R.T.	Area	c (mM)	C/C ₀	ln(C/C ₀)
0	6.401	1354245	0.100	1	/
5	6.406	1163132	0.0859	0.858879	/
10	6.397	1105614	0.0816	0.816406	/
15	6.402	1045246	0.772	0.771829	/
20	6.398	940884	0.0695	0.694766	/
25	6.395	915244	0.0676	0.675833	/
30	6.403	882242	0.0651	0.651464	/

Expt No: 5-18

Probe cpd: LNR

pH: 3

System: sole-Ozone with [O₃] at 0.0171 mM and [SO₄²⁻] at 0.01 M

T (min)	R.T.	Area	c (mM)	C/C ₀	ln(C/C ₀)
0	6.287	1242150	0.0921	1	/
5	6.282	775998	0.0575	0.624722	/
10	6.285	510958	0.0379	0.41135	/
15	6.290	374404	0.0278	0.301416	/
20	6.293	221116	0.0164	0.178011	/
25	6.284	135588	0.01	0.109156	/
30	6.291	96614	0.00716	0.07778	/

Expt No: 5-19

Probe cpd: LNR

pH: 3

System: sole-Ozone with [O₃] at 0.0171 mM and [HPO₄²⁻] at 0.01 M

T (min)	R.T.	Area	c (mM)	C/C ₀	ln(C/C ₀)
0	6.271	1242150	0.0921	1	/
5	6.264	761076	0.0564	0.612709	/
10	6.267	451710	0.0335	0.363652	/
15	6.275	281400	0.0209	0.226543	/

					<i>Cont'd</i>
20	6.278	187556	0.0139	0.150993	/
25	6.269	115958	0.0085	0.093353	/
30	6.271	107592	0.0079	0.086618	/

Expt No: 5-20
 Probe cpd: LNR
 pH: 7
 System: sole-Ozone with [O₃] at 0.0245 mM

T (min)	R.T.	Area	c (mM)	C/C ₀	ln(C/C ₀)
0	6.271	1267251	0.0940	1	/
4	6.265	479336	0.0356	0.378249	/
8	6.261	169516	0.0126	0.133767	/
12	6.259	53463	0.0039	0.042188	/
16	6.273	25544	0.0019	0.020157	/
20	6.268	12059	0.00089	0.009516	/

Expt No: 5-21
 Probe cpd: LNR
 pH: 7
 System: sole-Ozone with [O₃] at 0.0245 mM and [Cl⁻] at 0.01 M

T (min)	R.T.	Area	c (mM)	C/C ₀	ln(C/C ₀)
0	6.312	1278465	0.0948	1	/
4	6.307	556456	0.0413	0.435253	/
8	6.305	246994	0.0183	0.193196	/
12	6.311	135754	0.0101	0.106185	/
16	6.308	82878	0.0061	0.064826	/
20	6.302	56027	0.0042	0.043824	/

Expt No: 5-22
 Probe cpd: LNR
 pH: 7
 System: sole-Ozone with [O₃] at 0.0245 mM and [SO₄²⁻] at 0.01 M

T (min)	R.T.	Area	c (mM)	C/C ₀	ln(C/C ₀)
0	6.285	1267891	0.0940	1	/
4	6.289	534301	0.0396	0.421409	/
8	6.281	206395	0.0153	0.162786	/
12	6.277	73465	0.00545	0.057943	/
16	6.279	39404	0.0029	0.031078	/
20	6.283	16995	0.00126	0.013404	/

Expt No: 5-23
 Probe cpd: LNR
 pH: 7
 System: sole-Ozone with [O₃] at 0.0245 mM and [HPO₄²⁻] at 0.01 M

T (min)	R.T.	Area	c (mM)	C/C ₀	ln(C/C ₀)
0	6.323	1287106	0.0954	1	/
4	6.327	294155	0.0218	0.22854	/
8	6.321	69892	0.0052	0.054302	/
12	6.319	10508	0.00078	0.008164	/
16	6.328	0	0	0	/

Expt No: 5-24

Probe cpd: LNR

pH: 7

System: sole-Ozone with $[O_3]$ at 0.0245 mM and $[CO_3^{2-}]$ at 0.01 M

T (min)	R.T.	Area	c (mM)	C/C ₀	ln(C/C ₀)
0	6.278	1291817	0.0957	1	/
4	6.288	497665	0.0369	0.385244	/
8	6.281	227899	0.0169	0.176418	/
12	6.287	123784	0.0092	0.095822	/
16	6.276	50925	0.0038	0.039421	/
20	6.283	2618	0.0019	0.020165	/

The evolution of TOC, varied ions and pH during the decay process of LNR in sole-UV, sole-Ozone and UV/O₃ processes.

Expt No: 5-10

Probe cpd: LNR

pH: 6

System: sole-UV with 6 lamps at 254 nm

T (hr)	TOC (mg/L)	Cl ⁻ (mg/L)	NO ₃ ⁻ (mg/L)	NH ₄ ⁺ (mg/L)	pH
0	31.025	0.0782	0	0	6
0.5	30.563	4.716	0	0.0326	4.28
1	30.971	9.89	0	0.0484	3.97
1.5	31.235	14.43	0.0627	0.0652	3.74
2	30.671	16.94	0.0913	0.105	3.65
2.5	31.174	18.57	0.0475	0.139	3.62
3	30.712	19.52	0.0808	0.154	3.6
3.5	30.456	19.7	0.0627	0.186	3.58
4	31.302	19.79	0.0694	0.187	3.59

Expt No: 5-14

Probe cpd: LNR

pH: 6

System: sole-Ozone with $[O_3]$ at 0.0245 mM

T (min)	TOC (mg/L)	Cl ⁻ (mg/L)	NO ₃ ⁻ (mg/L)	NH ₄ ⁺ (mg/L)	pH
0	30.986	0	0	0	6.03
20	27.936	11.036	0.8317	0.545	3.45
40	25.856	14.186	1.347	0.934	3.36
60	25.056	15.050	1.467	0.846	3.34
80	24.646	15.678	1.645	0.923	3.32
100	23.976	15.922	1.774	0.756	3.30
120	23.170	16.109	1.872	0.743	3.30

Expt No: 5-16

Probe cpd: LNR

pH: 6

System: UV/O₃ with $[O_3]$ at 0.0245 mM and six lamps at 254 nm

T (min)	TOC (mg/L)	Cl ⁻ (mg/L)	NO ₃ ⁻ (mg/L)	NH ₄ ⁺ (mg/L)	pH
0	31.2	0.1	0	0	6.0
20	29.5	16.84	1.278	0.488	3.14
40	23.86	19.64	2.124	0.628	3.06
60	16.11	19.76	4.830	0.734	3.09

					<i>Cont'd</i>
80	8.763	20.31	9.497	0.931	3.11
100	5.943	20.48	15.49	1.005	3.08
120	4.313	20.41	15.92	1.120	3.05

Expt No: 6-1
 Probe cpd: LNR
 pH: 6
 System: TiO₂/H₂O₂ in dark

T (min)	R.T.	Area	c (mM)	C/C ₀	ln(C/C ₀)
0	6.450	1260079	0.0933	1	/
30	6.447	1229409	0.0910	0.97566	/
60	6.453	1202339	0.0890	0.954177	/
90	6.458	1186452	0.0878	0.94157	/
120	6.446	1165358	0.0863	0.924829	/
150	6.451	1161629	0.0860	0.92187	/
180	6.449	1158779	0.0858	0.919608	/

Expt No: 6-2
 Probe cpd: LNR
 pH: 6
 System: TiO₂/visible light at 420 nm (Hg lamps)

T (min)	R.T.	Area	c (mM)	C/C ₀	ln(C/C ₀)
0	6.401	1270871	0.0941	1	/
30	6.397	1187512	0.0879	0.934408	/
60	6.394	1161027	0.0860	0.913568	/
90	6.402	1155530	0.0855	0.909243	/
120	6.407	1142112	0.0846	0.898685	/
150	6.398	1131911	0.0838	0.890658	/
180	6.403	1132563	0.0839	0.891171	/

Expt No: 6-3
 Probe cpd: LNR
 pH: 6
 System: H₂O₂/visible light at 420 nm (Hg lamps)

T (min)	R.T.	Area	c (mM)	C/C ₀	ln(C/C ₀)
0	6.387	1260986	0.0934	1	/
30	6.381	1222732	0.0906	0.969663	/
60	6.385	1199610	0.0888	0.951327	/
90	6.390	1185675	0.0878	0.940276	/
120	6.384	1175093	0.0870	0.931884	/
150	6.381	1161098	0.0860	0.920786	/
180	6.385	1152873	0.0854	0.914263	/

Expt No: 6-4
 Probe cpd: LNR
 pH: 6
 System: TiO₂/H₂O₂/visible light at 420 nm (Hg lamps)

T (min)	R.T.	Area	c (mM)	C/C ₀	ln(C/C ₀)
0	6.397	1225617	0.0908	1	/
30	6.394	564596	0.0418	0.460663	/
60	6.402	340863	0.0252	0.278115	/

90	6.393	184365	0.0137	0.150426	/
120	6.405	104228	0.0077	0.085041	/
<i>Cont'd</i>					
150	6.401	49488	0.0036	0.040378	/
180	6.395	19761	0.0015	0.016123	/

Expt No: 6-5

Probe cpd: LNR

pH: 6

System: TiO₂/visible light at 420 nm (Hg lamps) with the addition of 1 M MeOH

T (hr)	R.T.	Area	c (mM)	C/C ₀	ln(C/C ₀)
0	6.387	1271203	0.0942	1	/
1	6.381	1267219	0.0939	0.996866	/
2	6.390	1272020	0.0943	1.000643	/
3	6.385	1272730	0.0943	1.001201	/

Expt No: 6-6

Probe cpd: LNR

pH: 6

System: TiO₂/H₂O₂/visible light at 420 nm (Hg lamps) with the addition of 1 M MeOH

T (hr)	R.T.	Area	c (mM)	C/C ₀	ln(C/C ₀)
0	6.378	1280145	0.0949	1	/
0.5	6.371	1251096	0.0927	0.977308	/
1	6.374	1250299	0.0927	0.976686	/
1.5	6.382	1235490	0.0916	0.965117	/
2	6.379	1234108	0.0915	0.964038	/
2.5	6.384	1235531	0.0916	0.965149	/
3	6.380	1230164	0.0912	0.960957	/

Expt No: 6-7

Probe cpd: LNR

pH: 6

System: TiO₂/visible light at 420 nm (Hg lamps) with the purge of O₂

T (hr)	R.T.	Area	c (mM)	C/C ₀	ln(C/C ₀)
0	6.290	1249873	0.0926	1	/
0.5	6.287	923787	0.0684	0.739105	/
1	6.293	868554	0.0643	0.694914	/
1.5	6.295	782862	0.0580	0.626353	/
2	6.285	731343	0.0542	0.585134	/
2.5	6.289	665062	0.0493	0.532104	/
3	6.296	599453	0.0444	0.479611	/

Expt No: 6-8

Probe cpd: LNR

pH: 6

System: WO₃/visible light at 420 nm (Hg lamps)

T (hr)	R.T.	Area	c (mM)	C/C ₀	ln(C/C ₀)
0	6.305	1270659	0.0941	1	/
1	6.309	1165833	0.0863	0.917503	/
2	6.313	1118633	0.0828	0.880357	/
3	6.304	1078960	0.0799	0.849134	/

Expt No: 6-9

Probe cpd: LNR

pH: 6

System: WO₃/visible light at 420 nm (Hg lamps) with the purge of O₂

T (hr)	R.T.	Area	c (mM)	C/C ₀	ln(C/C ₀)
0	6.324	1261721	0.0934	1	/
1	6.327	918077	0.0680	0.727639	/
2	6.329	735073	0.0544	0.582596	/
3	6.321	633415	0.0469	0.502025	/

Expt No: 6-10

Probe cpd: LNR

pH: 6

System: WO₃/H₂O₂/visible light at 420 nm (Hg lamps)

T (hr)	R.T.	Area	c (mM)	C/C ₀	ln(C/C ₀)
0	6.316	1285019	0.0951	1	/
0.5	6.311	929283	0.0688	0.723167	/
1	6.319	713703	0.0528	0.555403	/
1.5	6.308	546032	0.0404	0.424921	/
2	6.312	422521	0.0313	0.328805	/
2.5	6.305	340903	0.0252	0.26529	/
3	6.309	250219	0.0185	0.19472	/

Expt No: 6-11

Probe cpd: LNR

pH: 6

System: ZnO/visible light at 420 nm (Hg lamps)

T (hr)	R.T.	Area	c (mM)	C/C ₀	ln(C/C ₀)
0	6.296	1275087	0.0944	1	/
1	6.291	1041614	0.0771	0.816896	/
2	6.287	886906	0.0657	0.695565	/
3	6.293	769894	0.0570	0.603797	/

Expt No: 6-12

Probe cpd: LNR

pH: 6

System: ZnO/visible light at 420 nm (Hg lamps) with the purge of O₂

T (hr)	R.T.	Area	c (mM)	C/C ₀	ln(C/C ₀)
0	6.330	1237474	0.0916	1	/
1	6.337	805727	0.0596	0.651106	/
2	6.328	585078	0.0433	0.472800	/
3	6.332	463443	0.0343	0.374507	/

Expt No: 6-13

Probe cpd: LNR

pH: 6

System: ZnO/H₂O₂/visible light at 420 nm (Hg lamps)

T (hr)	R.T.	Area	c (mM)	C/C ₀	ln(C/C ₀)
0	6.321	1261549	0.0934	1	/
1	6.326	1039443	0.0770	0.823942	/
2	6.325	865096	0.0640	0.685741	/
3	6.329	769502	0.0570	0.609966	/

Expt No: 6-14

Probe cpd: LNR

pH: 6

System: TiO₂/H₂O₂/visible light at 420 nm (Hg lamps) with TiO₂ dosage of 0.05 g/L

T (min)	R.T.	Area	c (mM)	C/C ₀	ln(C/C ₀)
0	6.287	1231360	0.0912	1	0
30	6.281	1043715	0.0773	0.847612	-0.16533
60	6.285	983049	0.0728	0.798344	-0.22522
90	6.290	890814	0.0660	0.723439	-0.32374
120	6.293	840361	0.0622	0.682466	-0.38204
150	6.288	798880	0.0592	0.648779	-0.43266
180	6.291	767769	0.0569	0.623513	-0.47239

Expt No: 6-15

Probe cpd: LNR

pH: 6

System: TiO₂/H₂O₂/visible light at 420 nm (Hg lamps) with TiO₂ dosage of 0.1 g/L

T (min)	R.T.	Area	c (mM)	C/C ₀	ln(C/C ₀)
0	6.303	1244935	0.0922	1	0
30	6.298	993990	0.0736	0.798427	-0.22511
60	6.301	885585	0.0656	0.71135	-0.34059
90	6.307	775105	0.0574	0.622607	-0.47384
120	6.295	708608	0.0525	0.569193	-0.56354
150	6.302	639186	0.0473	0.513429	-0.66664
180	6.306	577657	0.0428	0.464006	-0.76786

Expt No: 6-16

Probe cpd: LNR

pH: 6

System: TiO₂/H₂O₂/visible light at 420 nm (Hg lamps) with TiO₂ dosage of 0.2 g/L

T (min)	R.T.	Area	c (mM)	C/C ₀	ln(C/C ₀)
0	6.275	1268821	0.0940	1	0
30	6.271	843234	0.0625	0.664581	-0.4086
60	6.268	671211	0.0497	0.529004	-0.63676
90	6.276	531313	0.0394	0.418745	-0.87049
120	6.279	419260	0.0311	0.330433	-1.10735
150	6.267	361633	0.0268	0.285015	-1.25521
180	6.270	293336	0.0217	0.231188	-1.46452

Expt No: 6-17

Probe cpd: LNR

pH: 6

System: TiO₂/H₂O₂/visible light at 420 nm (Hg lamps) with TiO₂ dosage of 0.4 g/L

T (min)	R.T.	Area	c (mM)	C/C ₀	ln(C/C ₀)
0	6.292	1237803	0.0917	1	0
30	6.297	618862	0.0458	0.499968	-0.69321
60	6.291	366623	0.0272	0.296188	-1.21676
90	6.287	225272	0.0167	0.181993	-1.70378
120	6.290	132016	0.00978	0.106653	-2.23817
150	6.285	68726	0.00509	0.055523	-2.89097
180	6.289	30174	0.00224	0.024377	-3.71411

Expt No: 6-18

Probe cpd: LNR

pH: 6

System: TiO₂/H₂O₂/visible light at 420 nm (Hg lamps) with TiO₂ dosage of 0.8 g/L

T (min)	R.T.	Area	c (mM)	C/C ₀	ln(C/C ₀)
0	6.279	1288889	0.0955	1	0
30	6.274	659509	0.0489	0.511688	-0.67004
60	6.271	356634	0.0264	0.276699	-1.28483
90	6.278	180337	0.0133	0.139917	-1.9667
120	6.269	85208	0.00631	0.06611	-2.71643
150	6.273	35069	0.00259	0.027209	-3.60419
180	6.275	11036	0.00082	0.008563	-4.76025

Expt No: 6-19

Probe cpd: LNR

pH: 6

System: TiO₂/H₂O₂/visible light at 420 nm (Hg lamps) with TiO₂ dosage of 1.0 g/L

T (min)	R.T.	Area	c (mM)	C/C ₀	ln(C/C ₀)
0	6.268	1271565	0.0942	1	0
30	6.265	523961	0.0388	0.41206	-0.88659
60	6.261	257541	0.0191	0.202539	-1.59682
90	6.271	123976	0.0092	0.097499	-2.32792
120	6.269	41944	0.0031	0.032986	-3.41167
150	6.273	11958	0.00088	0.009404	-4.66664

Expt No: 6-20

Probe cpd: LNR

pH: 6

System: TiO₂/H₂O₂/visible light at 420 nm (Hg lamps) with H₂O₂ at 1 mM

T (min)	R.T.	Area	c (mM)	C/C ₀	ln(C/C ₀)
0	6.283	1294377	0.0959	1	0
30	6.279	798456	0.0592	0.616865	-0.48311
60	6.285	550740	0.0408	0.425487	-0.85452
90	6.281	469742	0.0348	0.36291	-1.0136
120	6.276	439437	0.0326	0.339497	-1.08029
150	6.279	409984	0.0304	0.316743	-1.14967
180	6.280	380696	0.0282	0.294115	-1.22378

Expt No: 6-21

Probe cpd: LNR

pH: 6

System: TiO₂/H₂O₂/visible light at 420 nm (Hg lamps) with H₂O₂ at 2 mM

T (min)	R.T.	Area	c (mM)	C/C ₀	ln(C/C ₀)
0	6.312	1312462	0.0972	1	0
30	6.309	757285	0.0561	0.576996	-0.54992
60	6.307	519924	0.0385	0.396144	-0.92598
90	6.311	383032	0.0284	0.291842	-1.23154
120	6.315	311572	0.0231	0.237395	-1.43803
150	6.308	219692	0.0163	0.167389	-1.78743
180	6.324	205883	0.0152	0.156868	-1.85235

Expt No: 6-22

Probe cpd: LNR

pH: 6

System: TiO₂/H₂O₂/visible light at 420 nm (Hg lamps) with H₂O₂ at 5 mM

T (min)	R.T.	Area	c (mM)	C/C ₀	ln(C/C ₀)
0	6.263	1216492	0.0901	1	0
30	6.267	668490	0.0495	0.549523	-0.59871
60	6.261	473384	0.0351	0.389139	-0.94382
90	6.269	329960	0.0244	0.271239	-1.30476
120	6.265	225545	0.0167	0.185406	-1.68521
150	6.259	142732	0.0106	0.117331	-2.14276
180	6.262	76583	0.00567	0.062954	-2.76535

Expt No: 6-23

Probe cpd: LNR

pH: 6

System: TiO₂/H₂O₂/visible light at 420 nm (Hg lamps) with H₂O₂ at 20 mM

T (min)	R.T.	Area	c (mM)	C/C ₀	ln(C/C ₀)
0	6.281	1300561	0.0963	1	0
30	6.285	646460	0.0479	0.497062	-0.69904
60	6.279	410909	0.0304	0.315948	-1.15218
90	6.275	271322	0.0201	0.208619	-1.56724
120	6.280	191455	0.0142	0.14721	-1.9159
150	6.286	103663	0.00767	0.079706	-2.52941
180	6.276	59635	0.00442	0.045853	-3.08231

Expt No: 6-24

Probe cpd: LNR

pH: 2.0

System: TiO₂/H₂O₂/visible light at 420 nm (Hg lamps)

T (min)	R.T.	Area	c (mM)	C/C ₀	ln(C/C ₀)
0	6.401	1218117	0.0902	1	0
30	6.397	1108853	0.0821	0.910301	-0.09398
60	6.392	1024753	0.0759	0.84126	-0.17285
90	6.395	937128	0.0694	0.769325	-0.26224
120	6.393	817074	0.0605	0.670768	-0.39933
150	6.398	781874	0.0579	0.641871	-0.44337
180	6.402	714553	0.0529	0.586605	-0.5334

Expt No: 6-25

Probe cpd: LNR

pH: 4.0

System: TiO₂/H₂O₂/visible light at 420 nm (Hg lamps)

T (min)	R.T.	Area	c (mM)	C/C ₀	ln(C/C ₀)
0	6.374	1242736	0.0920	1	0
30	6.371	703704	0.0521	0.566254	-0.56871
60	6.375	472868	0.0350	0.380506	-0.96625
90	6.380	302410	0.0224	0.243342	-1.41329
120	6.379	218716	0.0162	0.175996	-1.7373
150	6.372	156143	0.0116	0.125645	-2.0743
180	6.377	112286	0.0083	0.090354	-2.40402

Expt No: 6-26

Probe cpd: LNR

pH: 9.0

System: TiO₂/H₂O₂/visible light at 420 nm (Hg lamps)

T (min)	R.T.	Area	c (mM)	C/C ₀	ln(C/C ₀)
0	6.354	1253686	0.0928	1	0
30	6.357	971510	0.0719	0.774923	-0.25499
60	6.351	774305	0.0573	0.617623	-0.48188
90	6.358	645316	0.0478	0.514735	-0.66410
120	6.352	520149	0.0385	0.414896	-0.87973
150	6.360	441777	0.0327	0.352382	-1.04304
180	6.358	358713	0.0266	0.286127	-1.25132

Expt No: 6-27

Probe cpd: LNR

pH: 11.0

System: TiO₂/H₂O₂/visible light at 420 nm (Hg lamps)

T (min)	R.T.	Area	c (mM)	C/C ₀	ln(C/C ₀)
0	6.368	1211125	0.0896	1	0
30	6.361	1160797	0.0859	0.958445	-0.04244
60	6.370	1120696	0.0829	0.925335	-0.0776
90	6.373	1038921	0.0769	0.857815	-0.15337
120	6.365	983031	0.0727	0.811668	-0.20866
150	6.368	953499	0.0705	0.787284	-0.23917
180	6.364	944997	0.0699	0.780264	-0.24812

Expt No: 6-28

Probe cpd: LNR

pH: 6.0

System: TiO₂/H₂O₂/visible light at 420 nm (Hg lamps) with LNR at 0.0125 mM

T (min)	R.T.	Area	c (mM)	C/C ₀	ln(C/C ₀)
0	6.303	136536	0.0106	1	0
15	6.307	44414	0.00328	0.325291	-1.12303
30	6.304	17082	0.00126	0.12511	-2.07856
45	6.301	5436	0.000402	0.039814	-3.22354

Expt No: 6-29

Probe cpd: LNR

pH: 6.0

System: TiO₂/H₂O₂/visible light at 420 nm (Hg lamps) with LNR at 0.025 mM

T (min)	R.T.	Area	c (mM)	C/C ₀	ln(C/C ₀)
0	6.325	270356	0.021	1	0
15	6.321	81627	0.0063	0.301924	-1.19758
30	6.327	34601	0.00269	0.127983	-2.05586
45	6.320	13407	0.00104	0.04959	-3.00396
60	6.330	7339	0.00057	0.027146	-3.60654

Expt No: 6-30

Probe cpd: LNR

pH: 6.0

System: TiO₂/H₂O₂/visible light at 420 nm (Hg lamps) with LNR at 0.05 mM

T (min)	R.T.	Area	c (mM)	C/C ₀	ln(C/C ₀)
---------	------	------	--------	------------------	-----------------------

0	6.307	567024	0.0441	1	0
30	6.311	226381	0.0176	0.399244	-0.91818
60	6.306	126381	0.00986	0.223521	-1.49825
90	6.303	58368	0.00454	0.102937	-2.27363
120	6.309	26729	0.00208	0.047139	-3.05465
150	6.305	10364	0.00081	0.018278	-4.00206
180	6.312	2889	0.000224	0.005095	-5.27949

Expt No: 6-31

Probe cpd: LNR

pH: 6.0

System: TiO₂/H₂O₂/visible light at 420 nm (Hg lamps) with LNR at 0.2 mM

T (min)	R.T.	Area	c (mM)	C/C ₀	ln(C/C ₀)
0	6.334	2121586	0.165	1	0
30	6.337	1164476	0.0906	0.548871	-0.59989
60	6.329	928857	0.0724	0.438871	-0.82596
90	6.327	697305	0.0542	0.328672	-1.1127
120	6.336	553833	0.0431	0.261047	-1.34306
150	6.331	453176	0.0352	0.213602	-1.54363
180	6.332	333008	0.0259	0.156962	-1.85175

Expt No: 6-32

Probe cpd: LNR

pH: 6.0

System: TiO₂/H₂O₂/visible light at 420 nm (Hg lamps) with LNR at 0.3 mM

T (min)	R.T.	Area	c (mM)	C/C ₀	ln(C/C ₀)
0	6.401	2905111	0.226	1	0
30	6.405	1970198	0.153	0.678183	-0.38834
60	6.407	1605858	0.125	0.55277	-0.59281
90	6.411	1552800	0.121	0.534506	-0.62641
120	6.413	1379451	0.107	0.474836	-0.74479
150	6.408	1107886	0.0862	0.381358	-0.96402
180	6.415	977555	0.0760	0.336495	-1.08917

Expt No: 6-33

Probe cpd: LNR

pH: 6.0

System: TiO₂-Rutile/visible light at 420 nm (Hg lamps)

T (min)	R.T.	Area	c (mM)	C/C ₀	ln(C/C ₀)
0	6.361	1289595	0.0954	1	/
60	6.367	1277282	0.0945	0.990452	/
120	6.362	1293499	0.0957	1.003027	/
180	6.369	1297954	0.0960	1.006482	/

Expt No: 6-34

Probe cpd: LNR

pH: 6.0

System: TiO₂-Rutile/H₂O₂/visible light at 420 nm (Hg lamps)

T (min)	R.T.	Area	c (mM)	C/C ₀	ln(C/C ₀)
0	6.351	1297705	0.0960	1	/
30	6.347	770063	0.0570	0.593404	/
60	6.342	526076	0.0389	0.40539	/

Cont'd

90	6.345	394854	0.0292	0.304271	/
120	6.350	289458	0.0214	0.223054	/
150	6.348	182800	0.0135	0.140864	/
180	6.346	108328	0.0080	0.083477	/

Expt No: 6-35

Probe cpd: LNR

pH: 6.0

System: TiO₂-Anatase/visible light at 420 nm (Hg lamps)

T (min)	R.T.	Area	c (mM)	C/C ₀	ln(C/C ₀)
0	6.341	1276360	0.0944	1	/
60	6.337	1224667	0.0906	0.95950	/
120	6.335	1103951	0.0816	0.864921	/
180	6.338	1033800	0.0765	0.80996	/

Expt No: 6-36

Probe cpd: LNR

pH: 6.0

System: TiO₂-Anatase/H₂O₂/visible light at 420 nm (Hg lamps)

T (min)	R.T.	Area	c (mM)	C/C ₀	ln(C/C ₀)
0	6.325	1289886	0.0954	1	/
30	6.330	1138572	0.0842	0.882692	/
60	6.334	1029422	0.0761	0.798072	/
90	6.328	930395	0.0688	0.72130	/
120	6.323	841231	0.0622	0.652175	/
150	6.327	797858	0.0590	0.618549	/
180	6.329	700657	0.0518	0.543193	/

Expt No: 7-1

Probe cpd: LNR

pH: 6.0

System: TiO₂/visible light at 420 nm (Xe lamp)

T (hr)	R.T.	Area	c (mM)	C/C ₀
0	6.297	1256883	0.0929	1
1	6.291	1236006	0.0914	0.98339
2	6.295	1260618	0.0932	1.002972
3	6.298	1229645	0.0909	0.978329
4	6.302	1219304	0.0901	0.970102
5	6.305	1242436	0.0918	0.988506

Expt No: 7-2

Probe cpd: LNR

pH: 6.0

System: H₂O₂/visible light at 420 nm (Xe lamp)

T (hr)	R.T.	Area	c (mM)	C/C ₀
0	6.287	1272421	0.0940	1
1	6.285	1287253	0.0951	1.011657
2	6.282	1271037	0.0939	0.998912
3	6.290	1278273	0.0944	1.004599
4	6.287	1275998	0.0942	1.002811
5	6.281	1280966	0.0946	1.006716

Expt No: 7-3
 Probe cpd: LNR
 pH: 6.0
 System: TiO₂/visible light at 420 nm (Xe lamp) with the purge of O₂

T (hr)	R.T.	Area	c (mM)	C/C ₀
0	6.271	1299544	0.0960	1
1	6.268	1259369	0.0930	0.969086
2	6.277	1294599	0.0956	0.996195
3	6.273	1278221	0.0944	0.983592
4	6.269	1297487	0.0958	0.998417
5	6.272	1279827	0.0945	0.984828

Expt No: 7-4
 Probe cpd: LNR
 pH: 6.0
 System: TiO₂/H₂O₂/visible light at 420 nm (Xe lamp)

T (hr)	R.T.	Area	c (mM)	C/C ₀
0	6.287	1241190	0.0917	1
1	6.285	722468	0.0534	0.582077
2	6.281	589626	0.0435	0.475049
3	6.288	520714	0.0385	0.419525
4	6.279	451617	0.0334	0.363858
5	6.284	364837	0.0270	0.293941
6	6.289	279840	0.0207	0.225461

Expt No: 7-5
 Probe cpd: LNR
 pH: 6.0
 System: TiO₂/H₂O₂/visible light at 435 nm (Xe lamp)

T (hr)	R.T.	Area	c (mM)	C/C ₀
0	6.263	1230891	0.0909	1
1	6.259	867777	0.0641	0.704999
2	6.267	671621	0.0496	0.545638
3	6.261	605064	0.0447	0.491566
4	6.268	535182	0.0395	0.434792
5	6.259	457703	0.0338	0.371847
6	6.264	384167	0.0284	0.312105

Expt No: 7-6
 Probe cpd: LNR
 pH: 6.0
 System: TiO₂/H₂O₂/visible light at 450 nm (Xe lamp)

T (hr)	R.T.	Area	c (mM)	C/C ₀
0	6.279	1200510	0.0887	1
1	6.283	1007824	0.0745	0.839497
2	6.277	928834	0.0686	0.77370
3	6.281	871266	0.0644	0.725747
4	6.284	846020	0.0625	0.704717
5	6.276	802134	0.0593	0.668161
6	6.271	740152	0.0547	0.616531

Expt No: 7-7
 Probe cpd: LNR
 pH: 6.0
 System: TiO₂/H₂O₂/visible light at 500 nm (Xe lamp)

T (hr)	R.T.	Area	c (mM)	C/C ₀
0	6.312	1245609	0.0920	1
1	6.315	1197814	0.0885	0.96163
2	6.317	1187476	0.0877	0.95333
3	6.325	1177657	0.0870	0.945447
4	6.311	1137605	0.0840	0.913292
5	6.313	1123529	0.0829	0.901992
6	6.320	1104071	0.0815	0.886371

Expt No: 7-8
 Probe cpd: LNR
 pH: 6.0
 System: TiO₂/H₂O₂/visible light at 435 nm (Xe lamp) with the addition of 100 mg/L NaN₃

T (hr)	R.T.	Area	c (mM)	C/C ₀
0	6.338	1252449	0.0925	1
1	6.342	1223521	0.0904	0.976903
2	6.345	1218288	0.0900	0.972725
3	6.337	1209783	0.0893	0.965934
4	6.340	1196017	0.0883	0.954943

Expt No: 7-9
 Probe cpd: LNR
 pH: 6.0
 System: TiO₂/H₂O₂/visible light at 435 nm (Xe lamp) with the addition of 100 mg/L HCO₃

T (hr)	R.T.	Area	c (mM)	C/C ₀
0	6.321	1232914	0.0911	1
1	6.325	1224112	0.0904	0.992861
2	6.328	1230054	0.0909	0.99768
3	6.319	1214110	0.0897	0.984749
4	6.326	1205188	0.0890	0.977512

Expt No: 7-10
 Probe cpd: LNR
 pH: 6.0
 System: TiO₂/H₂O₂/visible light at 435 nm (Xe lamp) with the addition of 100 mg/L tert-Butanol

T (hr)	R.T.	Area	c (mM)	C/C ₀
0	6.313	1241078	0.0917	1
1	6.315	1103941	0.0816	0.889502
2	6.320	1033978	0.0764	0.833129
3	6.311	977550	0.0722	0.787662
4	6.318	894539	0.0661	0.720776

Expt No: 7-11
 Probe cpd: LNR
 pH: 6.0
 System: TiO₂/H₂O₂/visible light at 435 nm (Xe lamp) with the addition of 3 g/L tert-Butanol

T (hr)	R.T.	Area	c (mM)	C/C ₀
0	6.309	1295706	0.0957	1
1	6.315	1280635	0.0946	0.988369
2	6.307	1278933	0.0945	0.987055
3	6.301	1265241	0.0934	0.976488
4	6.308	1256049	0.0928	0.969394

Expt No: 7-16
 Probe cpd: LNR
 pH: 6.0
 System: Ga₂O₃/H₂O₂/visible light at 420 nm

T (hr)	R.T.	Area	c (mM)	C/C ₀
0	6.331	1303676	0.0963	1
1	6.337	1305454	0.0964	1.001364
2	6.335	1298796	0.0959	0.996257
3	6.330	1296231	0.0957	0.994289
4	6.327	1302947	0.0962	0.999441

Expt No: 7-17
 Probe cpd: LNR
 pH: 6.0
 System: SiO₂/H₂O₂/visible light at 420 nm

T (hr)	R.T.	Area	c (mM)	C/C ₀
0	6.312	1297498	0.0958	1
1	6.309	1297399	0.0958	0.999924
2	6.305	1299132	0.0959	1.001259
3	6.301	1289854	0.0952	0.994109
4	6.308	1290321	0.0953	0.994469

Expt No: 7-18
 Probe cpd: LNR
 pH: 6.0
 System: Al₂O₃/H₂O₂/visible light at 420 nm

T (hr)	R.T.	Area	c (mM)	C/C ₀
0	6.328	1321100	0.0975	1
1	6.321	1307728	0.0966	0.989878
2	6.324	1300218	0.0959	0.984193
3	6.327	1315768	0.0971	0.995964
4	6.320	1306894	0.0964	0.989247

The evolution of TOC, varied ions and pH during the decay process of LNR in TiO₂/H₂O₂/Visible system.

Expt No: 7-12

Probe cpd: LNR

Ph: 6.0

System: TiO₂/H₂O₂/Visible light at 420 nm (Xe lamp)

T (hr)	TOC (mg/L)	Cl ⁻ (mg/L)	NO ₃ ⁻ (mg/L)	NH ₄ ⁺ (mg/L)	pH
0	27.514	0	0	0	6.00
2	/	1.2	0.0352	0.004	5.01
4	/	1.98	0.0485	0.023	4.23
8	26.0175	3.52	0.0798	0.0378	3.92
16	25.6565	6.43	0.186	0.109	3.68
24	23.9846	8.34	0.356	0.2036	3.56
32	22.9015	10.15	0.612	0.399	3.34
40	21.885	11.04	0.785	0.526	3.20
48	20.097	11.88	1.05	0.677	3.12
56	18.693	12.56	1.61	1.02	3.07
